THE UNIVERSITY OF CHICAGO

MODELING FLUORESCENCE PROPERTIES OF VOLTAGE-SENSITIVE PROBES IN SOLVENT AND EMBEDDED IN MEMBRANE USING MOLECULAR DYNAMICS

A DISSERTATION SUBMITTED TO
THE FACULTY OF THE DIVISION OF THE PHYSICAL SCIENCES
IN CANDIDACY FOR THE DEGREE OF
DOCTOR OF PHILOSOPHY

DEPARTMENT OF CHEMISTRY

BY
RACHAEL YOUNGWORTH

CHICAGO, ILLINOIS
MARCH 2023

TABLE OF CONTENTS

LIST OF FIGURES

LIST OF TABLES

ACKNOWLEDGMENTS

The work in this project would not have been possible without the guidance and support of Dr. Benoît Roux, I would like to thank him in particular for his patience and assistance during every stage of the process. I am extremely grateful to him and the other two members of my Thesis committee: Dr. Sarah King and Dr. Greg Voth for their advice and expertise.

Many thanks to all of the members of the Roux group for the helpful discussions and ideas. And, of course, I would like to thank my family and friends for their moral support over the years.

ABSTRACT

Voltage-sensitive probes inserted into membranes can be used to report back changes to their immediate environment, especially in regards to the membrane potential,[14,56,149] polarity,[119] ion concentration[39,40,70] and membrane composition.[28,56] Experimentally, the relative changes in the color of the fluoresced photons of voltage-sensitive probes can even be used to help track signal transmission across neurons in vivo.[104] However due to the sensitivity of these probes, there are many overlapping contributing factors to the exact color change, making it difficult to draw quantitative conclusions from studies in different systems. In order to investigate the degree to which different characteristics of a system contribute to the observed fluorescence changes of a probe molecule, atomic models have been developed. Rigorous force fields that treat induced polarization explicitly were created for the ground and excited state of the molecules of interest. Based on the Franck-Condon principle,[33,34,48] which generally states that electronic transitions are instantaneous as compared to any nuclear movements, the computational representation of the electronic component of excitation and emission is as simple as switching force field parameters for the probe molecule creating the Franck-Condon state. The intramolecular relaxation and surrounding solvent fluctuations can then be monitored in molecular dynamic simulations immediately after switching the state of the molecule. Considering the significance of the change in polarity for these probe molecules, parameters were developed for both a typical nonpolarizable force field and a polarizable Drude force field. First, the probe was simulated in a series of solvents with varying polarity, and second, the probe was simulated in a simple DPPC membrane in the presence of an applied transmembrane potential.

CHAPTER 1

INTRODUCTION

The interaction of light with matter

Most of the reality that surrounds us is constituted of atoms and molecules. It is a fundamental endeavor of theoretical chemistry to contribute to our understanding of the evolution and behavior of complex molecular systems in the most rigorous manner from the laws of physics. At the microscopic level, atoms and molecules are formed from nuclei and electrons, which are strongly associated with one another. In principle, the dynamical evolution of such systems obeys the laws of quantum mechanics (QM) and must be represented through the time-dependent nuclear-electronic wave function, which is obtained by solving the time-dependent Schrödinger equation.[120] However, this is often prohibitively complex, and to paraphrase Dirac,[41] even though the underlying QM laws are known, the difficulty is that these laws leads to equations that are "*much too complicated to be soluble*" in the case of complex molecular systems. Practical approximations must be made in order to make progress. For example, while molecules are expected to constantly move and undergo fluctuations at ambient temperature, it is reasonable to imagine that for any given configuration of the nuclei, the electrons occupy their lowest possible energy state known as the electronic ground or fundamental state. This is the foundational assumption of the Born-Oppenheimer approximation. While the electrons remain in their ground state, an effective and often adequate approximation is to adopt a purely classical treatment for the dynamics of the nuclei. In this case, their position is propagated according to Newton's law of motion $F = MA$ on an effective Born-Oppenheimer energy surface. However, this simple picture can be violated in a number of situations in which the electrons do not remain in their ground state. An important instance in which this occurs is when the electrons of a molecule are excited to higher energy states by absorbing the energy from light. The interaction of light

with matter is perhaps best explained by the concept of a "photon". The term photon was first popularized by Gilbert Lewis in 1926, extrapolating on the concepts of the quantized energies of light first proposed by Planck[145] and later by Einstein applying it to explain the photoelectric effect.[44] Lewis postulated that a photon associated with an electromagnetic wave at frequency ν carries a quantum of energy determined via Planck's constant h,[102]

$$E = h\nu \tag{1.1}$$

The energy of a photon can also be converted to corresponding units of wavelength as $\lambda = c/\nu$, where c is the speed of light. Individual photons only differ in characteristics like polarization, the direction in which they are moving, and the specific energy they possess.[102] Photons behave as both a particle and a wave, meaning that they are massless and move at the speed of light. The absorption of a photon of frequency $\tilde{\nu}_a$ allows for the excitation from ground to the excited state. Similarly, when the molecule returns from its excited to

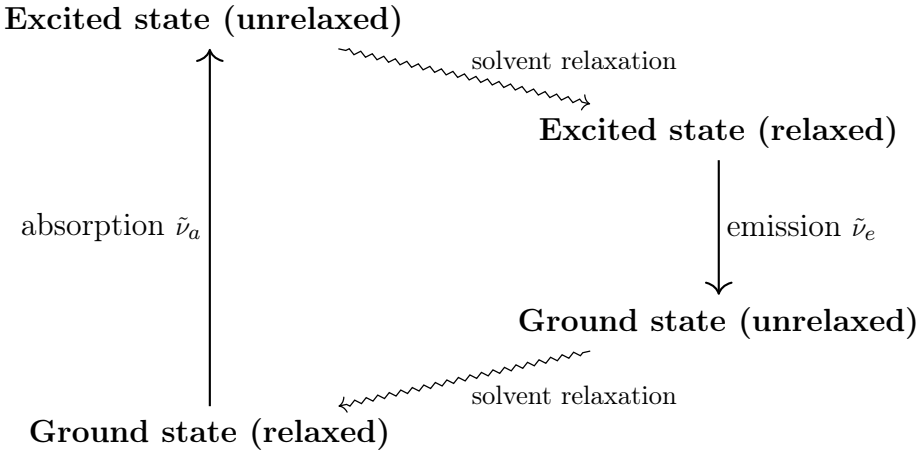

Figure 1.1: Simple Jablonski diagram of a fluorescence cycle[77] - The initial transition from the ground state to the Franck-Condon excited state corresponds to the absorption of a photon of frequency $\tilde{\nu}_a$. The final transition from the relaxed excited state to the unrelaxed ground state corresponds to the emission of a photon of frequency $\tilde{\nu}_e$. Due to solvent relaxation, the energy decreases from the unrelaxed Franck-Condon excited state to the relaxed excited state and from the unrelaxed ground state to the true relaxed ground state.

its ground state, there is emission of a photon of frequency $\tilde{\nu}_e$. As the simplest level, this offers a qualitative view of the process called fluorescence.

As illustrated in Figure 1.1, the absorption frequency $\tilde{\nu}_a$ is expected to be larger than the emission frequency $\tilde{\nu}_e$. This phenomenon, called the Stokes shift $\Delta\tilde{\nu}$, refers to the change in wavelength between the absorption $\tilde{\nu}_a$ and emission wavelength $\tilde{\nu}_e$.[180] Both absorption and emission can be expected to shift their exact transition energy in response to the immediate surrounding of the molecule. Solvent polarity tends to have a greater effect on emission energy differences than absorption energy differences due to how the solvent reorganizes in response to the excited molecule's dipole, which has a greater magnitude.[89] For this reason, the Stokes shift is particularly sensitive to changes in the immediate surroundings of the fluorescent molecule, making fluorescence a great tool to study that environment. The Lippert-Mataga Equation, Equation 1.2, is a simple model for a perfectly spherical fluorescent molecule of radius a embedded in a continuum dielectric solvent,[106,118]

$$\Delta\tilde{\nu} = \frac{2}{hc}\left(\frac{\varepsilon - 1}{2\varepsilon + 1} - \frac{n^2 - 1}{2n^2 + 1}\right)\frac{(\mu_E - \mu_G)^2}{a^3} + \Delta\tilde{\nu}^0 \tag{1.2}$$

where μ_E and μ_G are the magnitude of the dipole of the ground and excited states of the fluorescent molecule, respectively, and $\Delta\tilde{\nu}^0$ represents its Stokes shift in vacuum in the absence of any solvent. The equation relates the Stokes shift ($\Delta\tilde{\nu}$) of the fluorescing molecule in solvent in terms of the dielectric constant ε and refractive index n of that solvent. The portion of Equation 1.2 containing the solvent-dependent terms is,

$$\Delta f = \left(\frac{\varepsilon - 1}{2\varepsilon + 1} - \frac{n^2 - 1}{2n^2 + 1}\right) \tag{1.3}$$

where Δf is referred to as the orientation polarizability. The value of Δf determined for each solvent can be calculated for pure solvent systems with knowledge of that solvent's dielectric constant and its index of refraction. Orientation polarizability is a term that arises solely

from the molecular reorientation of the molecule, excluding any contribution from electronic mobility. The subtracted right-side term in the orientation polarizability definition, Equation 1.3, removes the contribution by electronic reorientation. In the case of solvents that do not have a permanent dipole, the dielectric constant is approximately the same as the index of refraction and thus its orientation polarizability is close to zero.

In principle, the Stokes shift of a fluorescent molecule in a series of solvents of different orientational polarizability should result in a perfect linear trend according to the Lippert-Mataga equation. In practice, there are deviations, though a general trend is still observable. Unsurprisingly, there are important limitations to the Lippert-Mataga equation based on a continuum dielectric treatment, especially in regards to accounting for specific interactions such as hydrogen bonding or internal charge transfers of the molecule of interest caused directly by the solvent interaction.[89] Nonetheless, this approximate treatment highlights the fact that simple classical models that ignore important QM aspects can still be useful to determine the effect of the environment on fluorescence. For example, to go beyond a simple continuum dielectric approximation for the solvent, one might resort to atomistic classical molecular dynamics simulations to determine the effect of the environment on fluorescence.

This discussion has so far left out a host of QM phenomena arising from the coupling between the electronic transition and the nuclear motion.[89,185] While the classical Franck–Condon principle pictures a vertical electronic transition occurring without changes in the positions of the nuclei,[33,34,48] there are non-radiative QM vibrational transitions associated with the reorganization of the nuclear configuration of the molecule caused by differences in the ground state and excited state potential energy surfaces.[89,185] For instance, the molecular geometry at the energy minimum as well as the shape (curvature) of the potential energy surface may differ for the two states. A simplistic representation of this is illustrated in Figure 1.2. Advanced QM treatment generally considers a Taylor expansion of the initial and final state potential energy surface around the ground state nuclear configuration and

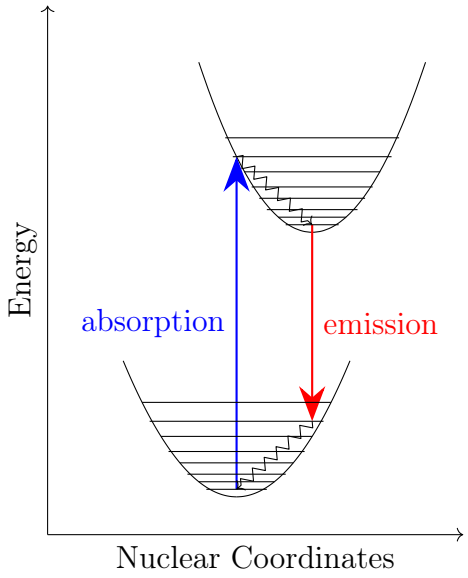

Figure 1.2: Energy transitions during the fluorescence cycle of a molecule between its ground and excited potential energy surfaces - electronic transitions colored blue for absorption and red for emission do not involve any nuclear motion (in accordance with the Franck-Condon principle) while the vibrational state transitions drawn as wavy black lines involve slight changes to the nuclear coordinates

the corresponding intramolecular vibrational states to account for the state-dependence of the energy minima and its coupling to the electronic transition.[45,79,134,184] For the sake of simplicity, these effects in the present work will be subsumed into environment-independent empirical offset constants for the excitation and emission.[198,200] Accounting for internal relaxation, the QM reorganization energies is expected to be on the order of about 1,000 cm^{-1} (2.859 kcal/mol) for one state. Assuming simple shifted harmonic potential energy surfaces, the difference between the absorption and emission frequency that is twice the reorganization energy, thus, the two offset constants of a fluorescent molecule are expected to differ by about 5 kcal/mol. While accounting for all QM effects is certainly essential for a complete and accurate simulation of optical spectra, including lifetime and line shapes, this simplification is justified because our main interest is a characterization of the influence of the molecular environment on the excitation and emission wavelengths.

Voltage-sensitive fluorescent dyes

The high sensitivity of fluorescent probe molecules to their environment is exploited in a broad range of biological studies. For example, probes that spontaneously insert into membranes can be used to report back changes in their immediate environment, especially in regards to membrane potential, polarity, ion concentration, membrane rigidity, and are even being used to track the transmission of the nerve impulse across neurons.[72,135,147] Voltage-sensitive styrylpyridinium dyes such as RH421,[54] RH160,[53] di-4-ANEPPS,[113] and di-8-ANEPPS (di-4- and di-8-amino-naphthyl-ethylene-pyridinium-propyl-sulfonate) are particularly interesting because they change their spectral properties in response to changes in membrane voltage.[5,56] Such dyes provide linear measurements of firing activity of single neurons, large neuronal populations or activity of myocytes, and for this reason, they are important tools to map the activity of the nervous system in the BRAIN Initiative (Brain Research through Advancing Innovative Neurotechnologies).[4] They are also used to monitor living organisms,[59] when integrated into medical devices. The dyes di-4-ANEPPS and di-8-ANEPPS have been used to probe the electric field and interfacial dipole potential of membrane bilayers due to their following properties: they respond linearly to membrane potential, an electrochromic mechanism underlies the response, they have no net charge at neutral pH, and they produce a spectral shift in response to voltage. Both di-4-ANEPPS, and di-8-ANEPPS bind to lipid membranes with their chromophore in the lipid head group region, where they are sensitive to the local electric field. The Stokes shift of di-8-ANEPPS has been used to examine variations in the interfacial membrane dipole potential associated with lipid composition and ions,[17,23,24,26,56,94,177,187,193] including the effect of cholesterol.[25,178] Interpretation of many experiments, however, is not straightforward due to the lack of information about the membrane-bound dye. For instance, the orientation of the dye molecule in the lipid bilayer has been subject to considerable controversy, with estimates of the angle relative to the membrane normal varying from 36° to 63°.[52,90,157] Detailed molecular

dynamics (MD) simulations of the dyes embedded in a solvated lipid membrane may help clarify many of these issues.

Molecular dynamics and classical force fields

Molecular dynamics (MD) simulation is a powerful theoretical approach to investigate the function of complex molecular systems.[85] It consists of calculating the position of the atoms as a function of time and using detailed models of the microscopic forces operating between them, by integrating numerically the classical equations of motion.[163] For the sake of computational efficiency, it is reasonable to approximate the Born-Oppenheimer QM potential energy surface by using a force field constructed from simple analytical and differentiable functions. The functional form used to represent the total potential energy of a molecule can essentially be broken down into additive components that each describe a different interaction between subsets of atoms. As an example, the CHARMM[16] function form of a nonpolarizable force field is shown in Equation 1.4.

$$\begin{aligned} E &= \sum_{\text{bonds}} K_{\text{b}}(b-b_0)^2 + \sum_{\text{angles}} K_\theta(\theta-\theta_0)^2 \\ &+ \sum_{\text{Urey}-\text{Bradley}} K_{\text{UB}}(r_{1,3}-r_{1,3;0})^2 + \sum_{\text{dihedrals}} K_\phi(1+\cos(n\phi-\delta)) \\ &+ \sum_{\text{nonbonded pairs}} \frac{q_i q_j}{4\pi\epsilon_0 r_{ij}} + E_{\text{min},ij}\left[\left(\frac{R_{\text{min},ij}}{r_{ij}}\right)^{12} - 2\left(\frac{R_{\text{min},ij}}{r_{ij}}\right)^{6}\right] \end{aligned} \tag{1.4}$$

In an all-atom MD simulation, each atom is considered explicitly, so each contributes to each summation term. These terms either describe bonded or nonbonded interactions. The first four terms (labelled bonds, angles, Urey-Bradley, and dihedrals) are the bonded terms, which describe geometry fluctuations as a product of a proportionality constant (to describe the stiffness of a harmonic oscillation) times the square of the difference between the distorted position (i.e. the bond when stretched or the angle when twisted) and an equilibrium

position. Consequentially, when a geometry feature is at an equilibrium position, its contribution to the overall potential energy is zero. There is a single optimal bond length, angle and Urey-Bradley (an angle bending term) computed. Dihedrals are a torsional angle around a bond with respect to the bonds linked to it at either end. In the case where four atoms are connected linearly (where the first atom is bonded to the second which is bonded to the third which is bonded to the fourth) and it is viewed along the bond between the second and third atom such that those two atoms overlap, the dihedral torsion is the angle between the positions of the first and fourth atom. Improper dihedrals consider the angles formed for a set of four atoms where there is one central atom directly bonded to the other three. The potential energy terms for these bonded contributions account for there being a number of energy minima via a cosine function and a multiplicity term.

The nonbonded interactions are the additional potential energy terms from the interaction between atoms separated by at least three bonds. These contributions are the electrostatic energy as represented by a Coulomb energy and van der Waals as represented by a Lennard-Jones potential. The Lennard-Jones potential energy is a function of interatomic distance, with an optimal distance corresponding to an energy minimum with depth E_{min}. The Coulomb energy term calculates interaction between the atomic charges of two atoms. If those charges are fixed and not allowed to vary, the force field is then described as additive or nonpolarizable. This is obviously an approximation because it is expected that the charge distribution of an atom or a molecule will be affected if it is subjected to an external electric field. This is the effect of induced polarization.

Polarizable force fields are expected to be more accurate in replicating the behavior of polar interactions, which is a particularly important component when modeling the effects of membrane potential and solvent polarity on transitions between ground and an excited state. In a polarizable force field, the charge distribution is adaptive and responds to external electric fields. There are several methods by which polarizability can be represented

as an extension of the nonpolarizable force field model such as with a fluctuating charge model, induced dipole model, and the classical Drude oscillator. Unlike the static point charges assigned in nonpolarizable models, the fluctuating charge model treats these charges as variables that change in response to its immediate environment, such as interactions with other molecules or geometrical alterations.[155,156] This method combines the creation of its atomic charges via electronegativity equilibration[136] and a Lagrangian approach to the treatment of the dynamical variables of a charge almost as if it were an atom. The CHARMM-FQ force field applies this fluctuating charge model to proteins, optimizing its electrostatics parameters to the small molecule charge responses to a dipolar probe.[138,139] Limitations due to how the charge flow is restricted to being only along bonds[179] results in this model's inability to properly model the polarization responses out of plane for something like an aromatic ring[156] and interactions in bifurcated hydrogen bonded systems.[11,109] In contrast, the induced dipole polarizable models do not allow the variance of its partial charges in response to external factors and instead adds inducible dipoles to each polarizable atom,[83] which was later improved upon to produce POSSIM (POlarizable Simulations with Second order Interaction Model).[103] Another extension of this idea was explored with the AMOEBA (Atomic Multipole Optimized Energetics for Biomolecular Applications) force field,[172] which returned to the concept of replacing the static partial charges like what was seen in the fluctuating charge model. The partial charges at each atomic center are then represented as permanent atomic multipoles which are composed of a charge, dipole and quadropole moments.[146,172]

The polarizable Drude model, based on the classical Drude oscillator, represents polarization by introducing a charged auxiliary particle that is attached to an atom via a harmonic spring.[42] This allows for a small separation of charge that is responsive to the local electric field. To a good approximation, it is adequate to introduce a Drude particle only for the non-hydrogen (heavy) atoms. For instance, it was shown that many of the properties of

water could be accurately modelled with only a Drude particle attached to its oxygen.[93] Fundamentally a Drude particle is a particle on a spring, and Hooke's Law describes the interaction with its parent atom as a classical oscillator.[92,99] The displacement vector of the Drude oscillator in response to an external electric field $\mathbf{E}$ is $\mathbf{d} = (q_D/k_D)\,\mathbf{E}$, yielding the induced dipole $\boldsymbol{\mu} = q_D\,\mathbf{d}$. Assuming a classical linear polarization response $\boldsymbol{\mu} = \alpha\,\mathbf{E}$, the effective polarizability coefficient ascribed to the atom is identified as,

$$\alpha \;=\; \frac{q_D^2}{k_D} \tag{1.5}$$

In principle, the inducible degree of freedoms (i.e., the displacement of the Drude oscillators) should be allowed to relax to the energy minimum for each fixed set of nuclear coordinates. Traditionally this condition is satisfied within a chosen tolerance by repeatedly adjusting the displacement of the Drude particles $\mathbf{d}$ in response to the total electric field $\mathbf{E}$, until self-consistency is reached. It is this "self-consistent field" (SCF) condition that confers the many-body character to polarizable models. However, the iterative SCF procedure (fixing the nuclei and adjusting the positions of the Drude particles via energy minimization) is computationally demanding, resulting in a considerable loss of efficiency for generating MD trajectories of large molecular systems. A popular alternative is to treat the inducible variables as dynamical degrees of freedom using an extended Lagrangian.[19] To remain as faithful as possible to the adiabatic dynamics of the initial SCF model, two independent thermostats are introduced: one at a temperature T for the physical degrees of freedom, and one at a lower temperature T^* for the inducible degrees of freedom. This led to the polarizable force field based on classical Drude oscillators with the dual-Nosé-Hoover thermostat.[93]

The ability of the extended Lagrangian method with dual-Nosé-Hoover thermostat to mimic the adiabatic propagation of the system on the SCF energy surface depends on the rate of energy flow between the physical degrees of freedom that are at a high temperature, and the inducible degrees of freedom that are at a low temperature.[167] The correct SCF en-

ergy can be recovered for a given configuration of fixed nuclei by minimizing the position of the Drude particles. From harmonic analysis, this difference in energy per oscillator between the extended Lagrangian and the SCF calculation is equal to 0.00298 (T^*/K) kcal/mol (or the Boltzmann constant multiplied by 3/2) where T^* refers to the lower temperature thermostat used for the Drude particles. When graphing the excess energy per oscillator from simulations as a function of T^*, the slope of the resulting line varies depending upon the mass assigned to the Drude particles. Since it was found to have the closest match to the slope produced through harmonic analysis, the generally recommended mass for Drude particles is 0.4 amu.[167] The use of the extended Lagrangian method was further validated by showing that the average potential energy differed by a factor of less than 0.1% when comparing a simulation performed under SCF conditions and one using dual-Nosé-Hoover extended-Lagrangian molecular dynamics, both at a nuclei temperature of 300 K. Additionally dual-Nosé-Hoover replica-exchange molecular dynamics performed with five replicas of temperatures ranging from 300 to 310K was also shown to agree within the same level of accuracy to the SCF reference model.[167]

Electronic structure and treatment of the excited state

The previous sections broadly described the effect of light on molecules in a very qualitative manner and introduced the basic concepts of MD simulations and classical force fields. Parameterization of the force field for a molecule implies the determination of the equilibrium structural parameters and the force constants for the internal energy terms (bonds, angles, dihedrals), as well as the partial charges, polarizability and Lennard-Jones parameters for the non-bonded interaction terms. General Automated Atomic Model Parameterization (GAAMP) is a tool to generate and optimize the parameters for both nonpolarizable and polarizable Drude force fields for any small molecule by generating the necessary ab initio calculations.[73] While a very powerful tool, GAAMP is somewhat limited by the size of

molecule it can handle efficiently and that it is only set up to fit its generated parameters to the electrostatic potentials of a molecule's ground state. High level ab initio calculations are necessary to map the electrostatic parameters of the molecule in its excited state. To enable a quantitative discussion of fluorescence, which requires consideration of excited states, it is necessary to adopt a rigorous QM framework.

Atomic and molecular orbitals

Orbitals describe the probability of an electron occupying a defined space, which can also be called a wave function in QM. Atomic orbitals can be defined by a series of unique quantum numbers: the principal quantum number (n), azimuthal (or angular momentum) quantum number (l), magnetic quantum number (m_l) and the electron spin quantum number (m_s). The principal quantum integer has values that refer to one of the discrete energy shells described in Bohr's atomic model. The greater the value, the higher the energy, and the further the shell exists from the atomic nucleus. The azimuthal quantum number is also an integer, though its range is restricted from zero to values equal to one less than the principal quantum integer. Its value refers to orbital shape, where zero corresponds to s-orbitals which are spherical, one corresponds to p-orbitals which are "dumbbell" shapes aligned along the x, y, or z axis, two represents d-orbitals and three refers to f-orbitals. The magnetic quantum number has integer values ranging from the negative of the azimuthal quantum number to the positive of the azimuthal quantum number and refers to the orbital angular momentum position in orientation space (differentiating between the one s-orbital, the three different p-orbitals, five d-orbitals and seven f-orbitals). Orbitals with the same principal and azimuthal quantum numbers are considered to be degenerate, because each has the same energy despite different conformations. Finally, the electron spin quantum number refers to the angular momentum of the electron and is given the value of either positive or negative 1/2 to indicate spins of the electron in opposite directions. Paired electrons in the

same orbital have opposite spin, which follows Pauli's exclusion principle of no two electrons having the same exact set of quantum numbers[140] since these two electrons do differ in the electron spin quantum number despite having the same other three quantum numbers.

When this is applied to molecules, an approximation of the corresponding molecular orbitals can be considered to be a linear combination of atomic orbitals.[100] Molecular orbitals can be divided into three types: nonbonding, bonding and antibonding orbitals.[71,125,126] Nonbonding orbitals contain unshared electrons and are the result of no direct interaction between the atomic orbitals. They are typically at the same energy level as the corresponding atomic orbital of the contributing atom. Both bonding and antibonding orbitals contain shared electrons, the difference lies in their respective energy levels. Bonding orbitals are the result of overlapping atomic orbitals, meaning that there is constructive interference between the two electrons resulting in an orbital of lower energy than the atomic orbitals that produced it.[176] The space defined by a bonding orbital can be considered to be between the two atoms forming the bond, thus electrons occupying bonding orbitals stabilize the molecule as a whole.[127] In contrast, antibonding orbitals are the result of destructive interference between electrons, resulting in a higher energy molecular orbital that defines its region as being on either side of the atoms forming the bond (rather than between them). If the antibonding orbital is occupied, the bond is expected to be destabilized.

Available electrons fill the orbitals starting from the lowest energy, creating the electronic configuration of the ground state. Electrons fill the available orbitals following the Pauli exclusion principle (which states that no two electrons can have identical electrons quantum numbers)[140] and Hund's rule (which states that before doubling up occupancy in an orbital of a given sublevel, each orbital is singly occupied with electrons with the same spin).[76] The last filled orbital, and thus the occupied orbital of the highest energy, is called the HOMO (highest occupied molecular orbital) while the next orbital above it that is unfilled is called the LUMO (lowest unoccupied molecular orbital). Molecules that gain sufficient

energy from a photon absorption can transition from its ground state to an excited state that inherently has higher energy. This is characterized by a movement of electrons between molecular orbitals across the HOMO-LUMO gap.

An excited state is described as either a singlet or a triplet state, depending upon the spin of the electron that was energized to jump to a previously unoccupied orbital. If the excited electron does not flip and is thus still paired with the electron it previously occupied an orbital with (meaning that the spins of these two electrons are antiparallel), the resulting excited state is a singlet. In the case were a flip does occur when the electron is excited to a new orbital, a former pair of electrons now have spins that are parallel resulting in a triplet state.[185] Transitions are forbidden between the ground state and a triplet state, the triplet state instead can only be reached due to interconversion from a singlet excited state.

Calculation of the wavefunction

Unlike molecular mechanics that uses classical Newtonian mechanics to represent molecular systems, ab initio calculations are derived from first principles based entirely on solving the Schrodinger equation[169] to acquire energy and a wavefunction (a mathematical representation of electron distribution). Hartree applied Schrodinger's one-particle equation to multiple electrons in a non-Coulomb central symmetric field where the potential is a function of the electron's distance from the nucleus. Thereby the overall wavefunction of an atom is represented as a product of individual one-electron wavefunctions or atomic orbitals.[64,65,69] His method involved successive approximation to create a self-consistent field, more explicitly: the solutions to each electron wavefunction in response to a general electrostatic field due to the other electrons was calculated iteratively for each electron until the solution of the total wavefunction no longer varied significantly. Self-consistency refers to the procedure of starting from an educated guess and performing iterations of the calculations until the result of an iteration is within an error tolerance to the previous iteration (in other words,

a relative consistency is reached).[15] One major issue with this initial formalism was that electrons were indistinguishable, meaning that electrons could have the same set of quantum numbers and thus violate the Pauli exclusion principle. This was solved by accounting for the spin electrons at the start of the calculation by considering only antisymmetric wave functions, treated as spin orbital determinants.[47,141,174] Slater wavefunctions are a determinant of each electron's spatial and spin orbitals, rather than just a simple product of them. Effectively this means that each spatial orbital is not occupied by more than two electrons and that the wavefunction is antisymmetric, thereby upholding the Pauli exclusion principle.[175] Incorporating exchange effects via Fock's equations[47] resulted in what would become known as the Hartree-Fock approximation, a size-consistent and variational method.[67] Size consistency refers to the property that the calculated energy of two molecules separated by an infinite distance is the same as the sum of the two calculated individually. The Hartree-Fock energy can be considered variational because its calculations are always seeking a lower, more correct energy (in other words, the energy calculated is always greater than or equal to the true ground state energy). Later this would be extended from atomic orbitals to molecular orbitals, after it was proven that reasonable initial guesses of the molecular orbital wavefunctions could be obtained with linear combinations of basis functions.[61,160]

Electron correlation, or the notion that the movements of an electron affects the others, is generally not handled explicitly in Hartree-Fock calculations. Apart from the restriction that paired atoms cannot have the same spin, the electron repulsion experienced by a given electron is a function of an averaged electrostatic field of the rest of the electrons. Hartree-Fock seeks the lowest energy configuration (the ground state), however there exist many other states of similar energies that could be considered simultaneously. One method to account for electron correlation is with Møller-Plesset (MP) calculations using perturbation theory,[121] a size consistent (but not variational) method. Another is configuration interaction (CI), which when applied to Hartree-Fock, provides a linear expansion of the Hartree-Fock wave-

function terms to now include excited states where electrons have been promoted to occupy virtual molecular orbitals. Slater determinants could be expanded to include components of several different electronic configurations,[35] thereby improving the estimation of systems that were poorly represented by a single configuration of Hartree-Fock calculations. A linear combination of equivalent state determinants, referred to as a configuration state function (CSF), are often used instead of Slater determinants as the terms in a CI expansion. Considering this 'superposition of configurations' in combination with his self-consistent field methods, Hartree showed an improved calculation of the energy values of oxygen ions[68] as compared to his prior calculations using only the ground state configuration.[66]

A full CI calculation — a method that is both size consistent and variational — considers all possible electron configurations. If only singly excited determinants are considered it is a CIS (configuration interaction singles) calculation, if both singly and doubly excited determinants are considered it is a CISD (configuration interaction singles and doubles) calculation. Both of these methods are still variational but no longer size consistent. And if in addition to the excitations from the ground state some excited configurations themselves are also considered in the same manner, it is a MRCI (multireference configuration interaction) calculation. These methods quickly become unwieldy with the increase in the size of a molecule when there are many electrons and too many possible molecular orbitals to occupy, and especially when excitations from multiple states are referenced. This necessitates some limitation of what configurations are considered important to characterize larger molecules.

Multi-configurational self-consistent field (MCSCF) is a method that combines the CI procedure where the spatial molecular orbitals used in the creation of the determinants are also optimized and SCF calculations. As a self-consistent field method, it requires many iterations to achieve convergence and needs to be simplified for larger molecules. Choosing only configurations necessary to calculating out the desired property is an important part of a MCSCF procedure, a particularly useful approach to this selection is encompassed in the

complete active space self-consistent field (CASSCF) version. CASSCF is not a variational method, though it can be size consistent, presuming that the chosen active space contains the correct molecular orbitals for the examined process. It is a multiconfigurational method, meaning that more than one set of occupancies or configurations of electrons distributed in molecular orbitals is considered simultaneously. CASSCF classifies theses orbitals into three categories: core, active and virtual. Core orbitals are doubly occupied by electrons, virtual orbitals are entirely unoccupied while the active orbitals have partial occupancy, the degree of which can fluctuate over the course of a transition. Unlike a single reference method that only considers core and virtual orbitals with a clean divide between the HOMO (highest occupied molecular orbital) and LUMO (lowest unoccupied molecular orbital), the active space of CASSCF can be considered to be spanning that divide. The selection of which orbitals are defined to be active is based on whether their occupancies change over the course of a transition, in this case the transition from ground to excited state. These configurations are represented mathematically as either Slater Determinants (an antisymmetrized product to describe electron spin-orbitals) or Configuration State Functions (which are linear combinations of Slater Determinants). The number of determinants and functions increases drastically with an increase in the number of active electrons, quickly making calculations more expensive. As a result, it is important to restrict the number of orbitals and electrons that are identified as active, but paramount that what is selected is sufficient to fully represent the transition.

Application to building excited state parameters

The general procedure to treat a molecule of interest such as di-8-ANEPPS follows the fluorescence cycle: starting with a geometry optimization, followed by a SA-CASSCF (state averaged CASSCF) calculation that equally weights the ground state along with a specified number of excited states above it, next the desired excited state is isolated representing the

instantaneous absorption transition, the excited state's geometry is optimized, then with the new geometry the ground state can be isolated to show the instantaneous emission step and finally another geometry optimization would recover the starting point. When choosing the number of states considered it is necessary to choose enough singlets and triplets such that all the states that are energetically between the ground and the state of interest are included as well as several states at a higher energy than the excited state of interest. If the excitation being studied is the first singlet, it is likely that only three total singlets need to be included: the ground state, the first singlet and the second singlet. Additionally, any triplets of similar energies need to be considered to distinguish them from the desired first singlet. During the SA-CASSCF step, orbitals have been categorized into core, active and virtual which give a general idea of which orbitals change occupancies between each of the considered states. This makes it a valuable starting point once a desired state is selected to be focused on entirely.

After converging a SA-CASSCF for the molecule that considers a sufficient number of states, the subsequent calculation puts all weight on the desired state and no longer averages over multiple states. Now the orbitals identified as active need to be important specifically for the transition from the ground to that isolated state. Often this step does not converge even with extended calculation time, but it does report its classifications of all the molecular orbitals before suspending the calculation. After observing the orbitals that were determined to be active, core and virtual, corrections can be performed manually. Since there is some knowledge of what some of the active orbitals should be, when these orbitals are identified in a different subspace they can be rotated into the active space before resuming the calculation until convergence is achieved.

Extracting the electrostatic potential data from the results of the CASSCF step that isolates the transition from the ground state to the desired excited state, allows for the generation of the excited state force fields. This was accomplished by using the charge-fitting

procedure within GAAMP. Using the excited state parameters generated, simulations can be performed with the molecule in its excited state. And for a given, independent snapshot of that simulation or one performed with the ground state parameters, an energy difference can be calculated that corresponds to the instantaneous electronic transition between states. These energies include contributions from the surrounding environment, but do not consider the changes in vibrational states that occur within the fluorescing molecule. Including both vibronic and environmental effects is necessary to calculate an accurate representation of the energy transition between the ground and excited state.

Approaches to accounting for contributions of vibrational transitions in an explicit solvent simulation can be classified as either static or dynamic. The dynamic method is based on the creation of linear and nonlinear time correlation functions of excitation energies, meaning that the fluorescing molecule and environment are on the same timescale. A less computationally expensive option is the static method, which only considers independent snapshots from simulation. The static method requires a separate calculation of the spectra density to determine the vibronic effects that are added in afterwards.[200] In this way, the contributions to the energy of the molecule of interest's transition from ground to excited state are separated into intermolecular interactions based on electrostatic interactions and intramolecular shifts in the vibrational modes. Molecular dynamics are used to find the long-range component of the excitation energy, but there are several means of finding the value of the vibrational coupling such as with harmonic analysis and single-point gradient quantum calculations.[97] Some studies only use the molecular dynamics simulations to produce the configurations of the molecule of interest in its specific surroundings to be used in QM optimizations and generating a Hamiltonian ensemble based on the Frenkel exciton model, rather than computing the Frank-Condon excitation energies directly.[98]

The average energy of vertical excitation (a Franck-Condon transition) is equivalent to the sum of the adiabatic excitation energy and contributions from changes in vibrational

modes and from temperature fluctuations.[198,200] This relationship means that in order to convert between the vertical excitation and the adiabatic excitation, all that is needed is a constant value which is independent of the specific solvent interactions with the molecule of interest. This constant, referred to as an offset throughout the rest of this Thesis, was not calculated directly and is instead an empirical value derived by fitting the vertical transition data to energy differences found in experimental studies.

General overview of this thesis

The focus of this study is on di-8-ANEPPS which is a zwitterion with a strong negative charge centered in its sulfonate group. The position of the corresponding positive charge shifts when the molecule is excited from the nitrogen in its pyridinium group to the nitrogen in its amino group. The bulk of the molecule is a conjugated structure, which facilitates a flow of charge when transitioning between its ground and excited state. The rest of the molecule is an amino group terminating in two hydrophobic octanes. It is a voltage-sensitive fluorescing probe whose absorption and emission properties can be directly influenced by its immediate surroundings. Di-4-ANEPPS, an identical molecule apart from having shorter carbon tails, is shown to have a maximum absorbance at 468 nm in lipid vesicles (493 nm in ethanol, 542 nm in chloroform and 470 nm in water). Its maximum emission is 640 nm in lipid vesicles (745 nm in ethanol and 675 nm in chloroform).[46]

During the course of the work for this project, it was deemed beneficial to run through all the stages of the project with a simpler molecule that still bore resemblance to the charge transfer excitation process of the probe. The molecule DMABN (4-(N,N-dimethylamino) benzonitrile) was chosen for this purpose. Similar to the di-8-ANEPPS probe, DMABN also has a conjugated ring that allows the flow of charge during the transition to its excited state. Both molecules also contain a tertiary amino group at the end of the conjugated section, for di-8-ANEPPS two octane chains are bound to the amino nitrogen while for DMABN it

is two methyl groups. Some of the additional factors to consider in the parameterization of DMABN is the fact that it exhibits dual fluorescence and the amino group's degree of twist, which has been investigated as an important component in the absorption and emission transition. The fluorescence from the first excited state is present in all solvents, while the second peak only appears in more polar solvents where it becomes the dominant feature. DMABN has been reported to having absorptions ranging from 281 nm to 291 nm when in solvents ranging from cyclohexane to acetonitrile, with corresponding emissions for its first excited state (LE or locally excited state) ranging from 342 nm to 353 nm. In the same study, emissions for its second excited state (ICT or intramolecular charge transfer state) are not reported for cyclohexane but are as high as 469 nm for acetonitrile.[8] Considering how the LE emission is consistently observable in all solvents, this work focuses on DMABN's transitions between the ground and LE state.

Chapter 2 of this thesis will first look at the solvents chosen for this work and calculate properties such as the dielectric constants of each when modelled with both nonpolarizable and polarizable Drude force fields. Chapter 3 will consider the smaller molecule of DMABN in a series of solvents to show the effect of differing solvent polarity on the fluorescence spectra of its LE state. Chapter 4 will follow much the same protocol as in Chapter 3, however the molecule under investigation is di-8-ANEPPS and the number of solvents considered is slightly increased. Chapter 5 takes the same parameters generated for di-8-ANEPPS in the previous chapter and applies them to a system where the probe molecule is inserted into a DPPC membrane and simulated under conditions of varying membrane potential. And finally, Chapter 6 is the overall conclusion of this study.

CHAPTER 2

PROPERTIES OF PURE SOLVENTS

The activity of fluorescent molecules, such as di-8-ANEPPS and DMABN, is highly dependent on its immediate environment. Thus, in addition to a detailed understanding of the molecule itself, the system into which it is placed needs to be well defined. In experiments, comparison between different solvents and between the responses of a molecule of interest solvated by those solvents is important. Computational models can help parse out what factors affect the results reported by this probe due to the precise control of the environment built in the theoretical space. This is the most direct strategy to validate the force fields generated for the molecules of interest in this study, since several studies exist exploring di-8-ANEPPS in a variety of polar solvents[94,119] and DMABN has also been studied in much the same manner.[8,60,131] Before simulating these molecules in various solvents, pure solvent properties such as heat of vaporization, density and dielectric constant are calculated for the theoretical models. The solvents selected for the present tests, in order of increasing polarity, are: benzene, diethylether, 1,1,1-trichloroethane, 1,1-dichloroethane, acetone, ethanol, methanol, acetonitrile, dimethylsulfoxide, and water. Two additional solvents for the di-8-ANEPPS simulations were included to better compare to available experimental data: chloroform and dichloromethane. All twelve of these solvents are characterized here in this chapter.

2.1 Theory

The heat of vaporization and density are common traits of neat liquids that are used to fit theoretical models and confirm that a given model provides a realistic representation of experiment. Before using these solvents to determine characteristics of other molecules, it is important to confirm that both the nonpolarizable and polarizable Drude parameters used

for these solvents produce reasonable values for these terms. Density was simply calculated as the total mass of the system divided by the ensemble average of the volume over the course of a constant pressure simulation. This is expressed in terms of the number of molecules placed in a system (N_{mol}), the molecular mass of a single solvent molecule (m), Avogadro's number (N_A) and the ensemble averaged volume ($\langle V \rangle$) in Equation 2.1:

$$\rho = \frac{m\, N_{\mathrm{mol}}}{N_A \langle V \rangle} \tag{2.1}$$

The heat of vaporization, the amount of energy required to transform one gram of a liquid into a gas, can be determined by comparing the difference in potential energy of a molecule in gaseous phase and in liquid phase as shown in Equation 2.2,

$$\Delta H_{\mathrm{vap}} = -\frac{\langle U_{\mathrm{liq}} \rangle + p \langle V_{\mathrm{liq}} \rangle}{N_{\mathrm{mol}}} + \langle U_{\mathrm{gas}} \rangle + RT \tag{2.2}$$

where $\langle U_{\mathrm{liq}} \rangle$ is the potential energy ensemble average of a simulated box of solvent, p and $\langle V_{\mathrm{liq}} \rangle$ refer to the constant pressure and ensemble averaged volume of that liquid simulation, N_{mol} is the number of molecules in that liquid simulation, $\langle U_{\mathrm{gas}} \rangle$ is the potential energy of a single molecule in vacuum, R is the gas constant and T is the constant temperature both the liquid and gas simulations were carried out under. The contribution of the $p \langle V_{\mathrm{liq}} \rangle$ term is negligible, meaning that an accurate calculation of the heat of vaporization can be found with the remaining terms after its removal:

$$\Delta H_{\mathrm{vap}} \approx -\frac{\langle U_{\mathrm{liq}} \rangle}{N_{\mathrm{mol}}} + \langle U_{\mathrm{gas}} \rangle + RT \tag{2.3}$$

The dielectric constant is a measure of a solvent's polarity, the higher the dielectric constant the more the solvent is able to insulate and stabilize solute charges. Equation 2.4 shows Kirkwood's formula[86] as derived by Neumann,[132] which directly relates fluctuations in the

total dipole of a system to the overall dielectric.

$$\varepsilon = \varepsilon_{\infty} + \frac{\langle \mathbf{M}^2 \rangle - \langle \mathbf{M} \rangle^2}{3\varepsilon_0 k_{\mathrm{B}} T \langle V \rangle} \tag{2.4}$$

where $\mathbf{M}$ is the total dipole of a configuration, found by summing the xyz components of the molecular dipole moments of each solvent molecule, $\boldsymbol{\mu}_i$, in a given frame of simulation.

$$\mathbf{M} = \sum_i \boldsymbol{\mu}_i \tag{2.5}$$

An ensemble average is taken for the total dipole moment and volume over the course of the simulation. This simulation is performed under constant pressure and temperature, meaning that along with the Boltzmann's constant and vacuum permittivity, the temperature term remains constant. Kirkwood's formula is employed here to calculate the theoretical dielectrics based on the ensemble averages of its dipole. This dielectric constant is the static dielectric constant as it is essentially the response of the system under an electric field at a frequency of zero. Using this equation to calculate the dielectric constants of fluids is well established.[88]

There is a high frequency component, ε_{∞}, referred to as the optical or dynamic dielectric constant, this induced polarization term is equivalent to the square of a solvent's refractive index. The refractive index arises from electron polarizability and is thus a high-frequency term accounting for a more instantaneous change. In a nonpolarizable simulation, there is no electronic polarization occurring when the nuclei do not move, so this term is equal to 1. In the polarizable models the isolated movements of the Drude particle can be considered to be solely electronic. A multitude of additional simulations can be performed at a much lower temperature where only the Drude particles are allowed to move freely, each starting from snapshots taken from the previously performed simulation used to find the static dielectric

constant. Again, the same Kirkwood formula can then be used in the analysis of the results to convert the measured ensemble averaged dipole to a dielectric value. This dynamic dielectric constant term representing the instantaneous electronic relaxation can then be incorporated into the calculation of the static dielectric constant for the polarizable parameters in Equation 2.4.

The change to the static dielectric constant of the polarizable Drude force fields is modest, since instead of just adding a 1 the value added can now range from 1 to 2. Meaning that the updated static dielectric constants of the polarizable Drude force fields will not be drastically different from those found for the nonpolarizable force fields. However, the effect of the dynamic dielectric constant will be most obvious when looking at the values calculated for the orientation polarizability term. Referring back to the representation of a solvent's effect on the spectra of a molecule, orientation polarizability in Equation 1.3 ($\Delta f = \left(\frac{\varepsilon-1}{2\varepsilon+1} - \frac{n^2-1}{2n^2+1}\right)$): for nonpolarizable parameters, the specific contribution from electronic polarization is not accounted for, so the index of refraction is considered to be equal to 1 and causes the right-side term to disappear entirely. For Drude parameters, the dynamic dielectric constant found by considering only the movements of the Drude particles is used directly as the square of the index of refraction.

2.2 Procedure

Initial verification of the solvent properties was carried out to compare the density, heat of vaporization and dielectric constants for both the nonpolarizable and polarizable Drude models to compare to the corresponding experimental values. Each solvent was represented as a box built with Packmol[117] to be 40 x 40 x 40 $Å^3$, where the number of solvent molecules was determined by its experimental density at 298 K. The same box size and number of solvent molecules was used when a molecule of interest is included in Chapters 3 and 4 of this Thesis. The pure solvent boxes were minimized, equilibrated at constant volume for 5

ns, and equilibrated for an additional 5 ns under constant pressure with NAMD.[144]

The average volume of the box during the constant pressure portion of the simulation was then used to compute the density of the solvent. The heat of vaporization was calculated from the average potential energy of the box of pure liquid and the average potential energy of a single molecule of the given solvent in vacuum via Equation 2.3. The single molecule simulation was run for 1 ns at 298 K, the same temperature of the box simulation. The potential energy values were extracted directly from the NAMD output for all systems. The static dielectric properties of the pure solvents were also characterized with the constant pressure liquid box simulation data. CHARMM[16] was used to calculate the dipole of each frame from the simulation, separated into its xyz components. The quadratic fluctuations of the average total dipole, along with the average volume, and temperature, can be converted to the dielectric constant for the solvent based on the Kirkwood formula, stated with Equation 2.4.

In addition to this static dielectric constant, the dynamic (or optical) dielectric constant was found for the polarizable Drude solvent systems. Ten independent simulations starting from random frames of the initial equilibration were run for 10 ps each at a temperature of 10 K where only the Drude particles of the polarizable parameters were allowed to move freely. The average of these ten dielectric constants of a given solvent derived by following the same calculation as for the static dielectric constant from such systems, was designated as the dynamic dielectric constant. Each solvent's static dielectric constant for the polarizable systems was then updated with the dynamic dielectric constant. Then using Equation 1.3, these dielectric constants were then used to find the orientation polarizability for each of the simulated solvents. These computed values for the orientation polarizability of both the nonpolarizable and polarizable Drude solvents will be used in Chapters 3 and 4 when creating the Lippert plots that show the dependence of the spectral properties of the molecules of interest on the orientation polarizability of the solvent.

Experimental data for the heat of vaporization and density of neat liquids was taken from the National Institute For Standards and Technology (NIST) Chemistry WebBook (https://webbook.nist.gov/chemistry). Experimental data for the static dielectric constant and index of refraction of neat liquids was taken from SpringerMaterials Interactive (https://materials.springer.com/).

2.3 Results

The densities for each solvent considered are reported in Table 2.1 from experimental sources as well as those found in this work for the nonpolarizable and polarizable Drude models. Looking first at the nonpolarizable representations of the twelve solvents, the predicted density averaged around a 4% error as compared to experiment, where the closest prediction was for the density of water which had an error of less than one percent. The polarizable Drude model was very similar in these regards, being the most accurate for its approximation of water's density and having a very similar average percent error around 3.5%.

Solvent	Experimental (g/cm^3)	Nonpolarizable (g/cm^3)	Drude (g/cm^3)
Benzene	0.9	0.8	0.9
Diethylether	0.7	0.7	0.7
Chloroform	1.5	1.4	1.8
Trichloroethane	1.3	1.3	1.3
Dichloromethane	1.3	1.2	1.2
Dichloroethane	1.2	1.1	1.1
Acetone	0.8	0.7	0.8
Ethanol	0.8	0.8	0.8
Methanol	0.8	0.7	0.8
Acetonitrile	0.8	0.8	0.8
Dimethylsulfoxide	1.1	1.1	1.1
Water	1.0	1.0	1.0

Table 2.1: Density of pure solvent for both the nonpolarizable and polarizable Drude force fields

The predicted heat of vaporization for each solvent, calculated for the nonpolarizable and polarizable Drude models displayed in Table 2.2, was less accurate as compared to the predicted densities. The nonpolarizable models for benzene and water produce heats of vaporization particularly close to those from experiment. When considering all twelve

solvents, the heats of vaporization calculated for the nonpolarizable model overall has an average percent error of about 5.5%. The polarizable Drude model was particularly accurate with its estimation of water's heat of vaporization, but when considering all twelve solvents a higher average percent error of 9% was found.

Solvent	Experimental (kcal/mol)	Nonpolarizable (kcal/mol)	Drude (kcal/mol)
Benzene	8.1	8.1	9.1
Diethylether	6.5	7.5	7.2
Chloroform	7.6	7.6	9.9
Trichloroethane	7.8	8.3	7.4
Dichloromethane	7.0	7.2	6.3
Dichloroethane	7.3	7.7	7.8
Acetone	7.5	7.9	8.2
Ethanol	10.1	10.5	10.1
Methanol	9.0	9.0	9.2
Acetonitrile	7.9	8.6	8.6
Dimethylsulfoxide	12.5	14.5	14.1
Water	10.5	10.5	10.5

Table 2.2: Heat of vaporization of pure solvent for both the nonpolarizable and polarizable Drude force fields

The static dielectric constants calculated for each solvent with both the nonpolarizable and polarizable force fields are generally in-line with experimental values, as shown in Table 2.3. In almost every case, the polarizable Drude force field dielectric constants are closer to those found in experiment, especially in regards to the differentiation of some of the middling solvents of acetone, ethanol and methanol. Additionally, the polarizable Drude model as compared to the nonpolarizable model has a much more accurate estimation of the two extremes (benzene and water). The solvents are ordered in terms of the increasing dielectric constant reported in experiment, an order which is largely maintained by the polarizable Drude values and is only deviated from with its estimations of the dielectric constant of chloroform being lower than that of diethylether. In contrast, the nonpolarizable model has many instances where the order is not quite in-line with the experimental values.

Although the calculated static dielectric constants for both nonpolarizable and polarizable Drude models are comparable, when converting from the dielectric constant to orien-

Solvent	Experimental	Nonpolarizable	Drude
Benzene	2.3	1.0	2.2
Diethylether	4.2	4.7	4.9
Chloroform	4.8	4.1	3.5
Trichloroethane	7.1	5.2	5.5
Dichloromethane	8.9	8.6	6.4
Dichloroethane	10.1	7.6	8.6
Acetone	20.5	20.0	16.9
Ethanol	24.9	15.3	22.3
Methanol	32.6	25.0	27.8
Acetonitrile	35.7	19.8	39.7
Dimethylsulfoxide	46.8	66.2	58.7
Water	78.4	96.6	82.3

Table 2.3: Static dielectric of pure solvent for both the nonpolarizable and polarizable Drude force fields

tation polarizability (Equation 1.3: $\Delta f = \left(\frac{\varepsilon-1}{2\varepsilon+1} - \frac{n^2-1}{2n^2+1}\right)$), the differences become more pronounced. For the nonpolarizable model the dynamic dielectric constant, ε_∞, is essentially equal to 1. For the polarizable Drude model it can be calculated out by freezing all but the Drude particles, observing the resulting net dipole and converting that to a dielectric constant — in this case the dynamic dielectric constant — which are reported for each solvent in Table 2.4. Each term is pretty close to the expected experimental values, which are determined by squaring a generally accepted value of the refractive index of each solvent. The dynamic dielectric constant was also used in the calculation of the static dielectric constant calculated for the polarizable Drude solvent models that was shown in Table 2.3 resulting in its improved estimation of the static dielectric constant as compared to those found with the nonpolarizable force fields.

This seemingly small difference of incorporating a dynamic dielectric constant whose value is closer to 1.5 or 2 (in contrast to 1) results in a noticeable difference between the estimations of the orientation polarizabilities as calculated by the nonpolarizable and polarizable Drude models. The orientation polarizability of the polarizable Drude data is much closer to experimental results (whose orientation polarizability is derived from accepted values for the experimental solvent's dielectric and index of refraction). All of the orientation polarizabilities for the nonpolarizable model are calculated to be greater than the corre-

Solvent	Experimental	Drude
Benzene	2.3	2.2
Diethylether	1.8	2.0
Chloroform	2.1	1.6
Trichloroethane	2.1	1.4
Dichloromethane	2.0	1.6
Dichloroethane	2.0	1.7
Acetone	1.8	2.1
Ethanol	1.8	1.5
Methanol	2.1	2.1
Acetonitrile	1.8	1.8
Dimethylsulfoxide	2.2	2.7
Water	1.8	1.7

Table 2.4: Dynamic dielectric constant (ε_∞) of pure solvent for the polarizable Drude force field

sponding experimental values, so much so that the nonpolarizable orientation polarizability of diethylether is found to be larger than the experimental orientation polarizability of water. Ultimately the pure solvent dielectrics found for the polarizable Drude force fields is much more in line with accepted values for each respective solvent's constants than those found from the nonpolarizable force fields, as can be seen in a direct comparison in Table 2.5.

Solvent	Experimental	Nonpolarizable	Drude
Benzene	0.0	0.0	0.0
Diethylether	0.2	0.4	0.2
Chloroform	0.1	0.4	0.2
Trichloroethane	0.2	0.4	0.3
Dichloromethane	0.2	0.4	0.2
Dichloroethane	0.2	0.4	0.3
Acetone	0.3	0.5	0.2
Ethanol	0.3	0.5	0.3
Methanol	0.3	0.5	0.3
Acetonitrile	0.3	0.5	0.3
Dimethylsulfoxide	0.3	0.5	0.2
Water	0.3	0.5	0.3

Table 2.5: Orientation polarizability of pure solvent for both the nonpolarizable and polarizable Drude force fields - the dynamic dielectric constant for the nonpolarizable model is considered to be 1

Most of the specific parameters used to characterize each solvent, both nonpolarizable and polarizable Drude, were taken from the Toppar files used in CHARMM-GUI[81] and are thus pretty robust. However, the polarizable Drude versions of acetonitrile and dimethylsulfoxide were not available in that list of parameters. The optimization of these parameters was

accomplished by starting with an estimation from GAAMP[73] followed by an optimized fitting to their respective Lennard-Jones parameters, heat of vaporization and density.[165,166] In the analysis of di-8-ANEPPS in solvents, two additional solvents were included to more directly compare to the available experimental papers: chloroform and dichloromethane (necessitating both of them being included in this solvent dielectric calculation procedure to determine the dielectric constants of both represented with nonpolarizable and polarizable Drude force fields). Similarly to acetonitrile and dimethylsulfoxide, an initial version of the parameters for these two solvents was first generated with GAAMP[73] and, for the Drude force fields, have the same optimization of the Lennard-Jones parameters performed as described above.[165,166]

It is important to note that, even for the accepted values for the dielectric and orientation polarizability of these solvents, the order of the solvents in terms of the dielectric constants do not necessarily match the order in terms of orientation polarizabilities. However, the trends are generally consistent with the increasing dielectric constant of the solvent as they are with increasing orientation polarizability. For consistency, all solvent effects are listed in order of increasing dielectric constant of solvents derived from experiment, both in this chapter and subsequent chapters. This is despite the fact that this order is not quite the same as for the experimental orientation polarizability and is also somewhat different from the orders of constants calculated for the nonpolarizable and polarizable Drude models.

CHAPTER 3

SIMULATING THE ABSORPTION AND FLUORESCENCE OF DMABN IN DIFFERENT SOLVENTS

3.1 Introduction

Luminescent probes that are highly sensitive to their environment allow for the tracking of changes to polarity, ion concentration and other factors. DMABN (4-(N,N-dimethylamino) benzonitrile) is a valuable probe for this purpose due to the large change in polarity between its ground and excited states, the exact magnitude of which is dependent on its surroundings. DMABN is a small molecule composed of a benzene ring with a nitrile group on one end and an amino group bonded to two methyls at the other end. The most intriguing characteristic of DMABN is that it exhibits dual fluorescence. Two different emission energies with somewhat overlapping spectra can be monitored, allowing for better characterization of the system. The first excited state is called the locally excited (LE) state and is characterized by a movement of charge over the conjugated ring structure. In nonpolar solvents and in the gas phase, the fluorescence of DMABN is entirely attributed to the transition from the LE state. In more polar environments, emission occurs from both the LE and the second excited state: an intramolecular charge-transfer (ICT) state.

Since its discovery, DMABN has been investigated with a variety of different tools to determine the exact mechanism of its excitation and emission with the intention of then using the small molecule as a versatile probe of multiple characteristics of a system. Not only can its dual fluorescence provide two wavelengths whose relative intensity can be measured as a function of environmental changes shifts such as in polarity, but the physical characteristics a surrounding system can dictate to what extent each excited state is favored and be monitored as well. DMABN has already been shown to be useful as a probe of the molecular weight of polymers because its fluorescence is affected by its restricted geometry

due to the size of the cavity it occupies amongst a polymer matrix.[2,3] Other applications of the probe include determining the critical micelle concentration of a surfactant,[105] detecting dissolved organic matter concentrations based on the variance of the phototransformation rate constant of DMABN,[101] and investigating solvation structure and dynamics of ionic liquids like imidazolium with the time-resolved infrared spectroscopy of DMABN.[6]

The geometry of DMABN in its excited states is still somewhat contentious, almost entirely surrounding the position of the amino group (specifically to what degree it is twisted and whether or not it is wagging out of the plane of the aromatic ring). The ground state is generally accepted to be consistently flat in the plane. And while there exists evidence that supports the LE state as being flat as well,[22,50,142,171] it has also been reported to exhibit a slight angle of its amino group.[116,150] In contrast, the ICT state is commonly associated with a much greater twist of that amino group. Additionally, a consensus on the exact interconversion mechanism between the two excited states has not been reached. The prevailing model is based on femtosecond stimulated Raman spectroscopy studies that elucidated an initial relaxation of the LE state in about a third of a picosecond, followed by a rapid internal conversion between the LE and ICT state occurring within 2 picoseconds, and finally vibrational relaxation of the ICT state that occurs over the course of 6 picoseconds involving twisting of the amino group and other geometry changes.[153,154]

However, the scope of this paper is to investigate solely the LE state and observe its sensitivity to the polarity of a solvent environment. Computationally investigating its properties allows for the total isolation of this excited peak from the ICT state. Though the ICT state is dominant, particularly in more polar environments, its fluorescence is not observed in every situation. The transition to and from the LE state is ever-present, even in systems where the fluorescence peak of the ICT state partially overlaps it, and thus cannot be ignored when modeling the dual fluorescence of DMABN. The ability of the LE state of DMABN to capture the electrostatics of its immediate environment as the probe molecule

is considered in a series of solvents with varying polarity. The ground state force fields were prepared via GAAMP (General Automated Atomic Model Parameterization).[73] After performing CASSCF calculations to isolate the electrostatic potential properties of the LE state, separate parameters are generated with GAAMP's charge fitting procedure to represent just the LE state, allowing for it to be directly simulated with molecular dynamics.

The conversion between the ground and the LE state are performed by switching between force field files imitating the comparably instantaneous electronic transition, and then simulating the subsequent relaxation on the new potential energy surface. Absorption and emission wavelengths (found by comparing the energies calculated with the force fields of the two states for a given snapshot of simulation) were measured in systems of different solvents and used to display the sensitivity of the LE state to the surrounding solvent polarity. Taking the difference between these wavelengths gave a Stokes shift which, when graphed against the orientation polarizability of the given solvent, increases with the increasing polarity of the solvent. The absorption and emission steps are entirely to and from the LE state, removing the complication added by the possibility of transforming into the ICT state and fluorescing from that instead. Simulations were performed with both nonpolarizable and polarizable Drude force fields. Polarizable force fields that include Drude particles are shown to be more sensitive in modeling the molecule, resulting in a more accurate representation of the energy differences calculated from the transition.

3.2 Theory

3.2.1 Molecular Characteristics of DMABN

DMABN (shown in Figure 3.1) has a conjugated section, with two nitrogen on either end of this active site and is overall rigid. Some characteristics that must be considered carefully are related to the fact that the amino group is known to have different optimized twist angles

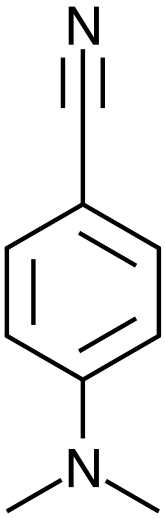

Figure 3.1: The structure of DMABN (4-(N,N-dimethylamino)benzonitrile)

for the ground and excited states and that the molecule has two main excited states that both contribute to the observed fluorescence. The existence of these two energetically similar excited states result in an observable dual fluorescence, making it an popular molecule to study since the discovery of this rare characteristic.[107,108] The states, the LE (locally excited) and the ICT (intramolecular charge transfer), produce overlapping peaks of varying intensity based on the polarity of the environment. Under more nonpolarizable conditions the LE state dominates, the excitation is entirely the result of reaching and emitting from the LE state. In more polar solvents a second peak, corresponding to the ICT state, appears and partially overlaps the LE emission spectra. As the surroundings' polarity is increased the peak of the ICT state becomes more prominent until it ultimately dominates the fluorescence spectra.

Experimentally it can be difficult to differentiate the two excited states, especially in more polar solvents, but theoretically the contribution of the LE state can be easily isolated. Many studies have been performed to investigate the specific mechanism of the fluorescence cycle, especially in regards to the interconversion between excited states.[151,152,196] The ICT state is commonly associated with a significant change in the angle of the amino group,

facilitating the favoring of its conformation over that of the LE state, referred to as the TICT (twisted internal charge transfer) state.[162] In addition to the amino twisting along its bond with respect to the rest of the molecule, there are also studies that investigate a wagging motion of the amino up or down out of the plane of the conjugated ring.[171] These changes in geometry are certainly favored by the ICT state, but can still occur while the molecule is in its LE state, likely facilitating interconversion. The parameterization of the LE state should involve particular consideration of this geometry feature.

Due to it primarily being the result of local excitation of the benzyl ring, the LE state has been depicted as being much more similar to the ground state: either perfectly planar or with a less extreme twist of the amino substituent, having a low oscillator strength especially in comparison to the ICT state. Several experimental studies support the planar LE state by IR spectroscopy[22] and rotational contour analysis,[142] as well as semi-empirical[50] and CASSCF calculations.[171] Though there does exist contrasting evidence of the ideal configuration actually being with a twist of the amino group with respect to the conjugated structure of 22° or more.[116] A TDDFT study yielded a pretty flat energy profile of this angle with a slight minimum at 32.5°.[150] Since in comparison to the ICT state the LE state does not involve any major conformational changes and the LE state is expected to fluoresce in each of the solvents selected for this study, it was selected as the state whose transitions would be investigated as the model system for the eventual investigation of di-8-ANEPPS. Additional steps were taken to find the optimal twist of the ground and LE state of DMABN to be reflected in the produced parameter sets, but largely the geometry optimization remained the same during a transition.

The observed optical spectrum of a molecule is affected by a number of factors, including non-radiative QM relaxation associated with the coupling between the electronic transition and the nuclear motions.[45,79,134,184] Differences in the molecular geometry at the energy minimum as well as the curvature of the potential energy surface between the ground and

excited states give rise to an internal reorganization energy, yielding a difference between the absorption and emission frequency that is on the order of about 2,000 cm^{-1}. For the sake of simplicity, these effects in the present work will be subsumed into environment-independent empirical offset constants for the excitation and emission.[198,200] Because of the QM factors affecting the absorption and emission process, two empirical energy offset constants expected to differ by about 5 kcal/mol are needed to model a given fluorescent molecule. Accounting for all QM effects is certainly essential for a complete and accurate simulation of optical spectra, but since the focus of this work is a characterization of the influence of the molecular environment on the excitation and emission wavelengths, the present simplification is justified.

The energies extracted in this study are vertical transitions, based on the Franck-Condon principle[33,34,48] that allows for the separation of the electronic transition from any movement of the nuclei due to a difference in timescale. In addition to this change, the molecule undergoes intramolecular transitions between its vibrational states immediately after the vertical transition. The offset constants that are derived empirically based on the fitting of the energy differences to experimental reports of absorption and emission of DMABN in a given solvent include the contribution to the overall transition energy from these non-radiative quantum mechanical transitions. Computational means of determining vibrational states generally rely on a Taylor expansion, either of both states' potential energy surfaces or of just the initial potential energy surface and determining the final potential energy surface from properties of the initial state (including the vertical transition energy).[45] Since the focus of the work presented here is not on elucidating these essential quantum mechanical effects, rather it is to investigate the effects of the surrounding environment on the excitation and emission of a molecule, an empirical constant is employed to account for its contribution to the transition energy.

3.2.2 Energy Calculations

After adding the offset constant, energy differences between the excited state and ground state can be converted to the wavelengths for the absorption and emission transitions. The difference between the emission and absorption, referred to as the Stokes Shift, can then be graphed against the orientation polarizability to form a Lippert plot which illustrates the overall linear relationship between the two. In order to get these energy differences, each system is simulated for an extended period of time when the molecule of interest is associated with either its ground or excited set of parameters. The ground state equilibration can be used to produce any number of examples of the ground state molecule in an optimized state. For each of these frames the energy at the ground state and the excited state can be calculated by independently considering the snapshot with either the ground or excited parameters of the molecule of interest. Parameters for the surrounding solvent are not changed regardless of which state the molecule of interest is currently in. If the source of the snapshot is the ground state, the difference between the two energies found from these two parameter sets represents the instantaneous electronic absorption from ground to excited state. Similarly, the excited state equilibration frames can be used to find the instantaneous electronic emission. The rest of the process of either absorption or emission is the intramolecular and intermolecular reorganization in response to the sudden shift caused by changing between the ground and excited force fields, and can be simulated by continuing to run molecular dynamics simulations with the second set of parameters after the force fields are switched.

The total energy of the system, the isolated energy of just the molecule of interest and the energy from the interaction between the molecule and its surroundings is calculated for each considered snapshot from simulation. The isolated energy of just the molecule of interest was found by first extracting the coordinates of the molecule and calculating the energy when the surrounding solvent is no longer present. The interaction energy is the

difference between the total energy and the energy of the isolated molecule of interest. For the polarizable Drude model there is an additional complication due to the presence of Drude particles. The general procedure depends on the separation of the instantaneous electronic transition (modelled by switching parameter sets) and the slower geometry relaxation that follows it. Drude particles are a theoretical construct that contain part of the charge from their respective heavy atoms and are also updated by a parameter set switch in terms of the literal partial charge and polarizability. But simply changing the parameter file does not allow for the Drude particles to move to their ideal position, a movement that should be considered part of the electronic transition rather than an atomic change. Without allowing this update, the perceived energy differences for the immediate transition are drastically affected. Minimizing the position of the Drude particles effectively recovers the correct SCF energy. So, for the systems that are built with polarizable Drude model, each energy calculation needs to first involve a minimization of the Drude particle positions. Summarily the energy differences of a given snapshot from a polarizable Drude simulation are between the excited state energy after minimizing the position of the Drude particles with the excited state parameters and the ground state energy after minimizing the position of the Drude particles with the ground state parameters.

These energy differences extracted from classical MD simulation only consider the effect of the environment on the electronic transition and thus cannot be converted directly to wavelengths, instead they need to be corrected with an offset value. This offset is informed by the difference between the energy reported for the molecule of interest in vacuum from molecular dynamic simulations and quantum dynamics from CASSCF calculations. It is an empirical value that accounts for intramolecular changes that occur during the conversion between the ground and excited state, including geometrical differences and vibrational transitions, that are not accounted for directly in the calculation. For a given molecule of interest and a given parameter set (either ground or excited, nonpolarizable or polarizable

Drude), each of its energy terms is modified with the same offset. Each force field model of DMABN has two offset constants, added to energies from ground and excited states simulations. The exact values of these offsets are determined by fitting the energies directly with the available experimental data for the solvents it has in common with those considered in this study.

Although the ground and excited state of a molecule can experience the same vibrational transitions, the energies and oscillation frequencies associated with those movements is not the same. The process of exciting an electron to a higher orbital introduces a greater degree of antibonding character resulting in equilibrium positions being looser (such as longer bond lengths) and different force constants restricting the motion to that equilibrium position. Excitation occurs when there is a great deal of overlap between the vibrational ground state wavefunction and that of the excited state. From there the vibrational transitions to the lowest energy excited state result in a different wavefunction that will allow for an emission to the ground state vibrational state it most resembles.[7] Because there are differences in the transitions between vibrational states within either the ground or excited state, a given offset is either accounting for energy contributions from the transition from higher excited vibrational states to the energetically lowest vibrational state of the excited state or vibrational transitions within the ground state. Thus, the exact values for the absorption and emission transition for the same molecule of interest will be different. As an example, the DMABN polarizable Drude absorption and DMABN polarizable Drude emission offsets should be similar but not identical. These offset terms incorporate the added energy changes that result from intramolecular quantum mechanics transitions into the total energy transition calculated as an effect of the surrounding environment.

3.3 Methods

3.3.1 Parameterization of DMABN

The parameterization of DMABN was largely accomplished with the help of GAAMP (General Automated Atomic Model Parameterization).[73] This program is designed to improve upon an initial guess from CGenFF (CHARMM General Force Field)[186] or GAFF (general Amber force field)[190] for small molecules with additional calculations of the electrostatic potential of the overall molecule, optimizing of the more mobile dihedral angles and calculating the effect of placing water molecules near potential hydrogen bond donors and acceptors. GAAMP was used in its entirety to create the ground state parameters for DMABN, using its default settings and fitting its initial values to the results of a CGenFF guess of its partial charges. Each step optimizing its geometry was performed with HF/6-31G* except for the electrostatic potential calculations when applying Drude particles (which used B3LYP/aug-cc-pVDZ). Both nonpolarizable and Drude force fields were generated in this manner for DMABN in its ground state. GAAMP has the limitation that its initial guess for partial charges and protocol for calculating the electrostatic potential of a molecule is based on it being in its ground state, meaning that there is no way to directly use this tool to generate excited state parameters.

In order to isolate the excited state of DMABN, ORCA[128,129] was implemented to perform CASSCF calculations. First the orbitals of the ground state are generated and observed with a simple BP86 def2-SVPD def2/J calculation. This step includes a geometry optimization, which showed a preference for the conjugated ring of DMABN being flat and the amino substituent to sit flat in the same plane. Since the molecular coordinates are set so that the molecule sits in the $X - Y$ plane with little to no atomic protrusions along the z-axis, the pz orbitals that have significant occupancy are the ones that are most likely to be important in any transition (particularly those that correspond to the conjugated ring). The

majority of the important occupancies resemble the typical patterns for benzene orbitals, since DMABN is essentially a benzene ring with substituents, making the recognition of these orbitals simpler. After ensuring that the ground state can be easily analyzed by itself, the first CASSCF calculation that considers the interactions of equally weighted states can be performed (called SA-CASSCF or state-averaged CASSCF). For the molecule DMABN there are 12 electrons and 11 orbitals in its complete active space, however it has been shown in computational studies that a CAS(6,7) (in which 6 electrons and 7 orbitals are considered in the active space) is sufficient.[195] This reduced active space size will be used for this and proceeding steps to save computation time. Additionally the orbital set reached by the CAS(6,7) study reported by Xu et al. was used to aid in the process of recognizing and rotating in the necessary orbitals to the active space.

During the state-averaged CASSCF step, many excited states are weighted equally along with the ground state in a def2-SVP def2-SVP/C calculation. Once again, the orbitals that can be extracted and visualized from this step can be used to help steer the following steps. Within the active space should be orbitals that are expected to play a role in the excitation in general, which in this case are ones with significant pz character around the conjugated ring. The next step involves isolating the state of interest from the output of the series of equally averaged states. Once the weight is entirely upon the state of interest (in this case the first excited singlet state), the results of the calculation entirely reflect that state. Additional runs of this calculation with various convergence criteria, such as orbstep SuperCi and switchstep DIIS, are used to reach a final conclusion that contains all of the expected orbitals in the active space that match other work with DMABN considered with CASSCF.[195] During the process, each output's active orbitals are visualized and switched out with orbitals that better match the expected set should the need arise. The final selection of orbitals in the active space for the excitation of DMABN are shown in Figure 3.2.

Once the set of active orbitals was settled upon, matching the set described by Xu et

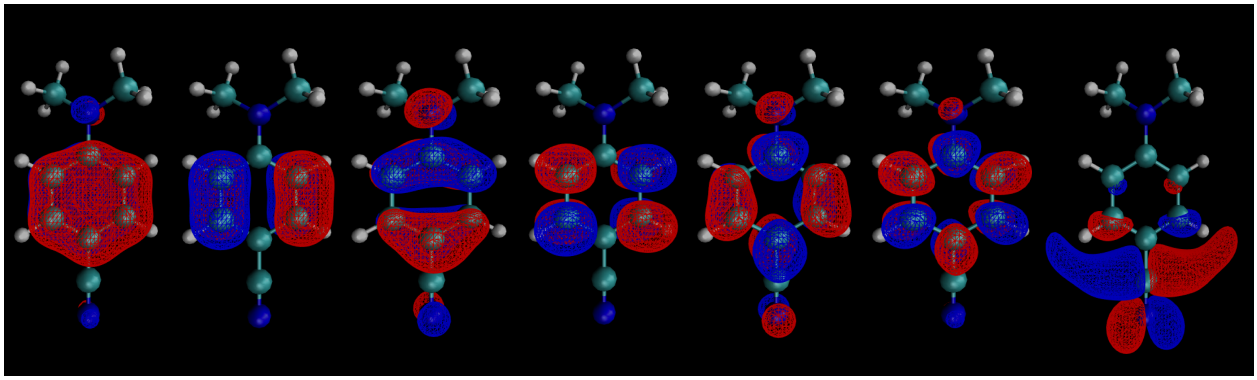

Figure 3.2: Active orbitals of the excitation of DMABN - converged to through CASSCF calculations

al.,[195] the electrostatic potential was determined for a large number of positions surrounding the excited molecule with CASSCF ab initio calculations. This was then used as the target data in the ESP charge fitting protocol utilized in GAAMP, producing the partial charge force field data. The output from the converged initial electronic transition step of the CASSCF calculations that produces the Franck-Condon excited state was used in conjunction with the GAAMP charge fitting procedure to create a parameter set with new partial charges for the atoms that does not directly update the geometrical parameters. Only the steps of GAAMP that involved the electrostatic potential were implemented (since the geometry of the DMABN molecule is initially considered to not change significantly for the transition to the first excited state). In other words, the excited state partial charges were fit to a flat structure geometry consistent with its ground state. These GAAMP steps specifically were fitting the electrostatic potential data and performing additional fitting with test water molecules should hydrogen bond donors or acceptors be identified. These steps had to be somewhat modified to read in the results of the CASSCF calculations for the excited state as a starting point, and some additional changes were implemented when creating the excited set of polarizable Drude parameters. In this step, discrete calculations are performed for sixty-six systems of DMABN and a perturbing point charge placed in different positions in its vicinity.

The dipoles of the ground and the first excited singlet found by Xu et al, calculated

with CASSCF (6, 7) at with a 6-311G* basis set, were 6.41 and 6.25 Debye respectively.[195] Another study using CASPT2 calculated dipoles of 7.36 Debye for the ground state and 7.58 Debye for the LE state.[171] Both of these works found the difference in dipole to only be about 0.2 Debye. The result of this study's CASSCF step also found a difference in dipole between the two states of about 0.2 Debye: 6.815 and 6.665 Debye for the ground and the LE state. After creating the parameter files, the dipole of the isolated DMABN molecule in each snapshot of the molecule simulated in solvent was determined as well. The dipole for the ground state nonpolarizable parameters was found to be 7.53 Debye and for the ground state polarizable Drude parameters it was found to be 8.81 Debye. The excited state was built based on the CASSCF data and thus reflects the similar but slightly smaller LE state dipole. The dipole for the excited state nonpolarizable parameters was 6.78 Debye and for the excited state polarizable Drude parameters: 6.04 Debye. Despite the similar dipoles found via CASSCF, the work of Jamorski et al. show that the values of the dipoles heavily depend on the method used to calculate it.[78] This is true even experimentally: a range of 5-7 Debye for the ground state and 6-11 Debye for the LE state is generally accepted.[78,195] The dipoles of the models used in this study are based on fitting to the ESP data from the initial CASSCF calculations, which was consistent with aforementioned CAS(6,7) study of DMABN.[195]

Considering the Lippert approximation of the fluorescing molecule being a spherical cavity with shifting dipoles, this study also focuses on changes in the electrostatics rather than any geometry changes within the molecule. So far the parameterization has not accounted for any geometry difference between the ground and excited state, however there is a characteristic of DMABN that should be directly addressed. As was mentioned before, the only geometrical feature known to shift between the ground and excited state is the twist angle of the amino group. A dihedral scan was performed with ORCA for every ten-degree rotation of the amino substituent with respect to the conjugated ring. This revealed the optimum

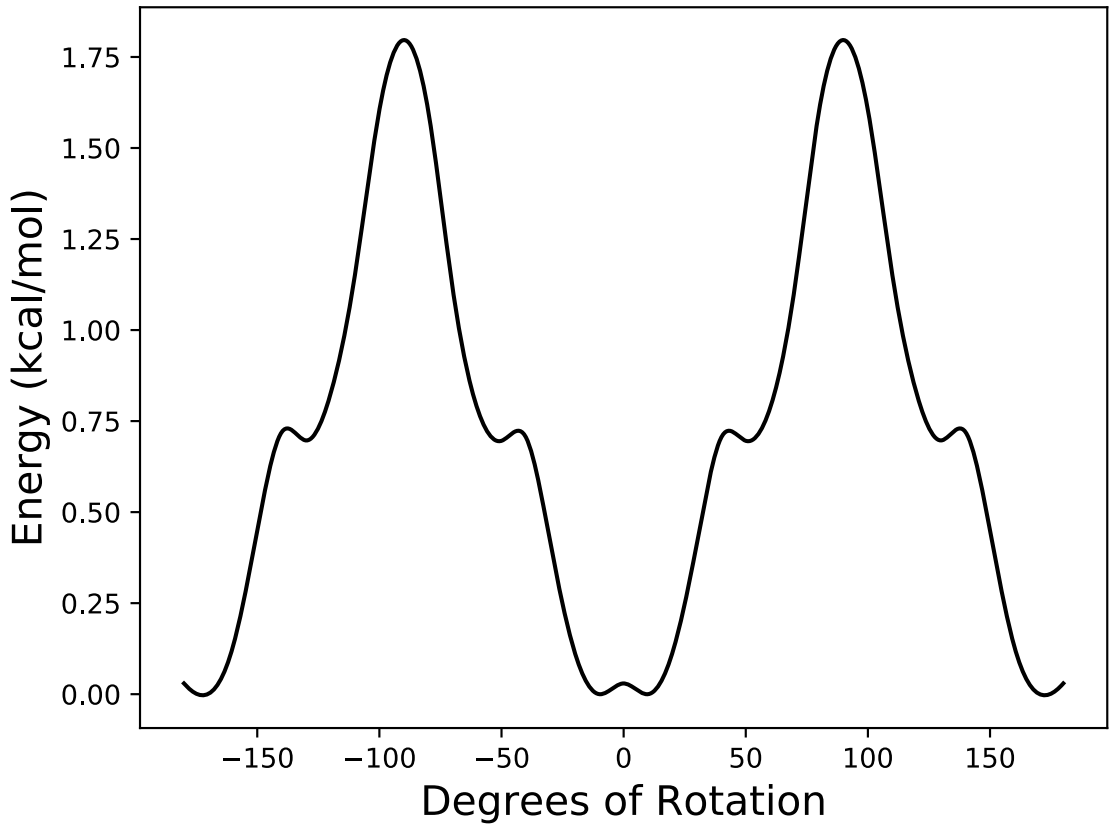

Figure 3.3: Dihedral scan of the ground state of DMABN - the selected dihedral is across the bond connecting the amino group to the conjugated ring

degree of twist for the two states of interest which was then directly compared with short simulations, performed with NAMD,[144] of the molecule locked in those configurations to confirm. For the ground state the optimal angle did indeed center around zero, favoring a conformation where the amino group doesn't twist more than about 10° and strongly resisting a twist of 50° or more. The excited state on the other hand showed a local minima around zero, with wells at around 10°, as well as another minimum at closer to 50°. These dihedral scans are included in Figure 3.3 for the ground state and Figure 3.4 for the excited state. Some manual manipulation of the dihedral parameters in both the nonpolarizable and polarizable Drude force fields was performed to better reflect these QM dihedral scans. All

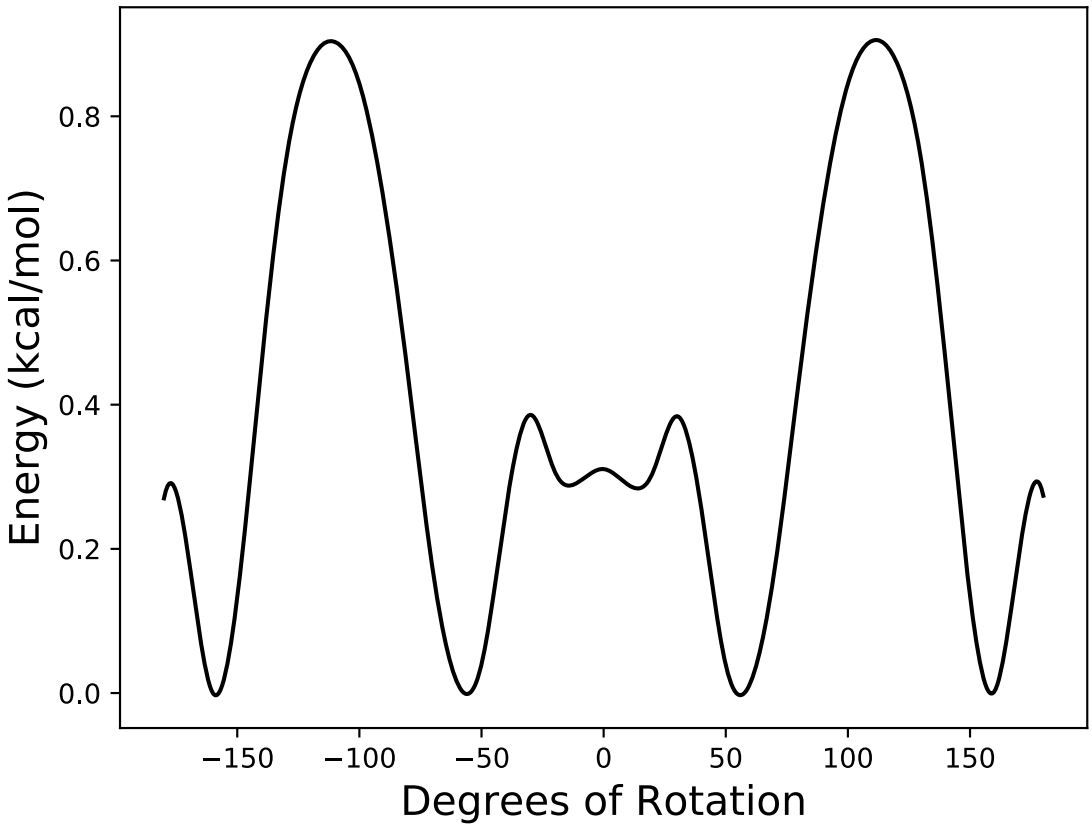

Figure 3.4: Dihedral scan of the excited state of DMABN - the selected dihedral is across the bond connecting the amino group to the conjugated ring

of this was to ensure that the MD simulations reproduce the characteristics revealed by the initial ORCA CASSCF isolation of the ground and LE states. Regardless the overall goal is to capture the electrostatics of the environment in terms of the shift in the dipole of the probe molecule and the reorientation of the dipoles of the surrounding solvent (as described in the assumptions of the Lippert-Mataga equation, Equation 1.2). Any energy difference between the ground and excited of DMABN due to their differing geometries will be accounted for in the added offset constants along with contributions from vibrational transitions.

3.3.2 Simulations in Solvent

Each solvated molecule system was prepared in the same way as the pure solvent boxes described in Chapter 2, with the same number of solvent molecules calculated before based on the respective solvents' experimental density. Packmol[117] was utilized in generating the initial starting positions of DMABN in each solvent 40 x 40 x 40 $Å^3$ cube. A wide range of solvents was used: benzene, diethylether, 1,1,1-trichloroethane, 1,1-dichloroethane, acetone, ethanol, methanol, acetonitrile, dimethylsulfoxide, and water. The bulk of their respective topology and parameter files for both the nonpolarizable and polarizable Drude force fields were taken from the CHARMM-GUI toppar files,[81] the exceptions are discussed in Chapter 2 of this Thesis. NAMD[144] was used to run 5 ns simulations at 298 K under constant volume simulations of each DMABN-solvent system using the force fields created for DMABN's ground state. Each of these runs was then repeated with the same settings, except that the DMABN force fields were switched with those of its excited state. Ultimately two sets of ground and excited force fields were prepared for DMABN, one that is nonpolarizable and another that is polarizable by incorporating in Drude particles. Since ten different solvents were investigated with either the ground or excited state of DMABN included, this means that twenty independent nonpolarizable simulations and twenty independent polarizable simulations were run.

A series of snapshots extracted from the trajectory of each of these simulations were analyzed with CHARMM[16] to calculate the energy of the system in the case where the parameters being read in are either for the ground state or for the excited state of DMABN. The parameters of the solvent are the same regardless of what state DMABN is currently considered to be. For simulations of the ground state of DMABN in a given solvent, energies are determined for every snapshot extracted using the ground state parameters of DMABN and using the excited state parameters of DMABN. The difference in energies for each ground state simulation snapshot shows the absorption or excitation energy (the instantaneous en-

ergy change between states before any rotations or relaxations can take place). Likewise, the difference between the energies calculated from snapshots of excited state simulations shows the emission.

The energies extracted for each parameter set are the total energy of the system as well as the energy of just the molecule of interest in whatever conformation it has reached while in the solvent simulation. This was accomplished by creating a separate coordinate file containing only the DMABN molecule from each snapshot and finding the energy difference when considering the ground or excited state parameters. The total energy differences calculated are the result of the sum of many intermolecular and intramolecular interactions of the solvent and DMABN. Subtracting the isolated DMABN energy difference from the total energy difference results in a value for the interaction energy between DMABN and the surrounding solvent. Each ground energy is subtracted from its respective excited energy to get the energies of transition for the total system, for the isolated molecule of interest and for the interaction energy between them. Every energy term is reported as an average of all the frames of simulation considered, along with a standard deviation of those values. The polarizable systems include the added complication of the Drude particles tethered to each heavy atom. Taking the instantaneous energy values for a given snapshot of the polarizable Drude simulation using the two separate parameter files for the ground and excited state respectively is not meaningful. Instead the given snapshot first has the positions of its Drude particles minimized with ground or excited parameters separately and those resulting energies are used in calculating the energy gap.

Each transition energy was then corrected with the offset energy to better match the precise values seen from experimental results. All absorption energies for a given molecule of interest modelled with a given parameter set have the same offset constant added (and a different, similar offset is added to all emission energies). The approximate value of this offset can be seen by comparing the transition energy found via QM methods to the difference in

energy reported by the ground and excited molecule independently analyzed in simulated vacuum. The exact value of the offsets was determined empirically by direct comparison of the energies obtained to those reported in experimental studies. In practice, the process of finding the specific offsets required a chi-square minimization of the energy terms calculated in this study to the results seen in experimental studies involving the same solute-solvent combinations.

The average energy gaps are then converted into the absorption wavelengths, emission wavelengths and Stokes Shift (the difference between the emission and absorption wavelengths). Graphing the Stokes Shift versus the orientation polarizability creates a Lippert plot, which shows the general linear trend of an increasing difference between the absorption and emission wavelengths of the molecule of interest as the dielectric of the solvent increases. In Equation 1.3 ($\Delta f = \left(\frac{\varepsilon-1}{2\varepsilon+1} - \frac{n^2-1}{2n^2+1}\right)$), it can be seen that the calculation of the orientation polarizability term is based on the solvent dielectric and index of refraction. For the polarizable Drude parameters set, the dielectric constant calculated from the pure solvent box simulations and index of refraction (equal to the square root of the dynamic dielectric constant) was used directly to find the orientation polarizability. It is important to note that the nonpolarizable model of pure solvent assumes the dynamic dielectric constant (and thus also the index of refraction) to be equal to 1 in all cases. When used directly to find the orientation polarizability, the results of the nonpolarizable model are noticeably shifted as compared to the experimental and polarizable Drude orientation polarizability when all graphed together. Each of these constants for the solvents selected for this work was determined for both the nonpolarizable and polarizable Drude models in Chapter 2 of this Thesis.

3.4 Results

For both the nonpolarizable and polarizable Drude data, a range of energy values for each DMABN-solvent combination is averaged and reported with their respective standard deviation and error (calculated via the block average method). The energies tabulated include the total energy difference of the system, the energy difference of the isolated DMABN and the energy difference of the interaction between the solvent and DMABN. This data is also represented as a series of histograms of the three energy differences in each of the considered solvents. Finally, the Stokes shift of DMABN in each solvent is graphed against the orientation polarizability of the solvent to produce two Lippert plots, one for the nonpolarizable force fields and one for the polarizable Drude force fields. For both parameter sets, the Stokes shift increased with the increasing polarizability of the solvent that surrounded the DMABN molecule. The results do not produce a perfectly linear progression, due to factors like the specific interactions between DMABN and the solvent molecules. In the case where the DMABN is in a theoretical series of the same solvent where the polarity is artificially altered, the resulting Stokes shifts would align more perfectly. The nonpolarizable and polarizable Drude results will be discussed separately before comparing them directly together. Additionally, the relaxation of the total energy of DMABN in a small subset of the solvents immediately after excitation is graphed to directly model that part of the fluorescence cycle. This was performed with both the nonpolarizable and polarizable Drude force fields allowing for the drop in energy as a function of time to be compared between the two models.

DMABN has been studied by others in a variety of different solvents, often displaying their results as overlapping spectra to show the shift in the maximum intensity of its absorption and emission. These results are not identical between studies, but do allow for the observation of general trends. There are even exceptions where the general positive trend matching increasing dielectric with increasing wavelengths is not followed by a given solvent. DMABN dissolved in hexane, diethylether and acetonitrile has results in a dielectric range of 1.88

to 35.688 according to Neubaur et al.'s results, which show an increase in the wavelengths of both the absorption and emission as the dielectric increases over this range.[131] Atsbeha et al. investigated the LE state of DMABN in cyclohexane, dioxane, dichloromethane and acetonitrile, which is approximately the same dielectric range. The absorption maximum wavelength mostly follows the same trend, but they show DMABN in dichloromethane to have the largest wavelength despite not having the highest dielectric. Their emission data starts with the lowest wavelength matching with DMABN in the lowest dielectric but the rest of the values essentially plateau instead of steadily increase.[8] The data reported by Haidekker et al. includes emission wavelengths of DMABN in benzene, ethylene glycol, glycerol and dimethylsulfoxide, which generally increase with dielectric, but DMABN in dimethylsulfoxide was found to have a smaller emission wavelength than it does in glycerol.[60] In summary, the general trends appear to be increases in wavelength with increasing dielectrics for both the absorption and emission, though there is definitely some ambiguity as to exactly how a specific solvent will behave and whether or not it properly follows that trend.

3.4.1 Nonpolarizable Solvent Models

In order to create the electrostatic potential data that was then fed into GAAMP to create the excited state parameters, DMABN's transition between ground and excited state was calculated with CASSCF. The energy difference between these states was found to be 106.74 kcal/mol. There are slight variations on this energy, based on exactly which basis set was used for the calculation and the exact geometry of DMABN, but all of these results were within about 3 kcal/mol of that value. When using NAMD[144] to analyze the flat optimized structure in vacuum, the energy difference of the excited state minus the ground state as represented by the nonpolarizable force field was found to be -4.84 kcal/mol. If the DMABN in vacuum is allowed to equilibrate, the average energy difference is closer to -5.47 kcal/mol. The offset term should be approximately equal to the difference between these energies calculated

by CASSCF and with the nonpolarizable force fields, meaning that each energy from the DMABN-solvent simulations needs to be corrected with about 100 kcal/mol. The exact value used for the correction was based on fitting the data closer to what was reported from experiment. Specifically the absorption and emission data for benzene, diethylether, ethanol, acetonitrile, dimethylsulfoxide and water from experimental studies[8,51,60,87,131,137,170] was fit directly with the corresponding data from this study. The offsets settled on were 102.569 kcal/mol for the absorption and 85.022 kcal/mol for the emission.

Each frame taken from the MD simulation was independently analyzed to determine the total energy of system in the case where DMABN was in its ground state and its excited state. Although the ground state is generally accepted to be entirely planar, after simulation in the solvents there would naturally be some twisting of the amino group and fluctuations in the other angles. This can be seen directly in the tabulated standard deviations of the energy differences of the isolated DMABN molecule. These slight variations in DMABN itself and in the specific interactions of the solvent with DMABN resulted in a range of reported energy differences, necessitating the average energies for each DMABN-solvent combination being used in analysis. These absorption energy averages, standard deviations and error values of DMABN in each solvent modelled with nonpolarizable force fields are given in Table 3.1. Three different absorption energies are reported: the overall energy of the total system, the energy of just DMABN isolated from its surroundings and the difference between these two energies which corresponds to the interaction between DMABN and the solvent.

The range of the total absorption energy was found to be approximately 4 kcal/mol from benzene to water, which corresponds to a range of about 12 nm. Although reported absorption is sparse in comparison to emission data, one example of absorption shifts in different solvents from Neubauer et al. shows a range of about 12 nm but from hexane to acetonitrile.[131] Another source reports a change of about 10 nm in the absorption wavelength of DMABN in cyclohexane as compared to in acetonitrile.[8] For a more direct comparison to

Solvent	All	stddev	error	DMABN	stddev	error	Interaction	stddev	error
Benzene	98.9	0.9	0.0	97.3	0.4	0.0	1.6	0.8	0.0
Diethylether	99.1	1.0	0.1	97.2	0.4	0.0	1.8	1.0	0.1
Trichloroethane	98.3	0.8	0.0	97.2	0.4	0.0	1.1	0.6	0.0
Dichloroethane	99.6	1.0	0.1	97.2	0.4	0.0	2.3	0.9	0.1
Acetone	100.3	1.3	0.1	97.2	0.4	0.0	3.1	1.2	0.0
Ethanol	100.2	1.4	0.1	97.2	0.4	0.0	3.1	1.4	0.1
Methanol	101.5	1.5	0.1	97.2	0.4	0.0	3.9	1.4	0.1
Acetonitrile	100.3	1.2	0.0	97.3	0.4	0.0	3.2	1.1	0.0
Dimethylsulfoxide	101.8	1.4	0.1	97.3	0.4	0.0	4.3	1.3	0.1
Water	103.2	1.7	0.0	97.3	0.4	0.0	5.7	1.6	0.0

Table 3.1: Absorption energy of DMABN in solvent using nonpolarizable force fields - energies include added offset

that study, the range of the data from this study from benzene to just acetonitrile is only about 4.5 nm. It is clear that the nonpolarizable data for DMABN understates the effect of an increased dielectric on the absorption activity of DMABN. Additionally the overall trend of the absorption data is backwards, the data from this study shows a decrease in wavelength (corresponding to an increase in the energy difference) with increasing dielectric when the opposite is shown with the data reported from experiment.[8,131] This may have to do with other papers only reporting the absorption of DMABN in a small number of solvents such as in hexane, diethylether, and acetonitrile[131] or in cyclohexane, 1,4-dioxane, dichloromethane and acetonitrile.[8] Apart from acetonitrile, the solvents chosen all have very low dielectric constants while the ten solvents considered in this study sample a wider range. Additionally, while some work shows an increase between each solvent listed,[131] others have exceptions where there is an increase for the first three solvents consistently until acetonitrile which exhibits a lower absorption wavelength than dichloromethane.[8] Although the absorption values are not being perfectly matched by this study's results, shown in Table 3.1, this is still acceptable as long as the Stokes shift trendlines ultimately match up. Looking at the energy differences taken of just the DMABN in the different poses reached during simulation, each solvent system results in an average value of around -5.3 kcal/mol (after adding in the offset this value is 97.2 kcal/mol) which is consistent with the DMABN equilibrated in vacuum values. The consistent value of the isolated DMABN absorption energy regardless

of solvent means that the changes in the total energy differences with increasing solvent dielectric are almost entirely due to changes in the surroundings in response to the transition of DMABN between its states. This also means that the trends of the interaction energy between DMABN and its surroundings mirrors the total system energy difference with a general increase with increasing dielectric.

Histograms of the absorption energy differences calculated from the ground state simulations are shown in Figures 3.5 and 3.6. First, looking at the total energy differences in the left column, it is immediately apparent that the histogram shifts its center to greater energies with the increasing polarity of the solvent (which corresponds to the values reported in Table 3.1). And it is apparent that the histogram also widens, indicating an increase in the standard deviation, and a greater number of configurations of DMABN and the surrounding molecules that result in different energy contributions. In the second column, representing the energy difference calculated for the DMABN molecule considered alone and in a vacuum taken from each frame of the trajectory, there is very little difference for these peaks between different solvent environments. This means that any geometry changes in the DMABN molecule itself due to the influence of solvent are extremely similar regardless of the identity of that solvent. The final column of histograms, showing the energy difference of the whole system after the contribution of the DMABN molecule itself is subtracted out, is not surprisingly very similar in shape to the first column of histograms. After removing the isolated DMABN energy, the interaction energy between the DMABN and the solvent is different depending upon the identity of the solvent, shifting to greater energy differences in solvents of greater polarity.

The emission from experimental studies[8,51,60,87,131,137,170] didn't always show that for each solvent with an increased dielectric constant the emission of DMABN would increase as well, but overall they do show that general trend to be true. From hexane to acetonitrile an increase of about 20 nm of the emission of DMABN has been reported,[131] but a similar

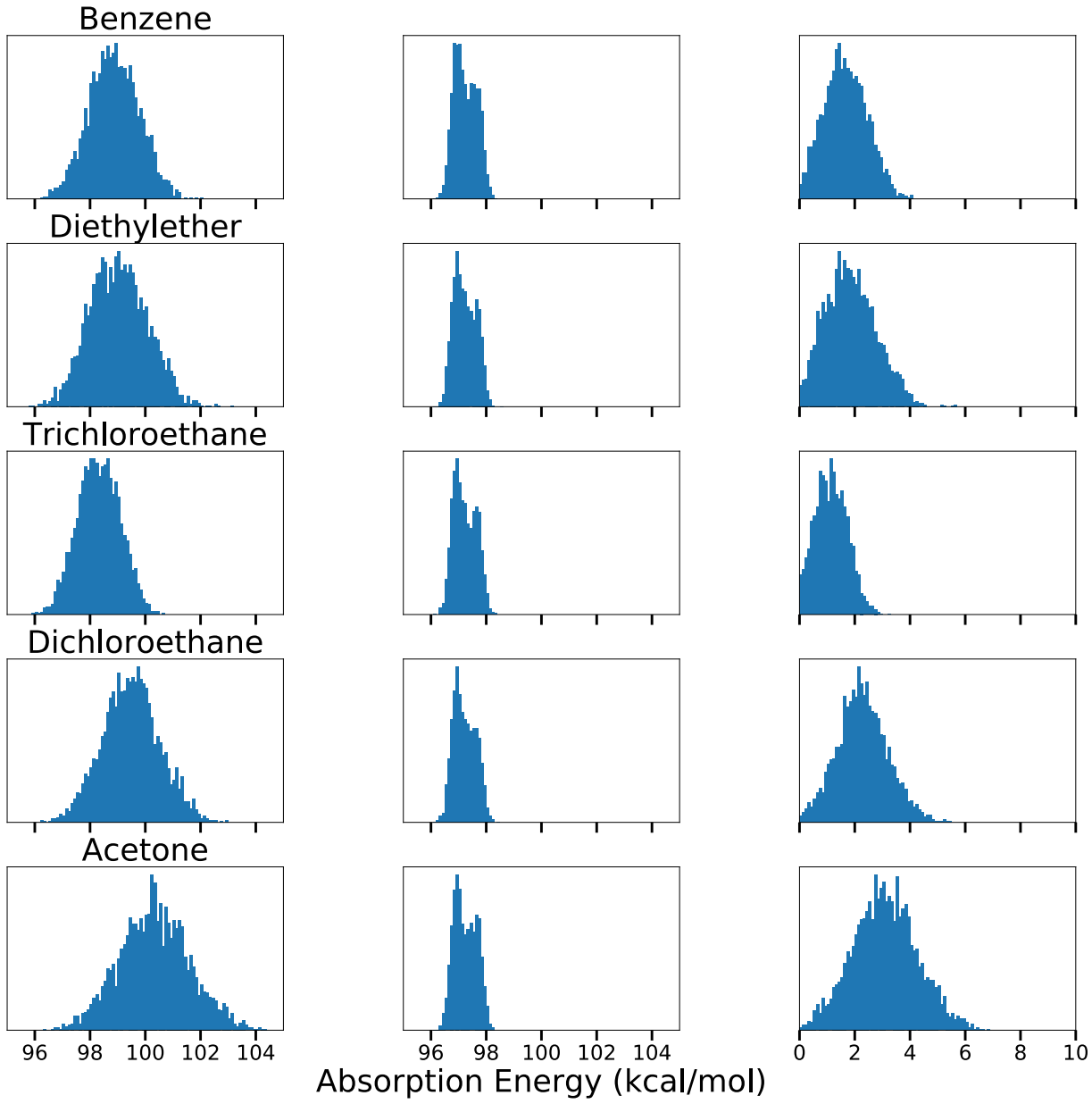

Figure 3.5: Histograms of the absorption energy of DMABN in solvent using nonpolarizable force fields Part 1 - left is the total absorption energy, middle is the absorption energy of just DMABN, and right is the absorption energy of the interaction between DMABN and the respective solvent

comparison of solvents (cyclohexane to acetonitrile) has found an increase of only about 11 nm.[8] Shown in Table 3.2, the results of this study underestimate the range of the wavelength, only showing a change of about 6.0 nm (1.35 kcal/mol) from benzene to water, which is very small in comparison to available experimental data. And again, the trend is in the opposite

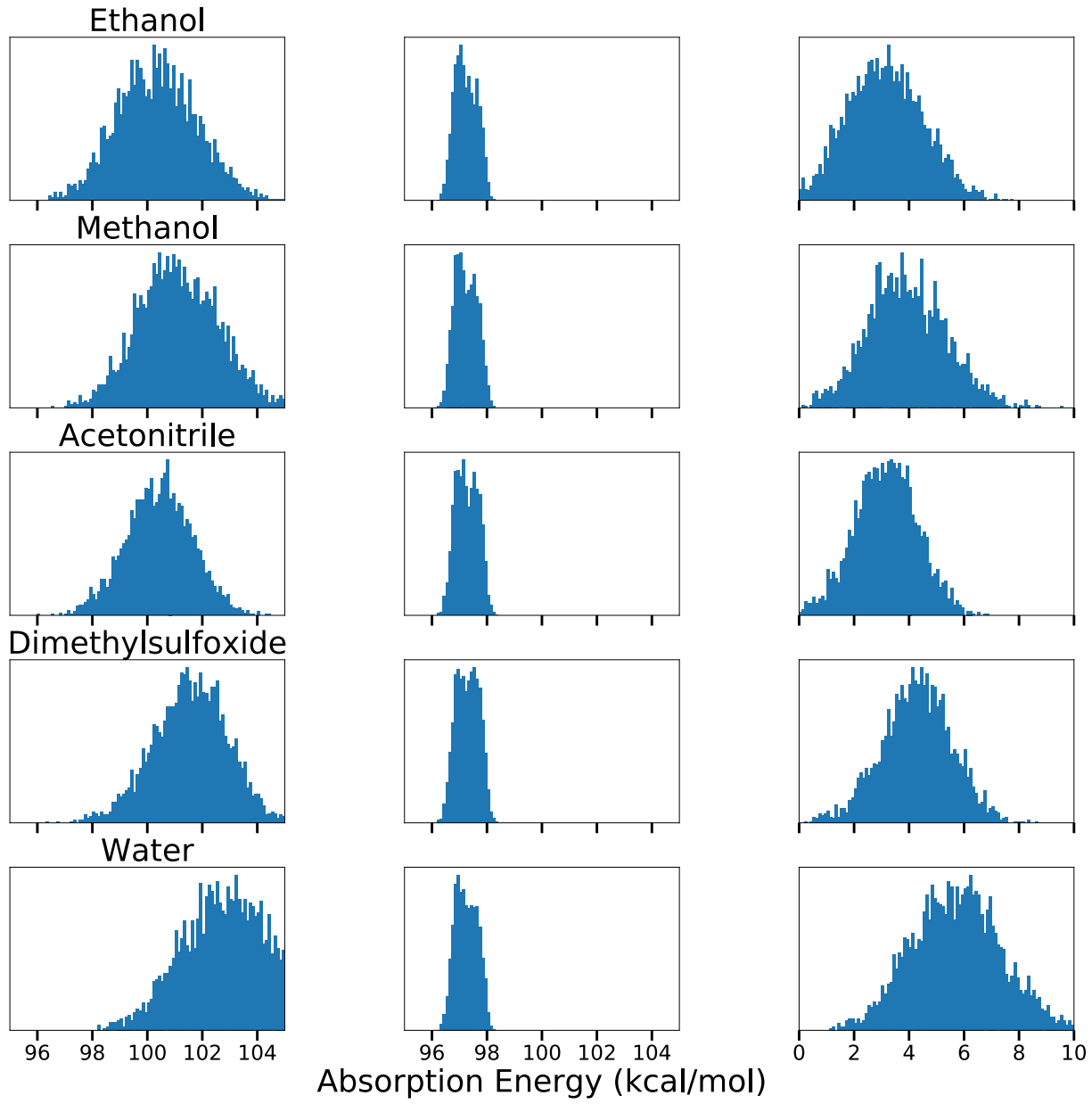

Figure 3.6: Histograms of the absorption energy of DMABN in solvent using nonpolarizable force fields Part 2 - left is the total absorption energy, middle is the absorption energy of just DMABN, and right is the absorption energy of the interaction between DMABN and the respective solvent

direction. The energy difference for just DMABN in these snapshots is slightly different than the absorption frames and the vacuum data (-5.6 kcal/mol before adding the offset, 79.4 kcal/mol after adding the offset) which is expected since the parameters for the excited state allows for slightly more twist of the amino group. The interaction energy, like that

Solvent	All	stddev	error	DMABN	stddev	error	Interaction	stddev	error
Benzene	79.8	0.8	0.0	79.4	0.3	0.0	0.4	0.8	0.0
Diethylether	79.9	0.9	0.0	79.4	0.3	0.0	0.5	0.8	0.0
Trichloroethane	79.8	0.7	0.0	79.4	0.3	0.0	0.4	0.6	0.0
Dichloroethane	80.3	1.0	0.1	79.4	0.3	0.0	0.9	1.0	0.1
Acetone	80.3	1.2	0.0	79.4	0.3	0.0	0.8	1.1	0.0
Ethanol	80.2	1.0	0.0	79.4	0.3	0.0	0.8	1.0	0.0
Methanol	80.5	1.2	0.0	79.4	0.3	0.0	1.0	1.2	0.0
Acetonitrile	80.2	1.2	0.0	79.5	0.3	0.0	0.9	1.1	0.0
Dimethylsulfoxide	80.7	1.3	0.1	79.4	0.3	0.0	1.2	1.3	0.1
Water	81.2	1.4	0.0	79.4	0.3	0.0	1.8	1.4	0.0

Table 3.2: Emission energy of DMABN in solvent using nonpolarizable force fields - energies include added offset

from the absorption, increases generally with increasing dielectric and mirrors the changes in the total energy emission.

The corresponding histograms of the emission energy differences calculated from the LE state simulations are shown in Figures 3.7 and 3.8. The general features of the emission histograms are quite similar to those seen for the absorption energy differences: the general widening of the data for the total energy differences with increasing polarity of the solvent and that the energy difference of just the DMABN molecule does not seem to change much regardless of what solvent simulation the conformation was extracted from. The differences lie in the exact values of the energy differences that were calculated and how much that value is shifted by the presence of different surrounding solvent. The standard deviations of the total energy difference for the system in a given solvent is practically the same for the absorption and the emission energies. The isolated energy difference of DMABN simulated in its excited state, shown in the middle column of histograms, still doesn't show any significant change regardless of the solvent from which it was taken. In fact, the standard deviation of the isolated DMABN from the excited state simulation is slightly smaller than was seen for the isolated DMABN extracted from the ground state simulation. Though, again, what is being graphed is the difference in energy for snapshots of a trajectory of simulation when the force fields applied to the system either ascribe the ground or excited state parameters

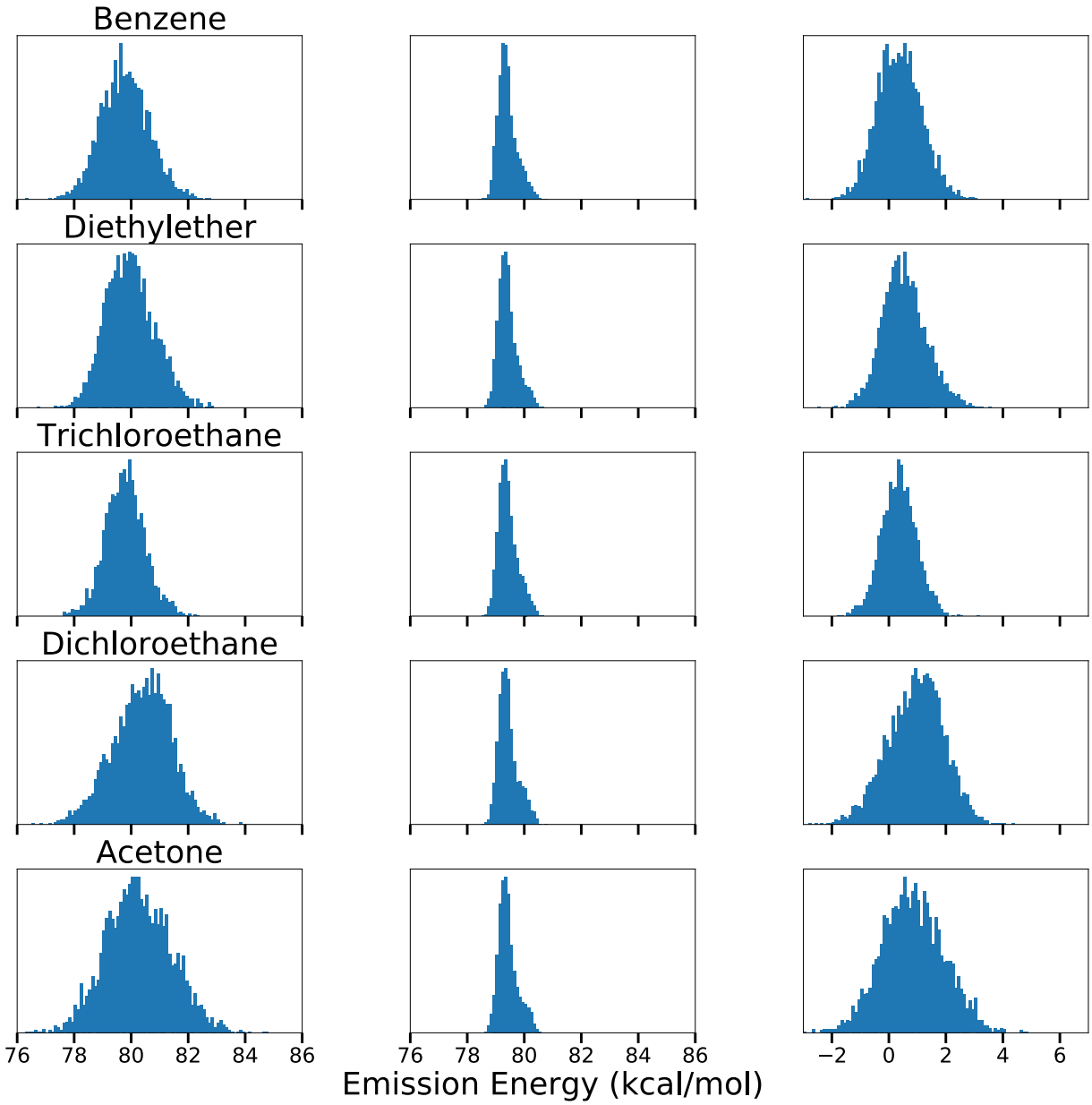

Figure 3.7: Histograms of the emission energy of DMABN in solvent using nonpolarizable force fields Part 1 - left is the total absorption energy, middle is the absorption energy of just DMABN, and right is the absorption energy of the interaction between DMABN and the respective solvent

to DMABN. The magnitude of that energy is entirely due to the internal differences of the ground and excited state of DMABN and the effect those differences have on the solvent. The final column of histograms clearly show the shift in energy: increasing in both the average value and standard deviation when DMABN in considered in solvents of increasing polarity.

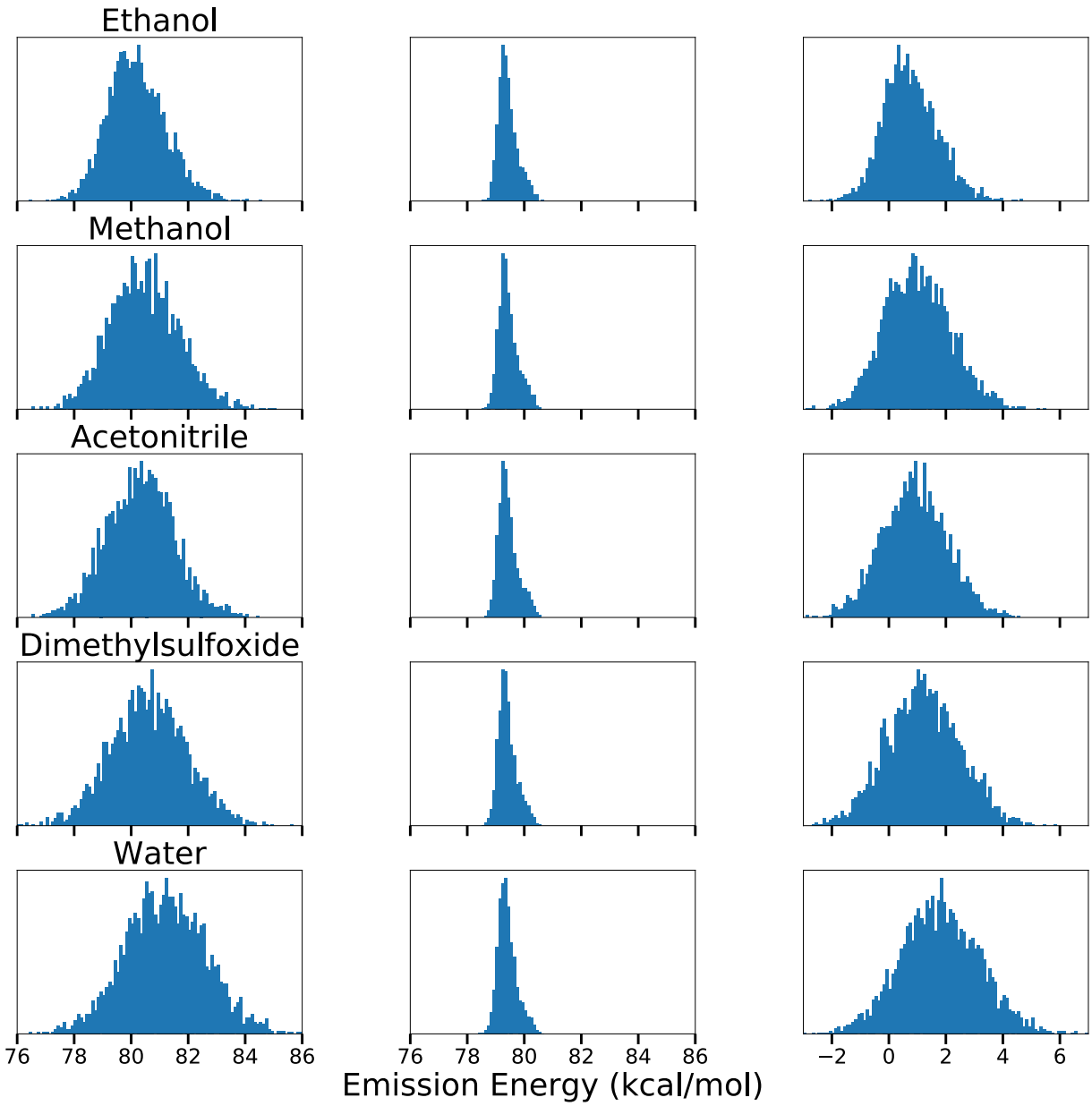

Figure 3.8: Histograms of the emission energy of DMABN in solvent using nonpolarizable force fields Part 2 - left is the total absorption energy, middle is the absorption energy of just DMABN, and right is the absorption energy of the interaction between DMABN and the respective solvent

Despite some disagreement between the experimental absorption and emission wavelengths, when the data from this work is converted into Stokes Shift (Table 3.3) and represented by a Lippert plot (Figure 3.9) the correct trend is observed. The Stokes shift (the

Solvent	Absorption	Emission	Stokes Shift
Benzene	289.2	358.3	69.1
Diethylether	288.6	357.7	69.1
Trichloroethane	290.8	358.5	67.7
Dichloroethane	287.2	356.1	68.9
Acetone	285.0	356.2	71.2
Ethanol	285.4	356.7	71.2
Methanol	281.8	355.2	73.4
Acetonitrile	285.0	356.5	71.5
Dimethylsulfoxide	281.0	354.5	73.5
Water	277.1	352.4	75.2

Table 3.3: Wavelengths of absorption, emission and Stokes shift of DMABN in solvent using nonpolarizable force fields

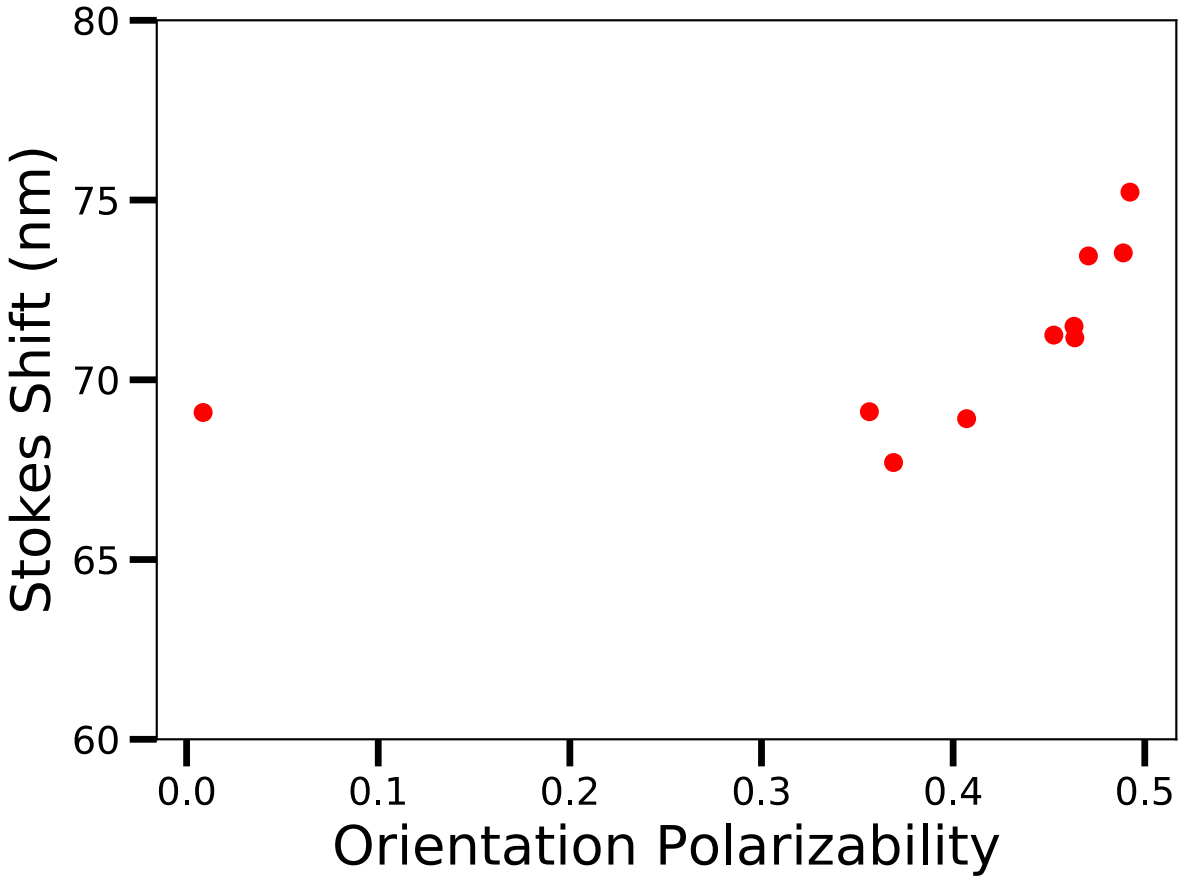

Figure 3.9: Lippert plot of DMABN in ten solvents using nonpolarizable force fields

difference between emission and absorption) increases with an increase in the orientation polarizability of the solvent, which is the desirable result. While the nonpolarizable parameters

are less than ideal in perfectly recreating the experimental wavelengths, the Drude parameter set is designed specifically to account for polar interactions and should be a better match.

3.4.2 Polarizable Drude Solvent Models

The approximate offset for the Drude parameters was found in the same manner as the nonpolarizable parameters: finding the difference between the energy of excitation from CASSCF calculations and vacuum simulation energy differences between the ground and excited state parameters. The CASSCF energy is still 106.74 kcal/mol (since this calculation is not based on using either parameter set). For the flattened geometry of DMABN (the optimized ground state and the Franck-Condon state reached by the instantaneous jump from ground to excited before relaxation has occurred), the energy was found to be 11.18 kcal/mol with the polarizable Drude force fields. If the molecule is allowed to be run in a short equilibration with polarizable Drude force fields, the average energy difference for the snapshots of simulation was found to be 12.12 kcal/mol. The offset will thus be also around 100 kcal/mol, though it is expected to be a slightly smaller offset than the nonpolarizable one due to the larger energy difference found for the polarizable Drude simulated DMABN in vacuum. And again, the exact value is the result of fitting to the available experimental data. The offsets settled on were 84.319 kcal/mol and 68.547 kcal/mol for the absorption and emission respectively. An important difference between the nonpolarizable and Drude data analysis is the handling of the Drude particles. The Drude particles are in an idealized position for the state that the equilibration was performed in, but if that snapshot was then analyzed with the other state's parameters those Drude particles are now in an unfavorable position. Since Drude particles are a means of separating charge, the update to their position should be part of the electronic transition between ground and excited state to recover the correct SCF energy. Thus, each frame first had its Drude particle positions minimized for the respective parameter file before the energy was calculated.

Solvent	All	stddev	error	DMABN	stddev	error	Interaction	stddev	error
Benzene	98.8	1.2	0.0	96.4	0.7	0.0	2.4	1.0	0.0
Diethylether	98.6	1.1	0.0	96.4	0.7	0.0	2.2	0.9	0.0
Trichloroethane	98.9	1.2	0.0	96.4	0.7	0.0	2.5	1.0	0.0
Dichloroethane	99.3	1.3	0.0	96.4	0.7	0.0	2.9	1.1	0.0
Acetone	99.7	1.4	0.0	96.4	0.7	0.0	3.3	1.2	0.0
Ethanol	100.5	2.0	0.1	96.4	0.7	0.0	4.1	1.9	0.1
Methanol	101.2	2.1	0.1	96.4	0.7	0.0	4.8	2.0	0.1
Acetonitrile	100.8	1.6	0.0	96.4	0.7	0.0	4.4	1.5	0.0
Dimethylsulfoxide	100.9	1.6	0.0	96.4	0.7	0.0	4.5	1.5	0.0
Water	104.2	2.5	0.0	96.4	0.7	0.0	7.8	2.4	0.0

Table 3.4: Absorption energy of DMABN in solvent using polarizable Drude force fields - Drude particles are minimized and energy includes added offset

As shown in Table 3.4, the range for the total absorption energy for the Drude parameters was about 5 kcal/mol (16 nm) from benzene to water, which is very similar to what was seen for the nonpolarizable parameters. The greater range is more in line with experimental data, however direction of the trend is still reversed (this study shows a decrease in absorption wavelength while experimental studies generally show an increase). In terms of the absorption, the Drude parameter set resulted in energy differences very similar to the nonpolarizable set with each data point in approximately the same place and the same progression with increasing solvent dielectric. Since the experimental data being compared to is the same as was for the nonpolarizable data, many of the same observations apply here. The average energy difference of just the DMABN poses isolated from the surrounding solvent they are extracted from is 12.1 kcal/mol (which corresponds to 96.4 kcal/mol after adding the offset) which is consistent with the energy difference seen for DMABN in vacuum. Since this energy contribution is relatively consistent, the interaction energy between the solvent and DMABN shows the same trend as the overall energy differences calculated for the absorption.

The histograms (Figures 3.10 and 3.11) of the energy differences between the ground and excited state polarizable Drude force fields for the NAMD simulations of the ground state (or in other words the absorption), are at a glance very similar to those seen in the nonpolarizable systems and the general trend of an increased standard deviation of these energies

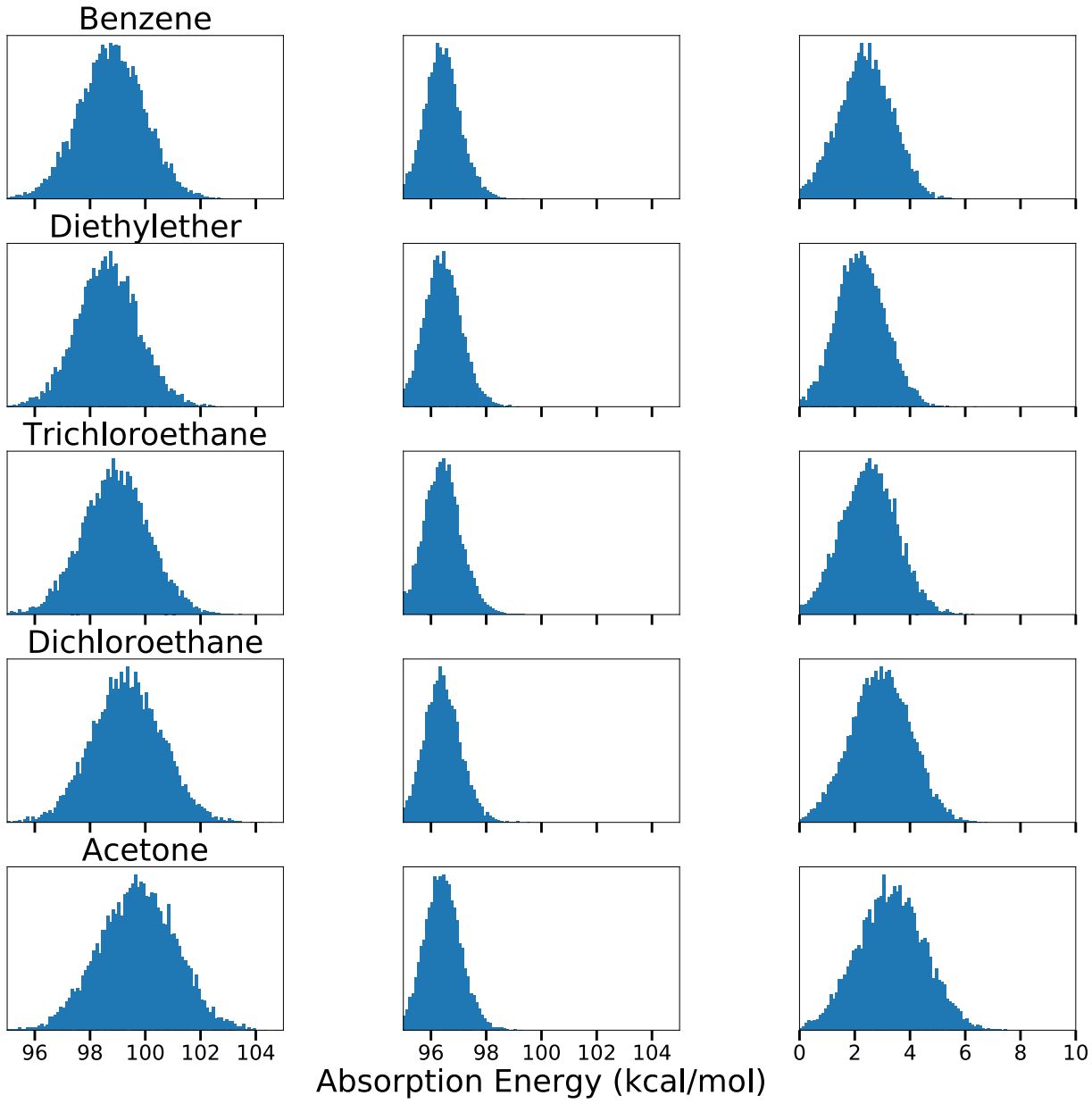

Figure 3.10: Histograms of the absorption energy of DMABN in solvent using polarizable Drude force fields Part 1- left is the total absorption energy, middle is the absorption energy of just DMABN, and right is the absorption energy of the interaction between DMABN and the respective solvent

with increasing solvent polarity is also observed. The standard deviation is slightly greater for an energy difference for a given solvent for the polarizable Drude force field version than the nonpolarizable, making the histograms slightly wider. And the shift of the peak from benzene to water is more drastic in the polarizable Drude histograms than was seen in the

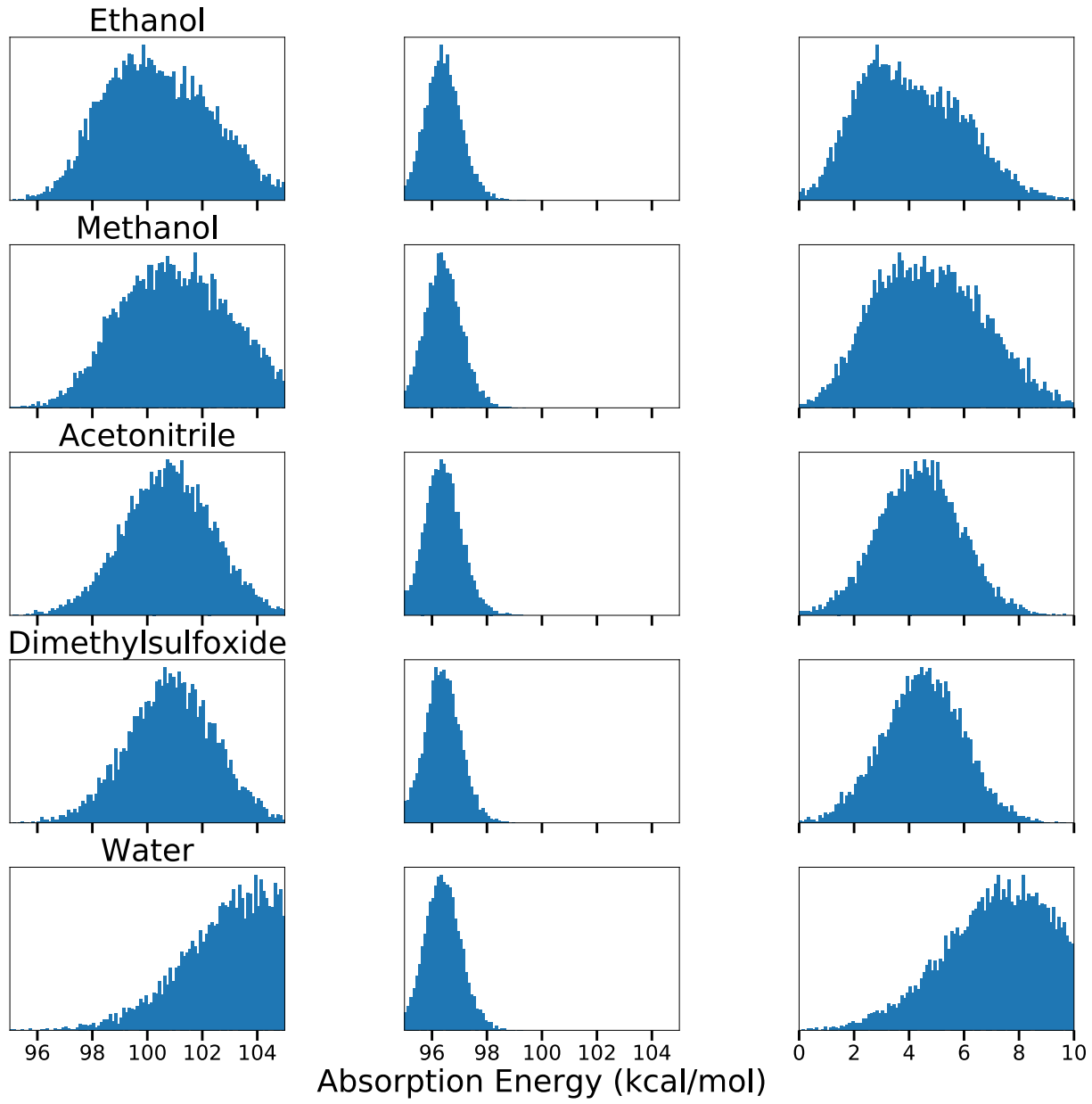

Figure 3.11: Histograms of the absorption energy of DMABN in solvent using polarizable Drude force fields Part 2 - left is the total absorption energy, middle is the absorption energy of just DMABN, and right is the absorption energy of the interaction between DMABN and the respective solvent

nonpolarizable histograms. The middle column, showing the range of energy differences of just the DMABN molecule extracted from each snapshot of the trajectory, is extremely consistent for each solvent system. This was also seen for the nonpolarizable isolated DMABN energy differences. However, in the polarizable Drude energy differences the standard devi-

ation is nearly twice as large, indicating that there are more conformations sampled by the DMABN molecule, or at least a greater energy difference between those conformations, when represented by the polarizable Drude force fields. But this remains consistent regardless of solvent, meaning that the third column of histograms (showing the differences in interaction energy between the DMABN and the surrounding liquid by subtracting out the isolated DMABN energy difference) has the same shape as the total energy difference histograms in the first column.

Solvent	All	stddev	error	DMABN	stddev	error	Interaction	stddev	error
Benzene	81.2	1.2	0.0	80.5	0.6	0.0	0.7	1.0	0.0
Diethylether	80.7	1.1	0.0	79.8	0.7	0.0	0.9	0.9	0.0
Trichloroethane	80.7	1.2	0.0	79.8	0.7	0.0	0.9	1.0	0.0
Dichloroethane	80.7	1.3	0.0	79.8	0.7	0.0	0.9	1.1	0.0
Acetone	80.6	1.4	0.0	79.9	0.7	0.0	0.8	1.3	0.0
Ethanol	80.6	1.3	0.0	79.8	0.7	0.0	0.8	1.1	0.0
Methanol	80.5	1.5	0.0	79.8	0.7	0.0	0.7	1.3	0.0
Acetonitrile	80.4	1.7	0.0	79.9	0.7	0.0	0.6	1.5	0.0
Dimethylsulfoxide	80.6	1.7	0.0	79.9	0.7	0.0	0.7	1.5	0.0
Water	78.3	2.0	0.0	79.9	0.7	0.0	−0.5	1.9	0.0

Table 3.5: Emission energy of DMABN in solvent using polarizable Drude force fields - Drude particles are minimized and energy includes added offset

Greater differences between the Drude parameter set and the nonpolarizable parameters are seen in the emission data, reported in Table 3.5. The total emission energy range is about 2.9 kcal/mol (about 13 nm), which is much more reasonable when compared to studies that had a range of about 20 nm (hexane to acetonitrile)[131] and 11 nm (cyclohexane to acetonitrile)[8] than the nonpolarizable model (which had a range of only 6 nm). And unlike the nonpolarizable results, the trend of the polarizable Drude systems matches the experimental one: both increase the wavelength of emission with increasing dielectric. The added complexity of the Drude particles resulted in a much closer approximation of the emission of DMABN in varying solvents than a simple nonpolarizable parameter set. The average isolated DMABN energy difference is 11.4 kcal/mol (corresponding to 79.9 kcal/mol after adding in the offset term), which is slightly smaller than that seen for absorption. This average is closer to the flat structure energy difference for DMABN in vacuum (11.18

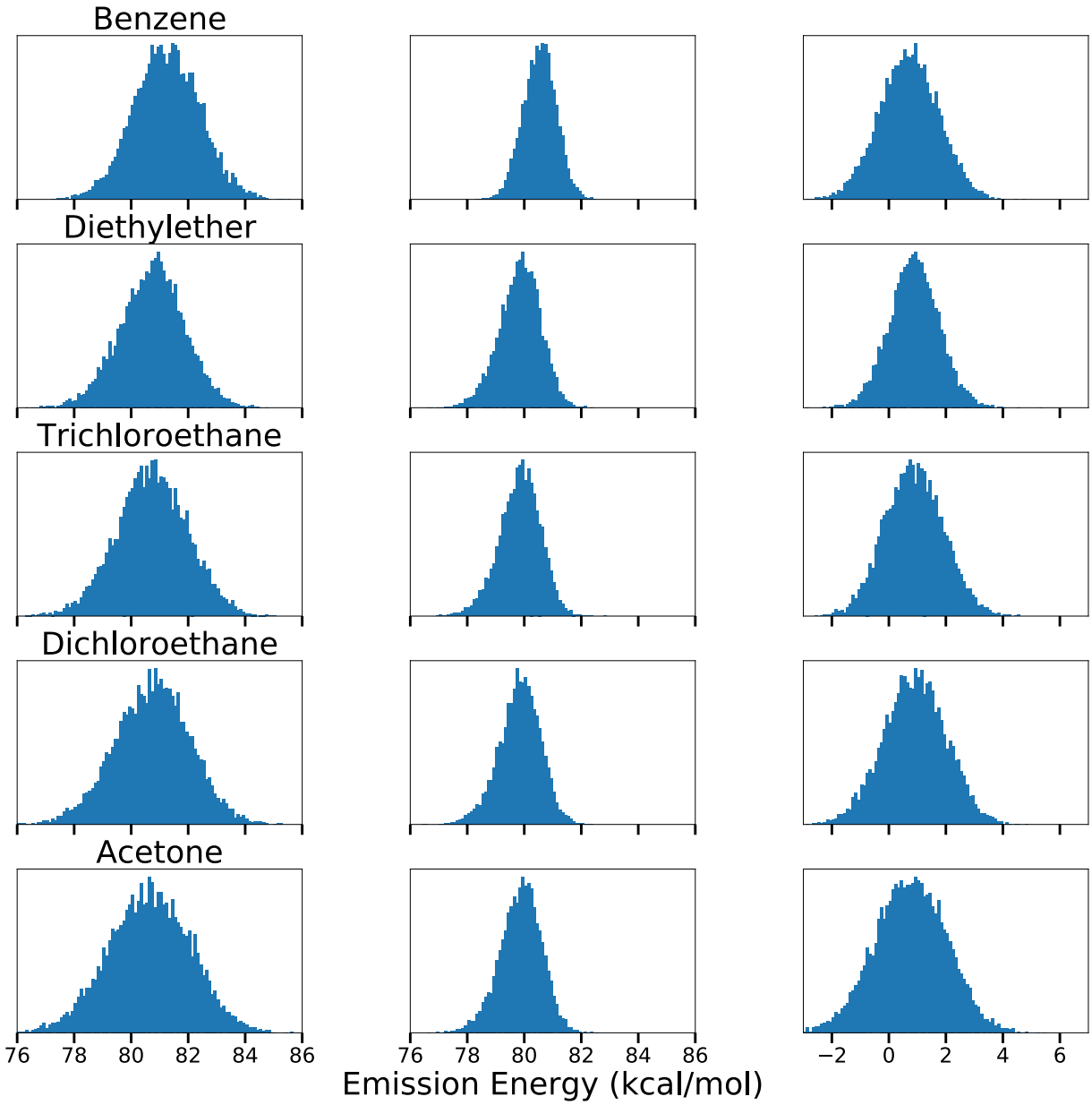

Figure 3.12: Histograms of the emission energy of DMABN in solvent using polarizable Drude force fields Part 1 - left is the total absorption energy, middle is the absorption energy of just DMABN, and right is the absorption energy of the interaction between DMABN and the respective solvent

kcal/mol) than to the average energy difference for the molecule simulated in vacuum (12.12 kcal/mol).

Similar to each of the sets of histograms of DMABN in solvents shown before, the polarizable Drude emission histograms shown in Figures 3.12 and 3.13 have an increase in the

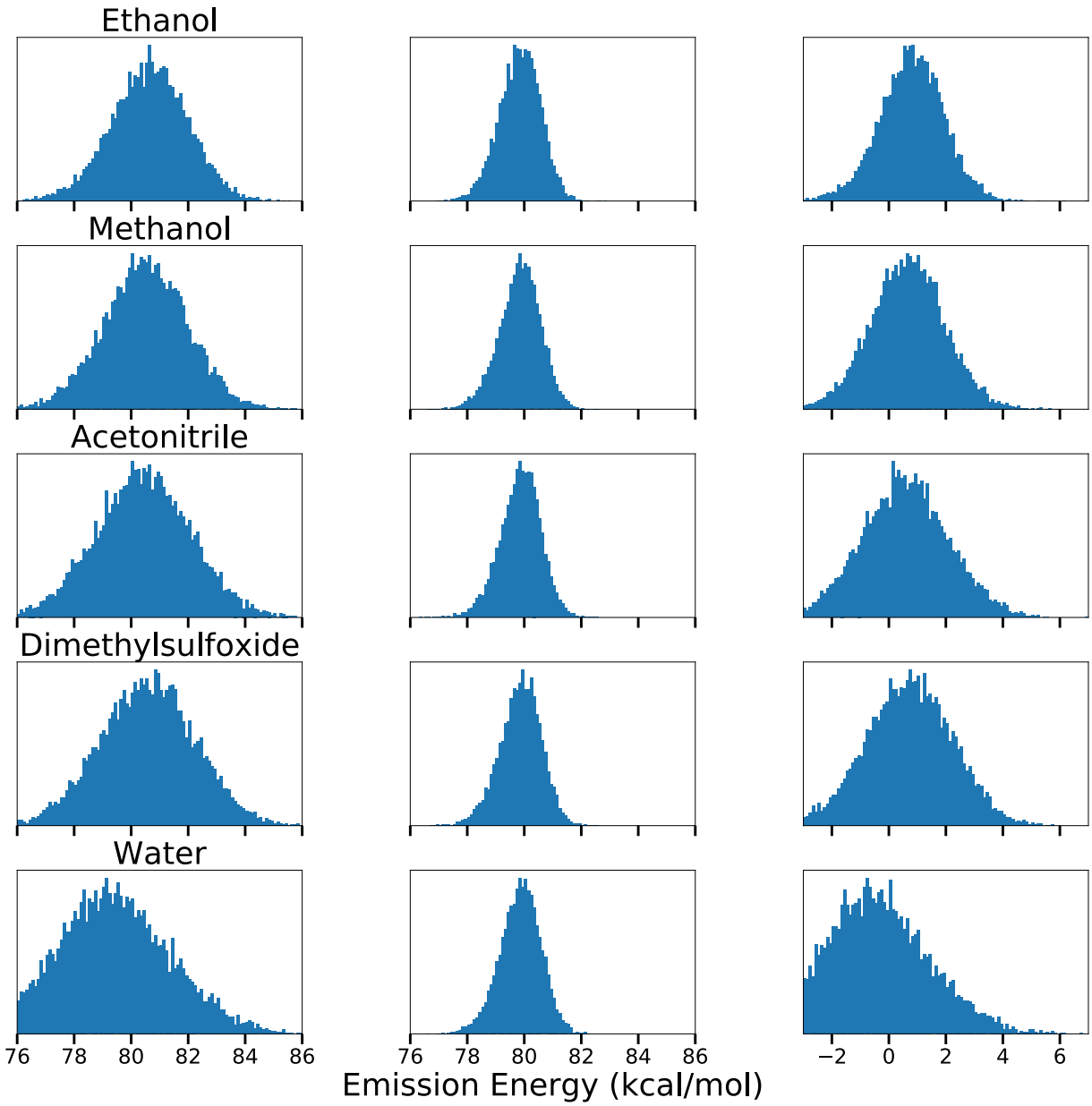

Figure 3.13: Histograms of the emission energy of DMABN in solvent using polarizable Drude force fields Part 2 - left is the total absorption energy, middle is the absorption energy of just DMABN, and right is the absorption energy of the interaction between DMABN and the respective solvent

standard deviation with increasing solvent polarity and have very consistent values for the isolated DMABN energy differences (the middle column). Unlike all the other histogram sets, it can be seen in the first and third column that the average energy difference decreases with the increasing polarity of the solvent. Comparing these histograms directly to the non-

polarizable emission histograms shows that there is a greater standard deviation of values in the energy differences calculated with the polarizable Drude force fields. Both the absorption and emission energy differences reflected this trend: the polarizable Drude version exhibits a greater standard deviation in all energy terms than those derived from the nonpolarizable simulations.

Solvent	Absorption	Emission	Stokes Shift
Benzene	289.5	352.0	62.5
Diethylether	289.9	354.2	64.3
Trichloroethane	289.1	354.2	65.1
Dichloroethane	287.9	354.2	66.3
Acetone	286.8	354.6	67.9
Ethanol	284.6	354.6	70.0
Methanol	282.7	355.2	72.6
Acetonitrile	283.8	355.5	71.8
Dimethylsulfoxide	283.5	354.9	71.5
Water	274.4	365.0	90.6

Table 3.6: Wavelengths of absorption, emission and Stokes shift of DMABN in solvent using polarizable Drude force fields

The Stokes shift of this data (Table 3.6) shows the desired increase of wavelength with increasing dielectric. The only data point that somewhat differs from the experimental Stokes shift trend line is water, however none of the experimental sources reported both the absorption and emission of water and thus cannot be included in the comparison. The work of Grabowski et al. shows the emission wavelength of DMABN in water to be around 365.9 nm or 360.4 nm[51] which is quite close to the value calculated in this work. The difference in their two estimates being whether the spectra was immediately determined for the freshly prepared solution or if five days were allowed to elapse before measurement. Perhaps if the work of Neubauer et al.[131] (which considered only hexane, diethylether and acetonitrile) and Atsbeha et al.[8] (which considered cyclohexane, 1,4-dioxane, dichloromethane and acetonitrile) included additional polar solvents the trendline produced here would line up even better. The positive trend in the Stokes Shift (as represented by the Lippert plot in Figure 3.14) and the closer match in the range and trend of emission wavelengths shows that the Drude parameter set is much better adept at predicting the fluorescent cycle of DMABN

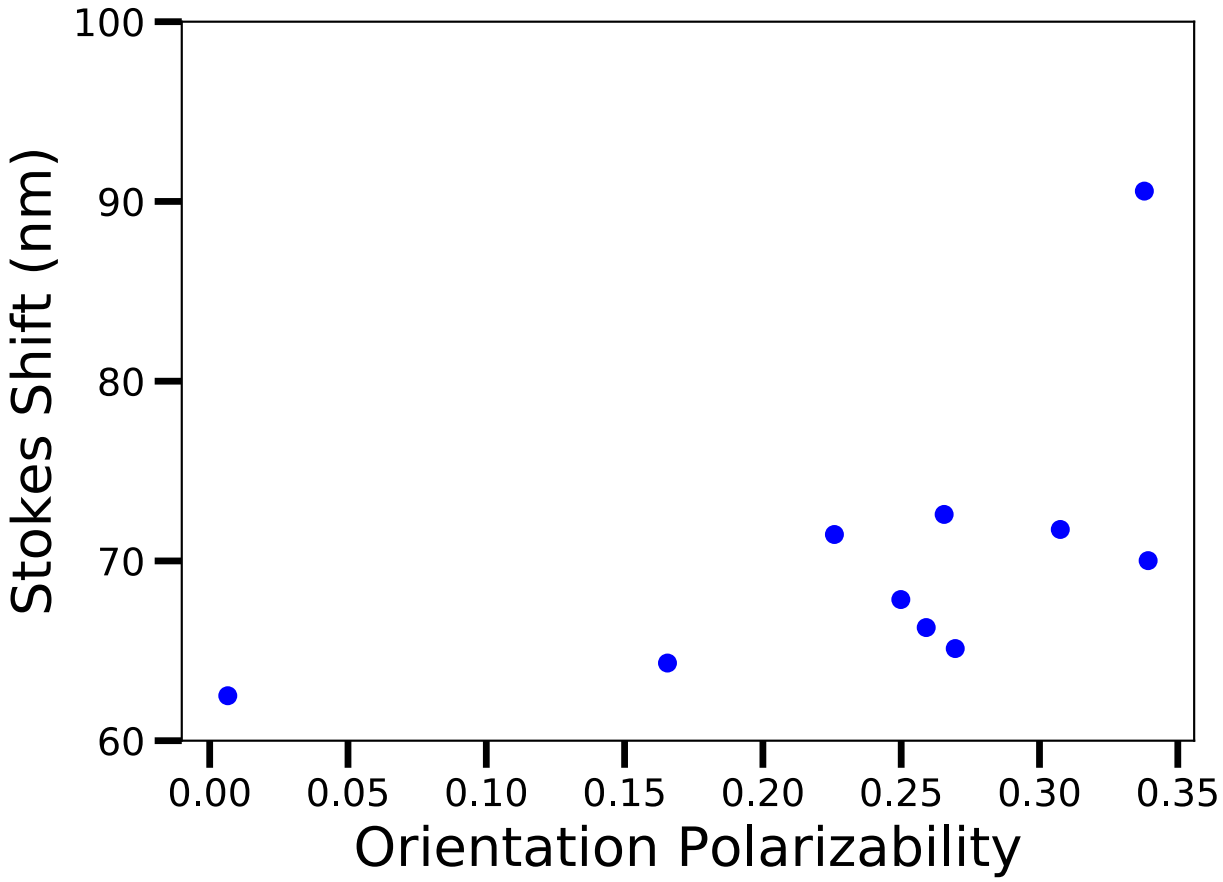

Figure 3.14: Lippert plot of DMABN in ten Solvents using polarizable Drude force fields

than the nonpolarizable set.

3.4.3 Simulating Relaxation after Excitation

In addition to the instantaneous energy change that can be extracted by analyzing the same snapshot with two different parameter files, the subsequent relaxation can be observed by running the simulation for a short period of time after the transition. To demonstrate this, fifty different snapshots were extracted from the ground state equilibration systems for DMABN in methanol, dimethylsulfoxide and water. Then each snapshot is treated as the starting point of a new simulation where the parameter set for DMABN was switched to its excited state version. After each femtosecond of simulation, the energy gap between the

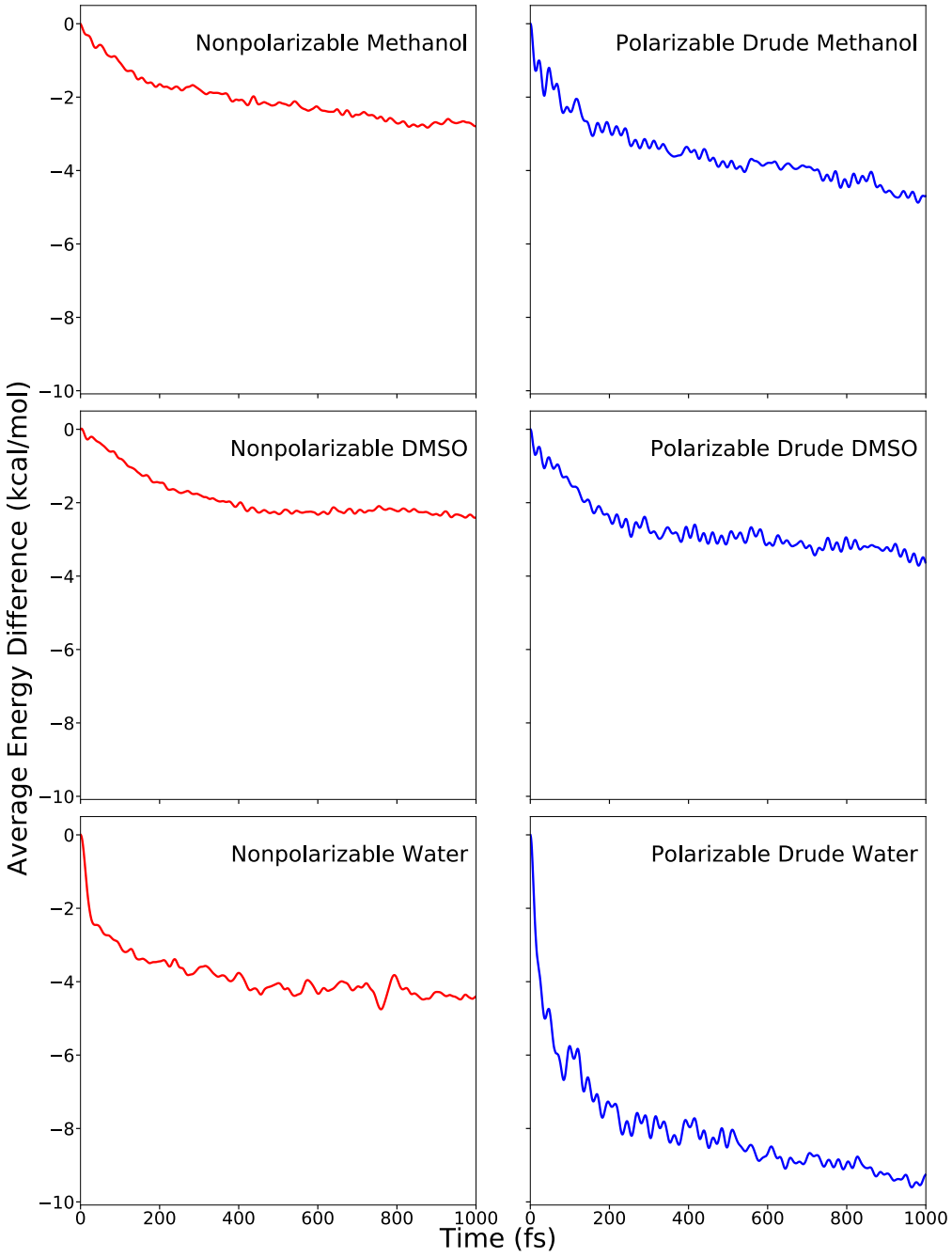

Figure 3.15: Relaxation of DMABN in three sample solvents immediately after excitation - left, in red, is using nonpolarizable force fields and right, in blue, is using polarizable Drude force fields

ground and the LE state is measured and averaged over the fifty iterations of DMABN in the given solvent for a total of 1000 fs. The energy at the starting time step was subtracted from each energy to more clearly display the change in energy over the course of the simu-

lation. This was performed with both the nonpolarizable and polarizable Drude force fields. Reported in Figure 3.15 is the relaxation of the total energy of the system as a function of time after an excitation in each of the three solvents considered.

Graphed on the left and in red is this relaxation performed with the nonpolarizable model while on the right and in blue is the relaxation performed with the polarizable Drude model. In every case, a sharper decline is seen in the first couple hundred femtoseconds that levels off before the end of the simulation; this is most noticeable in the water simulations. The total energy change is more significant in more polar systems like water, which in the nonpolarizable model shows a decrease of about 4.5 kcal/mol during the solvent relaxation while the other two solvents considered shows a decrease closer to 2.5 kcal/mol. The polarizable Drude model also shows the same trend of a greater change in energy for the more polar solvent system of water. However, the magnitude of that change is noticeably larger with polarizable Drude force fields: the water solvated DMABN shows a decrease of about 9.5 kcal/mol while the methanol system decreased by about 4.5 kcal/mol and dimethylsulfoxide system decreased by about 3.5 kcal/mol. As with the instantaneous energy differences calculated for the full regimen of solvents, the polarizable Drude force fields predict a larger energy difference range between solvents.

3.5 Discussion

Graphing both the nonpolarizable and polarizable Drude data together against the orientation polarizability calculated with each force field model, (along with experimental data) results in Figure 3.16 for the absorption wavelengths, Figure 3.17 for the emission wavelengths and Figure 3.18 for the Stokes Shift. The nonpolarizable results are graphed in red, polarizable Drude in blue and any available experimental data is graphed in black. The experimental data used in the absorption wavelengths graphs two sets of solvents, one of DMABN in hexane, diethylether and acetonitrile[131] and one of DMABN in cyclohexane,

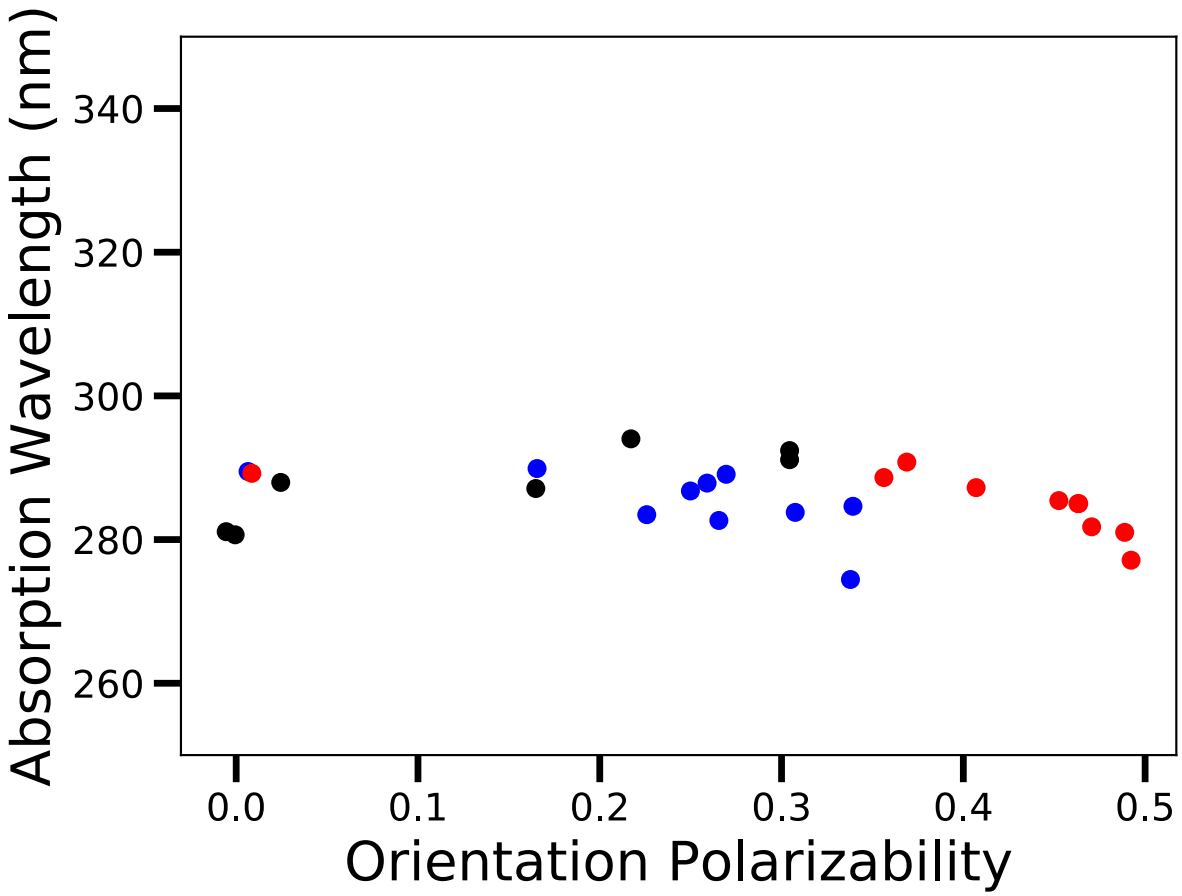

Figure 3.16: Absorption wavelengths of DMABN in solvent using nonpolarizable and polarizable Drude force fields, graphed with experimental data - nonpolarizable data is graphed in red, polarizable Drude data is graphed in blue, and experimental data is graphed in black

1,4-dioxane, dichloromethane, and acetonitrile.[8] Emission wavelengths graphed are from the previous two sets of solvents as well one of DMABN in benzene, ethylene glycol, glycerol and dimethylsulfoxide,[60] one of DMABN in cyclohexane, benzene, and dioxane,[170] one of DMABN in hexane, dibutyl ether, diethylether, and butyl chloride[87] and DMABN in aqueous solutions including pure water.[51] The Stokes shift graph is based on the experimental studies that included both the absorption and emission maximums of DMABN in their series of solvents.

The general trend of increasing Stokes shift with increasing orientation polarizability was clearly observed for both the nonpolarizable and polarizable Drude parameter versions of the

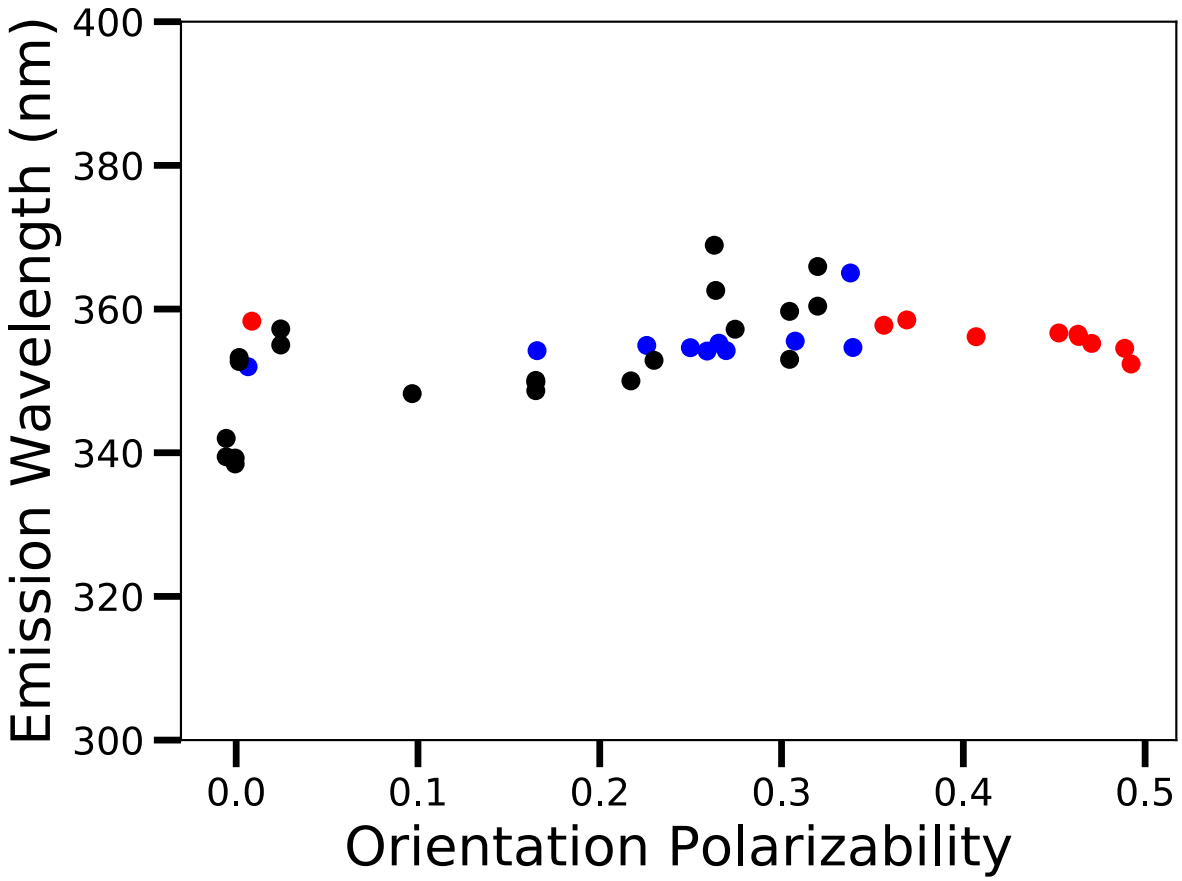

Figure 3.17: Emission wavelengths of DMABN in solvent using nonpolarizable and polarizable Drude force fields, graphed with experimental data - nonpolarizable data is graphed in red, polarizable Drude data is graphed in blue, and experimental data is graphed in black

DMABN-solvent systems. However, the sensitivity of the polarizable Drude version results in a greater range of data, from the least polar solvent of benzene being lower than the corresponding data point in the nonpolarizable version to the most polar solvent of water having a higher data point than the nonpolarizable version. According to the nonpolarizable model, the locally excited state first singlet of DMABN hardly changes based on its environment. While it is true that this transition does not involve nearly as much solvent reorganization as the transition for more complicated molecules like di-8-ANEPPS, the nonpolarizable model of the DMABN fluorescence cycle certainly underestimates the change with respect to solvent polarity. From benzene to water, the nonpolarizable change of wavelength is only 6.13

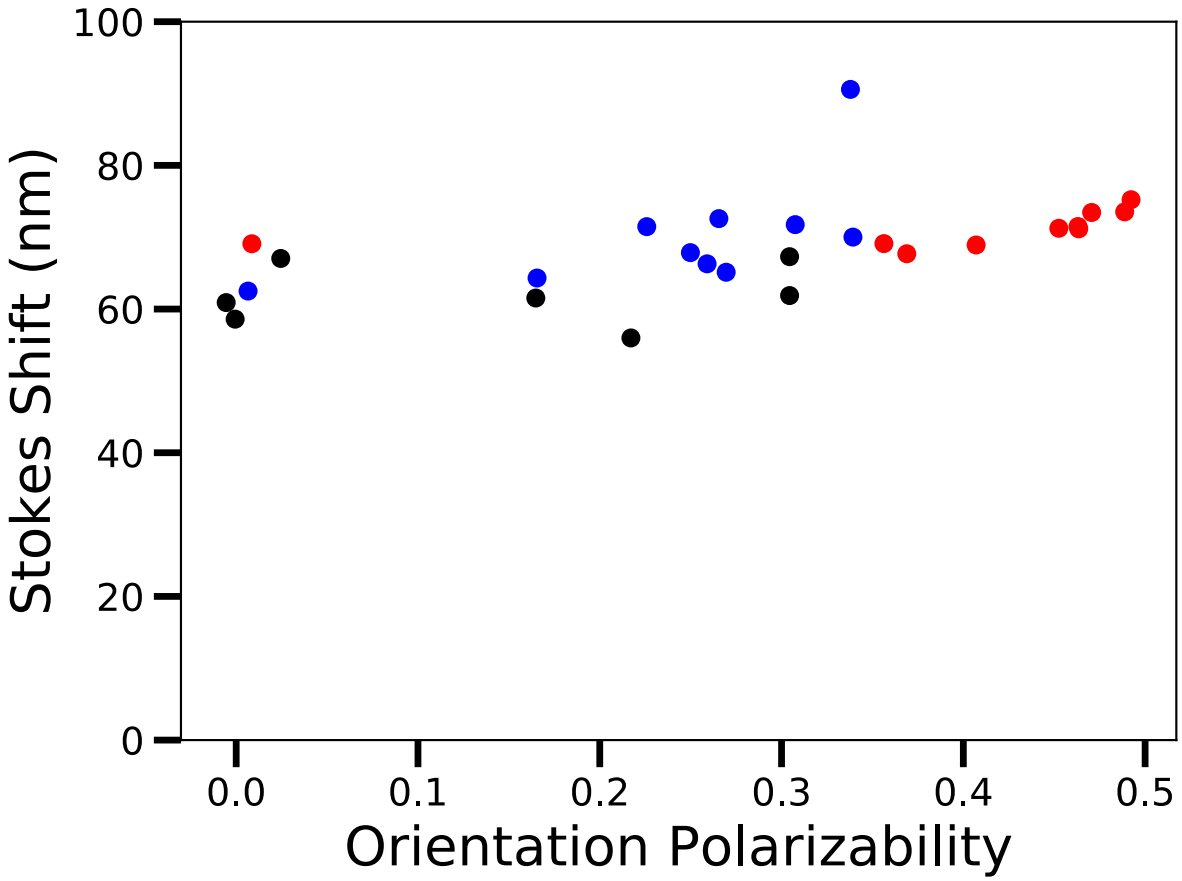

Figure 3.18: Stokes shift of DMABN in solvent using nonpolarizable and polarizable Drude force fields, graphed with experimental data - nonpolarizable data is graphed in red, polarizable Drude data is graphed in blue, and experimental data is graphed in black

nm (from benzene to dimethylsulfoxide it is 4.44 nm). In contrast the polarizable Drude model predicts the Stokes shift to change from benzene to water by 28.07 nm (from benzene to dimethylsulfoxide it is 8.97 nm). The DMABN in water data as represented by the Drude parameters seems to overestimate the difference between the absorption and emission, and that point is a bit of an outlier from the linear trend produced by the rest of the solvents. Removing it from consideration matches the polarizable Drude data much more cleanly to the available experimental data than the nonpolarizable data can match. Unfortunately, when studied experimentally, DMABN is often placed a in range of solvents that ends with either dimethylsulfoxide or acetonitrile as its most polar solvent so it is unclear if the polar-

izable Drude DMABN-water system behavior is an artifact of the method or a reflection of a true characteristic. Regardless, the greater range of the polarizable Drude data is overall more in-line with experiment, making it a better representation of the spectral properties of DMABN than the results when using nonpolarizable parameters.

Solvent	Nonpolarizable	Polarizable Drude	Experimental
Benzene	289.2	289.5	
Diethylether	288.6	289.9	287.1 [131]
Trichloroethane	290.8	289.1	
Dichloroethane	287.2	287.9	
Acetone	285.0	286.8	
Ethanol	285.4	284.6	
Methanol	281.8	282.7	
Acetonitrile	285.0	283.8	292.4 [131] 291.1 [8]
Dimethylsulfoxide	281.0	283.5	
Water	277.1	274.4	

Table 3.7: Absorption wavelengths of DMABN from nonpolarizable and polarizable Drude models compared to available experimental data

Despite how ultimately the absorption, emission and Stokes shift data of both the nonpolarizable and polarizable Drude models line up generally with the available data from experimental studies, some very noticeable differences can be seen when graphing against only the solvents that are in common. All of the absorption wavelengths are summarized together in Table 3.7. Of the ten solvents that were simulated, experimental values were found for only diethylether and acetonitrile. Only graphing the nonpolarizable and polarizable Drude results against these three experimental absorption wavelengths is shown in Figure 3.19. For each of these three, the wavelengths reported by the nonpolarizable model are closer to the experimental value. However, the difference between the nonpolarizable and polarizable Drude model is only about 1 nm in each case. In general, the difference between absorption wavelengths found by the two simulated models do not differ by more than 3 nm, and are very similar to one another.

There were more reports of the emission of the LE state of DMABN in various solvents than for the absorption, and thus there were more emission wavelengths that can be directly compared to. The experimental emission wavelengths of DMABN in benzene, diethylether,

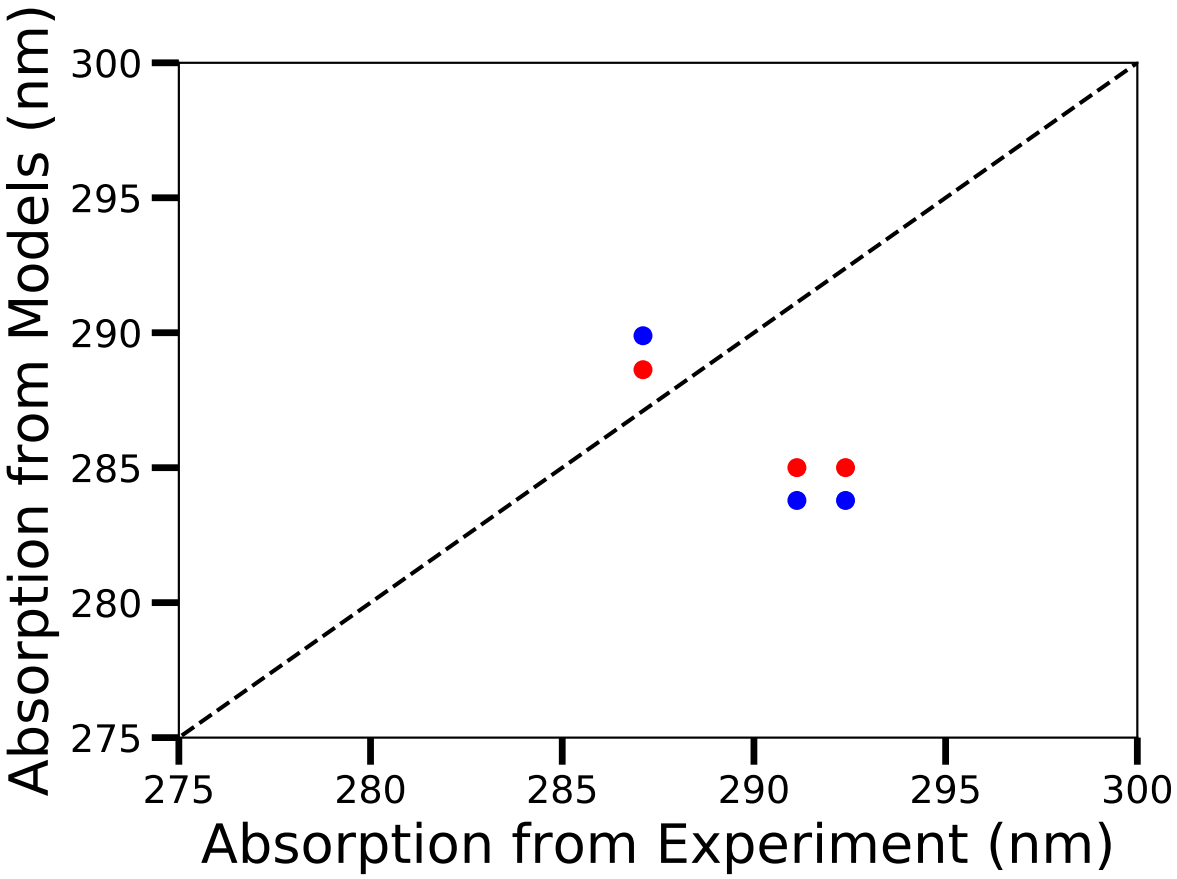

Figure 3.19: Absorption wavelengths of DMABN in solvent using nonpolarizable (red) and polarizable Drude (blue) force fields plotted against the available experimental data

Solvent	Nonpolarizable	Polarizable Drude	Experimental
Benzene	358.3	352.0	352.7 [60]
Diethylether	357.7	354.2	348.6 [131]
Trichloroethane	358.5	354.2	
Dichloroethane	356.1	354.2	
Acetone	356.2	354.6	
Ethanol	356.7	354.6	354 [8]
Methanol	355.2	355.2	
Acetonitrile	356.5	355.5	359.7 [131] 353 [8]
Dimethylsulfoxide	354.5	354.9	362.6 [60]
Water	352.4	365.0	

Table 3.8: Emission wavelengths of DMABN from nonpolarizable and polarizable Drude models compared to available experimental data

ethanol, acetonitrile and dimethylsulfoxide are listed alongside the emission wavelengths found for each solvent considered in this study with both the nonpolarizable and polariz-

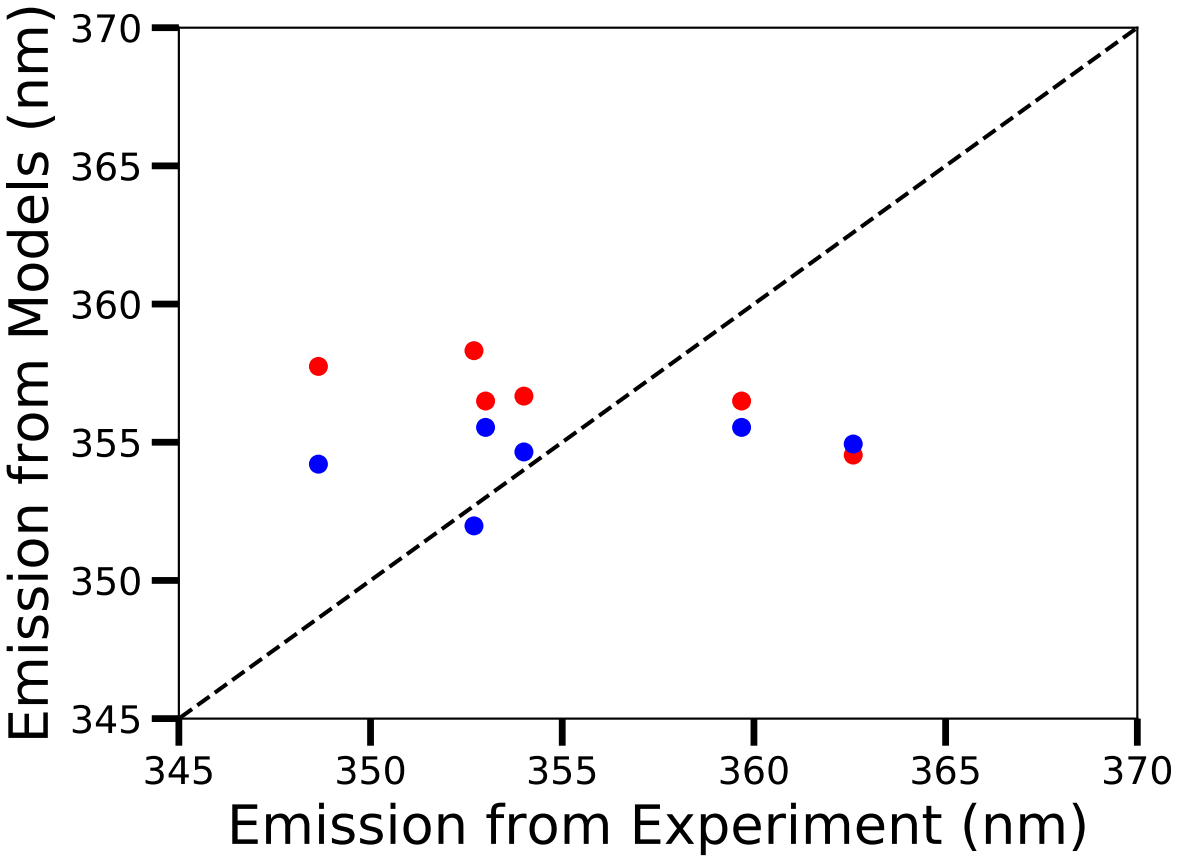

Figure 3.20: Emission wavelengths of DMABN in solvent using nonpolarizable (red) and polarizable Drude (blue) force fields plotted against the available experimental data

able Drude model in Table 3.8. Graphing the simulated emission data against the available experimental data results in Figure 3.20. It is immediately apparent that the polarizable Drude model has a closer approximation of the experimental wavelength in every case except for one of the values for acetonitrile: 359.7 nm.[131] The polarizable Drude model was particularly good at replicating the data for benzene, ethanol and for another reported emission of DMABN in acetonitrile (353 nm[8]) which all have very similar wavelengths ranging from about 352 to 355 nm. Overall the two simulated models differ much more in their calculated emission than they did in their absorption. This is particularly obvious when looking at benzene and diethylether. The experimental emission in benzene has been reported to be 352.7

nm[60] which is much closer to the polarizable Drude calculation of 352.0 nm than the 358.3 nm from the nonpolarizable model. Similarly, the experimental emission in diethylether has been reported to be 348.6 nm[131], which is closer to the 354.2 nm calculated with the polarizable Drude model than the 357.7 nm calculated with the nonpolarizable model.

Solvent	Nonpolarizable	Polarizable Drude	Experimental
Benzene	69.1	62.5	
Diethylether	69.1	64.3	61.5[131]
Trichloroethane	67.7	65.1	
Dichloroethane	68.9	66.3	
Acetone	71.2	67.9	
Ethanol	71.2	70.0	
Methanol	73.4	72.6	
Acetonitrile	71.5	71.8	67.3[131] 61.9[8]
Dimethylsulfoxide	73.5	71.5	
Water	75.2	90.6	

Table 3.9: Stokes shift of DMABN from nonpolarizable and polarizable Drude models compared to available experimental data

The available Stokes shift that can be directly compared to is only present if the experimental source reported both the absorption and emission wavelengths of DMABN in the given solvent, thus there are again only three experimental data points that correspond to solvents that were modelled. The Stokes shift from both the nonpolarizable and polarizable Drude model, as well as the available experimental data, are shown in Table 3.9 and graphed in Figure 3.21. The results between studies are often inconsistent: an example of this is apparent here in the Stokes shift where one study shows that in diethylether the Stokes shift is 61.5 nm[131] while in another study the Stokes shift in acetonitrile is practically identical at 61.9 nm.[8] Comparisons of the simulated models to experimental results is more appropriate for experimental results performed by the same study. Looking at the two Stokes shift from Neubauer et al. (61.5 nm in diethylether and 67.3 nm in acetonitrile), the polarizable Drude model better matches (64.3 nm in diethylether and 71.8 nm in acetonitrile) than the nonpolarizable model (69.1 nm in diethylether and 71.5 nm in acetonitrile). Considering how the polarizable Drude model was consistently closer to the available experimental emission wavelengths and that the absorption wavelengths are extremely similar between the two

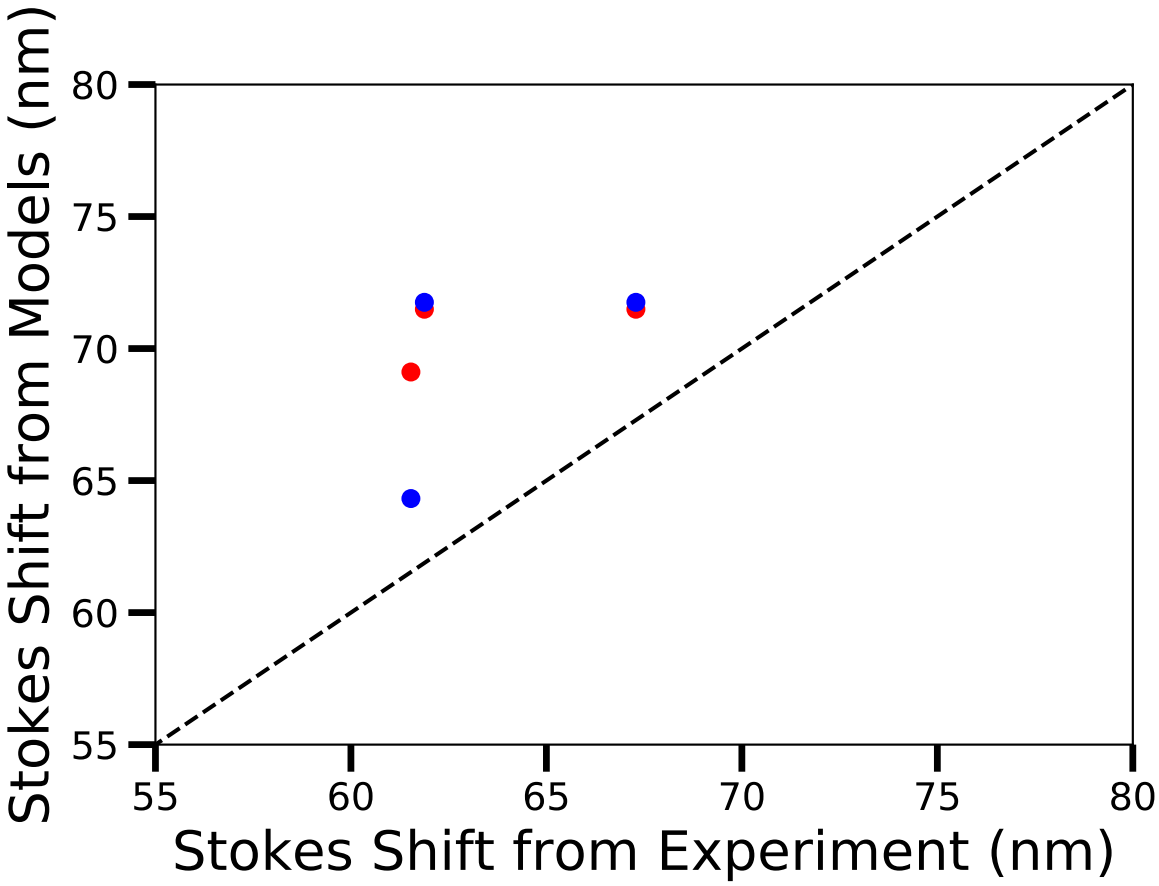

Figure 3.21: Stokes shift of DMABN in solvent using nonpolarizable (red) and polarizable Drude (blue) force fields plotted against the available experimental data

models, the polarizable Drude model better approximates the Stokes shifts as well.

3.6 Conclusion

This method of using force field files generated by GAAMP (supplemented with QM data of the excited state from CASSCF calculations) for molecular dynamics simulations has here been shown to be effective in modeling the transition between the ground and excited state of a molecule. The instantaneous electronic initial conversion is performed by manually switching the ground force fields for the corresponding excited force fields, while a short simulation afterwards simulates the relaxation of the Frank-Condon state to a relaxed excited

state. The inclusion of Drude particles further improves this representation, especially in regards to the interactions between DMABN and more polar solvents. Lippert plots allow for more direct comparison to other reports and a more visual representation of the effect of changing the surrounding solvent on the spectra of DMABN. Since the solvents are explicitly included in the systems, and not an implicit dielectric field imposing its polarizability on DMABN, their data points on the Lippert plot do not perfectly coincide with a straight line. But they do follow the general, expected trend of an increase in the Stokes shift with an increase in the polarizability of the surroundings. Though this series of MD simulations were performed for a relatively simple molecule that exhibits a small energy transition between its ground and first excited state, it can be clearly seen that this methodology can be applied effectively to more complex fluorescent probes and in more complicated environments.

CHAPTER 4

SIMULATING THE ABSORPTION AND FLUORESCENCE OF DI-8-ANEPPS IN DIFFERENT SOLVENTS

4.1 Introduction

Probe molecules are used to study the system they have been inserted into based on the observable changes in properties of the probe molecule itself in response to characteristics of that system. Ideally the probe gives consistent responses that are uncomplicated by other factors in the system. After it was observed that changes in fluorescence signals of dyes staining nervous tissues coincided with changes in membrane potential,[31,183] it became apparent that there could be such an organic molecule optimized for the purposes of monitoring that potential. These initial signals were too small to be used unless signal averaging was performed over a large membrane area, such was the case for a study with muscle fiber where a birefringence signal composed of the action potential and what was proposed to be the result of voltage shifts associated with calcium ion movement was investigated.[12] Early efforts to find a dye that exhibits a larger signal-to-noise ratio involved screening through hundreds of candidate molecules.[32,161]

Based on the molecules already known to exhibit some changes in their fluorescence as a function of membrane potential, attempts were made to actively design an optimal molecule for the monitoring of voltage changes across a membrane. Predictions of the optical properties of molecules was performed with simple molecular orbital theory calculations to characterize charge density in order to create probes that respond to membrane potential with primarily electronic rather than molecular movement.[112] This led to testing the spectral properties of a series of molecules based on the 4-(p-aminostyryl)-1-pyridinium (ASP) chromophore to verify the theoretical predictions and to find the version that can give consistent responses in a range of membrane preparations, especially in regards to interference

from chromophores intrinsic to those membranes.[111,114]

After branching out into more highly conjugated analogues of ASP, promising probes with a greater fractional change in their fluorescence signal were investigated such as RH160,[53] RH-421[54] and di-4-ANEPPS.[46] Di-4-ANEPPS has shown consistent potentiometric responses when tested in a wide variety of membrane environments: lipid vesicles, red blood cells, squid axon and guinea pig heart.[113] A relative fluorescence change for di-4-ANEPPS was found to be per 100 mV $9.52 \pm 0.02\%$ in A-431 cells, $8.6 \pm 1.4\%$ in rye protoplast, $3.7 \pm 2.0\%$ in a fungus spore, and $12.0 \pm 1.5\%$ in RBL cells.[55] Additional studies reported a change of 9% per 100 mV in a spherical lipid bilayer,[115] 9.5% per 100mV in HeLa cells,[43] up to 9% due to action potential amplitude (which is typically about 100 mV) in rat myocardium,[124] and 1% per 100mV in rat superior cervical ganglion.[21] A small adjustment was made to d-4-ANEPPS to improve its stability in a membrane and prevent it from being internalized: its hydrophobic carbon tails were extended from butane to octane to better anchor it with lipid tails.[110] Unsurprisingly, this new probe, called di-8-ANEPPS, has very similar spectral properties to di-4-ANEPPS.

These voltage-sensitive probes, designed to monitor changes in membrane potential, have been shown to also have a high sensitivity to solvent polarity. But it is difficult to distinguish the degree to which a given external factor influenced the perceived emissions when there are so many differences between the experimental systems the probe has been inserted into. With computational methods, it is possible to have complete control over the particular characteristics of the system and thus predict these interactions. This Chapter looks to investigate one of these probes, di-8-ANEPPS (di-8-amino-naphthyl-ethylene-pyridinium-propyl-sulfonate), by modeling each part of the transition between its ground and excited state surrounded by solvents of varying polarity with molecular dynamic simulations. This requires the direct assignment of the physical properties of the molecule (such as the bond lengths, angles, and dihedrals) as well as the partial charges for each atom of the molecule in its ground state

and in its excited state. GAAMP (General Automated Atomic Model Parameterization)[73] was used to prepare the initial parameter data, though additional revisions were made to tune the characteristics of the molecule to better match experiment. The ground and excited states of di-8-ANEPPS were simulated in a series of twelve solvents with increasing polarity to observe the probe's sensitivity to this property. Polarizable Drude force fields were also generated for the ground and excited state of di-8-ANEPPS to better account for the polar interactions within the molecule as well as between it and the surrounding solvent.

4.2 Theory

4.2.1 Molecular Characteristics of di-8-ANEPPS

The structure of Di-8-ANEPPS (shown in Figure 4.1) can be thought of as three overlapping sections: from the negatively charged sulfonate to the pyridinium nitrogen can be considered to be its head group, the conjugated pyridinium and naphthyl rings are the fused ring section, and the hydrophobic octane chains extending from the amino nitrogen are the tail group. In both its ground and excited state, di-8-ANEPPS is a zwitterion, meaning that it contains both a part that is strongly positive and a part that is strongly negative despite the overall molecule ultimately remaining neutral in charge. Regardless of state, the sulfonate at the top of the molecule is strongly negative. The difference between the states largely lies in the location of the corresponding positive charge that cancels this out. In the ground state, the positive charge is centralized on the pyridinium nitrogen, a placement that is separated from the negatively charged sulfonate by only a short propyl chain. Thus, the charge separation is relatively short and exists entirely in the head group of the molecule. In its excited state however, the conjugated structures of the pyridinium, ethylene and naphthyl rings allow for a flow of charge resulting in the positive center now being located on the amino nitrogen that spawns the two octane tails. As a result, the excited state has a much greater charge

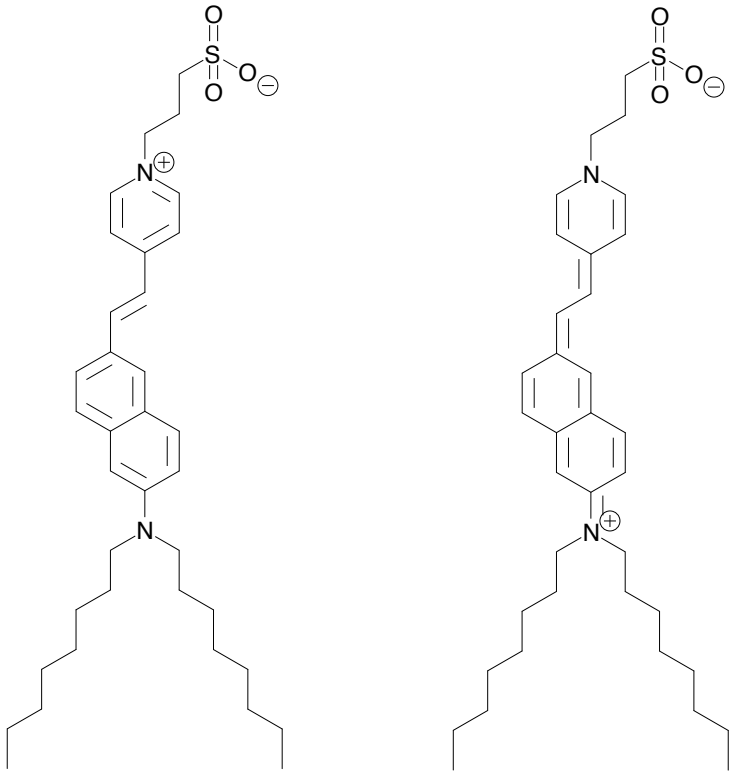

Figure 4.1: The Structure of di-8-ANEPPS (di-8-amino-naphthyl-ethylene-pyridinium-propyl-sulfonate) and a qualitative charge distribution of its ground and excited states.

separation and larger dipole that extends for the majority of the length of the molecule, only excluding the comparatively inactive carbon chains. The transition between states is entirely based on this charge transfer, and very little to no geometry rearrangements accompany it. The active site of the molecule, stretching from nitrogen to nitrogen, is largely immobile due to is conjugated structure.

4.2.2 Energy Calculations

Explanations of the energy calculations of the transition between the ground and excited state of di-8-ANEPPS in solvents are identical to those detailed in Chapter 3 of this Thesis for the investigation of DMABN in solvents. Details on how the energy terms were extracted

and analyzed can be found there, including the explanation of the empirically derived offset constants.

4.3 Methods

4.3.1 Parameterization of Di-8-ANEPPS

GAAMP (General Automated Atomic Model Parameterization)[73] was used to generate nonpolarizable and polarizable Drude force fields for the ground state of di-8-ANEPPS. This program is based on improving the partial charge assignments from either CGenFF (CHARMM General Force Field)[186] or GAFF (general Amber force field)[190] by fitting to electrostatic potential data from QM calculations and by fitting to the results of tests of compound-water interactions. Dihedral data is also optimized by fitting to the conformer energies resulting from a one-dimensional dihedral scan. Additionally, GAAMP can be used to generate polarizable force fields by adding and optimizing Drude particles. Drude particles are point charges that are tethered to a parent heavy atom via a harmonic spring that create a small distribution of the charge over each such atom. For comparison both nonpolarizable and polarizable Drude force fields are considered in this study. In actuality, a slightly shorter version of di-8-ANEPPS (di-4-ANEPPS) was parameterized directly with GAAMP just to cut down on the number of soft, flexible dihedrals that would need to be considered. The alkane chains were restored afterwards with parameters taken from saturated lipid tails that were then connected to the ends of the previously cleaved chains.

As with the parameterization of DMABN in Chapter 3, the excited state requires the generation of QM electrostatic potential data specifically representative of the desired state from another source that is then fit to by GAAMP's charge fitting procedure. Di-8-ANEPPS in particular has been studied before with CASSCF methods and simulated with mixed QM-MM methods.[158,168] The full pi system consists of 20 electrons and 19 orbitals, but

the computational study from Robinson et al. shows that the transition to the first excited singlet state can be fully represented by a CAS(6,6) (6 electrons and 6 orbitals) active space with a fragment of the full molecule.[158] The same procedure used to parameterize DMABN was applied to di-8-ANEPPS using ORCA.[128,129] Due to the transition from ground to excited states for both DMABN and di-8-ANEPPS involving reorganization of charge over the conjugated section, its active molecular orbitals largely concentrate their occupancy in pz atomic orbitals on those carbon (assuming the molecule lies in the $x-y$ plane). Because of this, it was easiest to recognize the molecular orbitals of interest by starting the molecule flat in the $x-y$ plane so that the desired reported occupancies were entirely of pz-character. Then the orbitals that are initially placed in the active space without any z-character can be rotated out in favor of the desired orbitals before continuing to converge the CASSCF calculation. Ultimately convergence was achieved at the def2-SVP def2-SVP/C level with orbstep SuperCi and switchstep DIIS convergence criteria included. The results of the CASSCF calculation of the isolated first excited singlet reflect the excited state after an instantaneous electronic transition from the ground state, meaning that the geometry of the molecule has not been updated since the initial ground state geometry optimization.

Initially attempts were made to replicate these orbital occupancies for the truncated structure used in the Robinson et al. study, which consists of only the fused ring section of the molecule (the rigid ring structure spanning from nitrogen to nitrogen without the propyl sulfonate or the octane chains).[158] The set of active space molecular orbitals all show high occupancy in a set of pz atomic orbitals located in the conjugated ring structure. Successfully characterizing the truncated molecule (shown in Figure 4.2) did not allow for an easy transition to utilizing the tools of GAAMP to convert the overall electrostatic potential surrounding the molecule to partial charges on each of its atoms. This cationic fragment does not account for contributions from the sulfonate that neutralizes the overall molecule. Additionally, defining the amino as primary rather than tertiary affects the treatment of all

dihedrals that include it and also affects the amino Nitrogen's accessibility when calculating its affinity as a hydrogen bond acceptor.

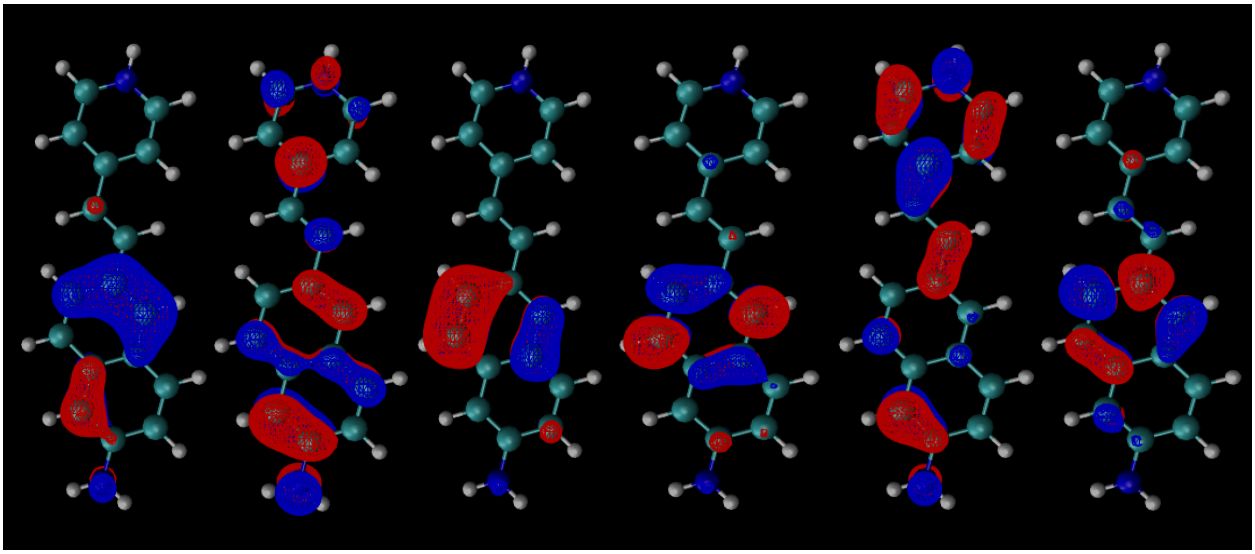

Figure 4.2: Active orbitals of the truncated di-ANEPPS fragment - converged to through CASSCF calculations

Repeating the procedure of calculating the QM electrostatic potential for di-4-ANEPPS (an identical structure to di-8-ANEPPS except that the carbon tails are shorter) was possible by rotating in the orbitals known to be in the active space for the truncated structure into the active space of this molecule. The orbitals of the active space for the excitation of di-4-ANEPPS to its first excited singlet state are shown in Figure 4.3. Then the same GAAMP steps as were used for DMABN in Chapter 3 were used for di-4-ANEPPS: running through all of the steps for the ground state and only using GAAMP's electrostatic potential fitting protocol for the excited state. GAAMP is designed for small molecules meaning that the sheer number of soft dihedrals (dihedrals that are identified to have a wide range of motion) present in the di-8-ANEPPS molecule would make the calculation very expensive. Because the important and more unique characteristics of the probe are entirely contained within the head group and fused ring structure, it was best to shorten the carbon tails for this step. Additionally, the electrostatic data generated with CASSCF was for the di-4-

ANEPPS structure, making it far more convenient to convert the molecule back into di-8-ANEPPS after the GAAMP portion of the procedure. Since even di-4-ANEPPS is a larger molecule than DMABN, the number of unique discrete calculations of the molecule with a perturbing charge is naturally more (one hundred sixty-four). There are more soft dihedrals to contend with, mostly occurring along the butane chains. And more hydrogen-bond acceptor calculations with test water molecules were necessary, three around the oxygen in the sulfonate head group and one for the amino nitrogen.

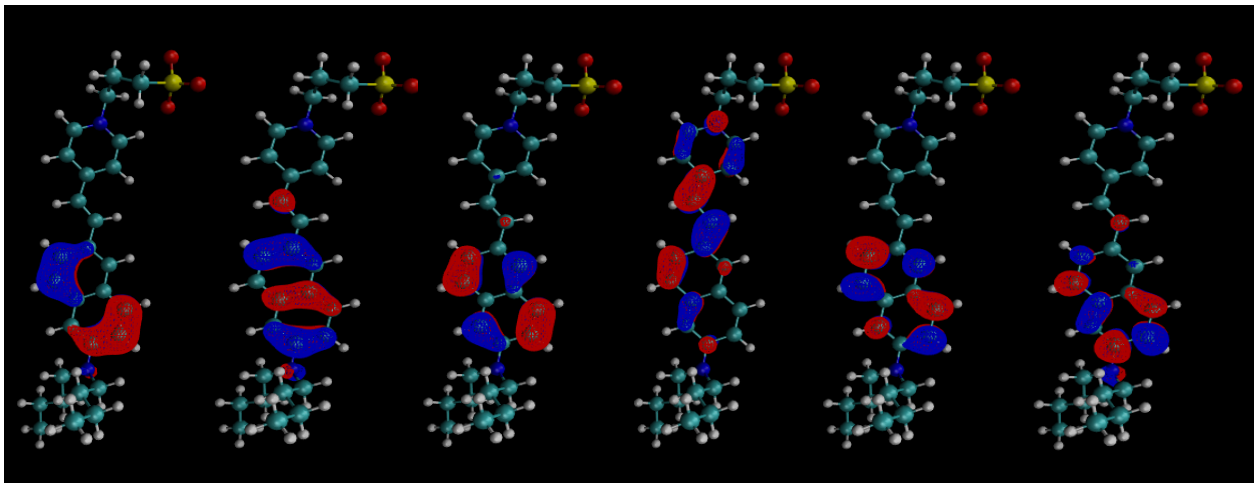

Figure 4.3: Active orbitals of di-4-ANEPPS - converged to through CASSCF calculations

Correcting these results to be for di-8-ANEPPS rather than di-4-ANEPPS was done at the very end of the GAAMP fitting steps since the extended carbonyl chains would not have any impact on the partial charges of the sulfonate or the conjugated rings. The modification to extend the butanes to octanes was a matter of taking the partial charge and geometrical parameter data from saturated lipid tails and essentially replacing one of the terminating hydrogen with the extended carbon chain. Some minor manual alterations were made to the partial charges of the previously terminating methyl to ensure everything is neutral. This was the same method used for the ground state extension from di-4-ANEPPS to di-8-ANEPPS, since the properties at the end of the alkane chains should not experience any electronic changes during absorption or emission.

Ultimately it was found that the Drude version of the parameters produced in this way did not behave as expected: after simulating them in various solvents the resulting trends were entirely inconsistent with the nonpolarizable model and with experimental data. The behavior of the simulated di-8-ANEPPS as represented by polarizable Drude force fields was extremely sensitive to even the slightest changes to its parameters. Considering the success that was found with the nonpolarizable di-8-ANEPPS in replicating the changes in the Stokes shift in solvents of varying polarity and in a simple membrane with varying voltage, a new version of the polarizable Drude parameters was generated. Instead of allowing the partial charges to be altered during the course of fitting the electrostatic potential data to create the polarizable Drude particles, the partial charges on each atom were held constant. Thus, the only difference between these two sets of ground state parameters is the inclusion of the Drude particles themselves, in other words the inclusion of polarizability terms. The same is true of the relationship between the nonpolarizable and polarizable Drude excited state parameters used in this work.

The truncated structure of di-8-ANEPPS was found by Robinson et al. to have a ground state dipole of 14.9 Debye and an excited state dipole of 3.4 Debye via a CASSCF(6,6) calculation.[158] The initial attempts to replicate the isolation of the correct orbital occupancies performed with a CASSCF(6,6) calculation, resulted in dipoles of 17.28 Debye and 4.56 Debye for the truncated structure. Another QM/MM study reported that for the full structure of the ground state dipole as 36.7 ± 2.7 Debye and the excited state dipoles as 48.3 ± 2.6 Debye (a change of 11.4 ± 1.7 Debye).[168] Using CASSCF(6,6) for the di-4-ANEPPS structure, dipoles of 22.34 and 33.14 Debye for the ground and excited state respectively were found, which exhibits a very similar change of 10.80 Debye. After generating parameter files with GAAMP based on this data and converting it to di-8-ANEPPS the change in dipole is largely maintained. The nonpolarizable force fields produce dipoles of 31.23 and 41.40 Debye for the ground and excited state, which is a change of 10.17 Debye. The final version

of the polarizable Drude force fields report dipoles of 28.71 Debye for the ground state and 37.59 Debye for the excited state, a difference of 8.88 Debye. The dipole calculation of the Drude parameter set can be converted to the exact same values as the nonpolarizable set if the Drude particles are restrained to the same coordinates as their respective parent atoms, effectively recreating the nonpolarizable point charges.

4.3.2 Simulations in Solvent

The molecular dynamics simulations of the ground and excited state of di-8-ANEPPS in solvents and their subsequent analysis follows the same procedure that was detailed in Chapter 3 of this thesis for the simulations of DMABN in solvents. The same ten solvents are used here, with the addition of chloroform and dichloromethane bringing up the total to twelve total solvents considered. The properties of these solvents as represented by both nonpolarizable and polarizable Drude force fields are reported and discussed in Chapter 2 of this Thesis.

4.4 Results

Di-8-ANEPPS was initially analyzed in the presence of the same set of ten solvents that were used for DMABN in Chapter 3, with nonpolarizable and polarizable Drude parameters generated for the ground and excited state. Two additional solvents: chloroform and dichloromethane were later included to directly compare to solvents seen in other work. In experimental studies, there is a marked decrease in the wavelength of the absorption with an increase in dielectric. The emission wavelength on the other hand is shown to increase in general but for solvents like water, there is a drastic drop. This is likely due to di-8-ANEPPS not being especially soluble in water. Di-8-ANEPPS has a flexible propyl tethering the polar sulfonate group to its comparably rigid conjugated ring structure composed of a pyridinium, ethylene and naphthyl ring which ends in an amino group with octane carbon tails. The pa-

rameters derived for this molecule do allow for some lateral twisting of the rings but is largely flat while the other parts are much more flexible. The charge separation greatly increases for the excited state version of the molecule, so greater variation in the exact conformation is to be expected. Greater interaction with the more polar solvents is also expected for the excited state of the molecule for this reason.

The generation of the Drude force fields was fraught with difficulty as the system was highly sensitive to slight changes in the partial charge distribution and the polarizabilities ascribed to each heavy atom. Additionally, each oxygen introduced the need for two lone pairs to be added to the system that resulted in an overly negative region of the molecule that interfered with measuring its other properties. In order to highlight the benefits of using a polarizable Drude parameter set, the differences between the two parameters sets was minimized. The partial charges are identical between the polarizable Drude and nonpolarizable parameters and the lone pairs are entirely cleaved from the molecule. The polarizabilities of each heavy atom (which determines how much of the charge is siphoned to the Drude particles) was calculated by using the charge fitting steps of GAAMP. So, in the case of the excited state, the electrostatic potential data derived from CASSCF calculations was fit to the excited state nonpolarizable partial charges. Thus, geometry is not updated between models and their only difference lies in the Drude particles tethered to each heavy atom.

The twelve solvents used for this study are (in order of increasing dielectric): benzene, diethylether, chloroform, 1,1,1-trichloroethane, dichloromethane, 1,1-dichloroethane, acetone, ethanol, methanol, acetonitrile, dimethylsulfoxide and water. The work of Le Goff et al. has a similar line up of solvents that encompass a similar range of dielectric with their set that includes many of the same solvents: chloroform, dichloromethane, hexanol, 2-propanol, acetone, ethanol, methanol, acetonitrile, ethanolamine, and water.[94] Our results will be most directly compared to this study. Additional experimental data from Matson et al. studies the effects of various alcohol solvents (and water) on the fluorescence cycle of di-8-ANEPPS.[119]

Another resource compared to is the work of Čmiel et al. which has data on a smaller pool of solvent systems and notably investigate di-4-ANEPPS instead.[29] Di-4-ANEPPS and di-8-ANEPPS only differ in the length of their carbon chains (either butane or octane), the active site of the molecule along its conjugated fused ring structure and the highly electronegative sulfonate group are identical and thus have extremely similar spectral properties.

4.4.1 Nonpolarizable Solvent Models

The parameters were built with a focus on accurately describing the shift in the dipole over the course of the transition to allow for the observation of the electrostatics of the surrounding environment. Other contributing factors to the energy calculations such as slight geometry differences and vibrational transitions are accounted for with two offset constants, one for the absorption and one for the emission. An estimation of the offset needed to convert the raw NAMD[144] simulation energy data into energies that reflect the actual transitions can be extracted by comparing the transition energy as calculated by CASSCF and in vacuum by molecular dynamics. In CASSCF, the energy between the ground and excited state of the truncated structure (where the molecule consists only of the conjugated ring structure spanning between and including the two Nitrogen) was found to be 63.390 kcal/mol. This calculation was repeated for di-4-ANEPPS which includes the added complication of the propyl sulfonate and butane, resulting in an energy of 85.366 kcal/mol. For both of these calculations, the molecule was in a flat posture in terms of its conjugated rings in the $x-y$ plane. Simulating the nonpolarizable ground and excited state parameters independently in vacuum and taking the difference in that energy yielded 36.081 kcal/mol. Taking the difference between the CASSCF transition energy of di-4-ANEPPS and the NAMD molecular dynamics estimation from the parameter sets results in 49.285 kcal/mol (27.309 kcal/mol when using truncated CASSCF data instead). In either case, this shows that the offset is expected to be significantly smaller for the di-8-ANEPPS energies

than it was for the DMABN energies. The exact offset used is determined by minimizing a chi square estimation of the seven solvents in common between those in this study and investigated by Le Goff et al. (chloroform, dichloromethane, acetone, ethanol, methanol, acetonitrile, and water).[94] This results in the offsets for the nonpolarizable model being 4.990 kcal/mol for the absorption energy and 10.044 kcal/mol for emission.

Solvent	All	stddev	error	Di8A	stddev	error	Interaction	stddev	error
Benzene	51.7	2.6	0.2	45.7	2.1	0.1	6.0	1.7	0.1
Diethylether	54.5	3.2	0.1	46.6	2.2	0.1	7.9	2.5	0.1
Chloroform	52.0	3.3	0.3	46.9	3.3	0.4	5.1	2.3	0.2
Trichloroethane	50.6	2.9	0.1	46.0	2.1	0.1	4.6	2.0	0.1
Dichloromethane	53.4	3.3	0.3	44.9	4.1	0.7	8.6	3.1	0.4
Dichloroethane	53.1	3.4	0.4	45.7	4.0	0.8	7.5	3.0	0.5
Acetone	58.3	3.5	0.1	45.7	2.2	0.1	12.7	2.9	0.1
Ethanol	58.9	3.7	0.2	40.6	2.5	0.2	18.3	3.5	0.3
Methanol	59.6	3.7	0.2	40.2	2.2	0.1	19.4	3.3	0.2
Acetonitrile	57.5	3.3	0.1	44.8	2.3	0.1	12.8	2.9	0.1
Dimethylsulfoxide	61.5	3.7	0.2	44.5	2.5	0.2	17.0	3.4	0.3
Water	60.5	3.9	0.1	43.8	2.4	0.1	16.6	3.6	0.1

Table 4.1: Absorption energy of di-8-ANEPPS in solvent using nonpolarizable force fields - energies include added offset

In Table 4.1 it can be seen that the range of the absorption energies from benzene to water is about 9 kcal/mol, which corresponds to a difference of about 77 nm in wavelength. This is a bit of an underestimate when compared to the range reported in Le Goff et al.'s work, which shows a change of 92 nm between chloroform and water.[94] Čmiel et al.'s work shows a decrease in wavelength of 40 nm between chloroform and dimethylsulfoxide[29] and Matson et al. shows a decrease in wavelength of 35 nm between decanol and water.[119] The trend of the absorption data from the nonpolarizable model lines up correctly, the absorption wavelength decreases with increasing the dielectric constant of the solvent and the magnitude is reasonably similar as well.

Graphing the energy differences from Table 4.1 as histograms in Figures 4.4 and 4.5 allows for a visualization of the average total energy difference (the first column) shifting with the increase in the solvent polarity. It also displays the variance in that average, which is slightly larger for the solvents with greater polarity. The middle column shows the histograms of

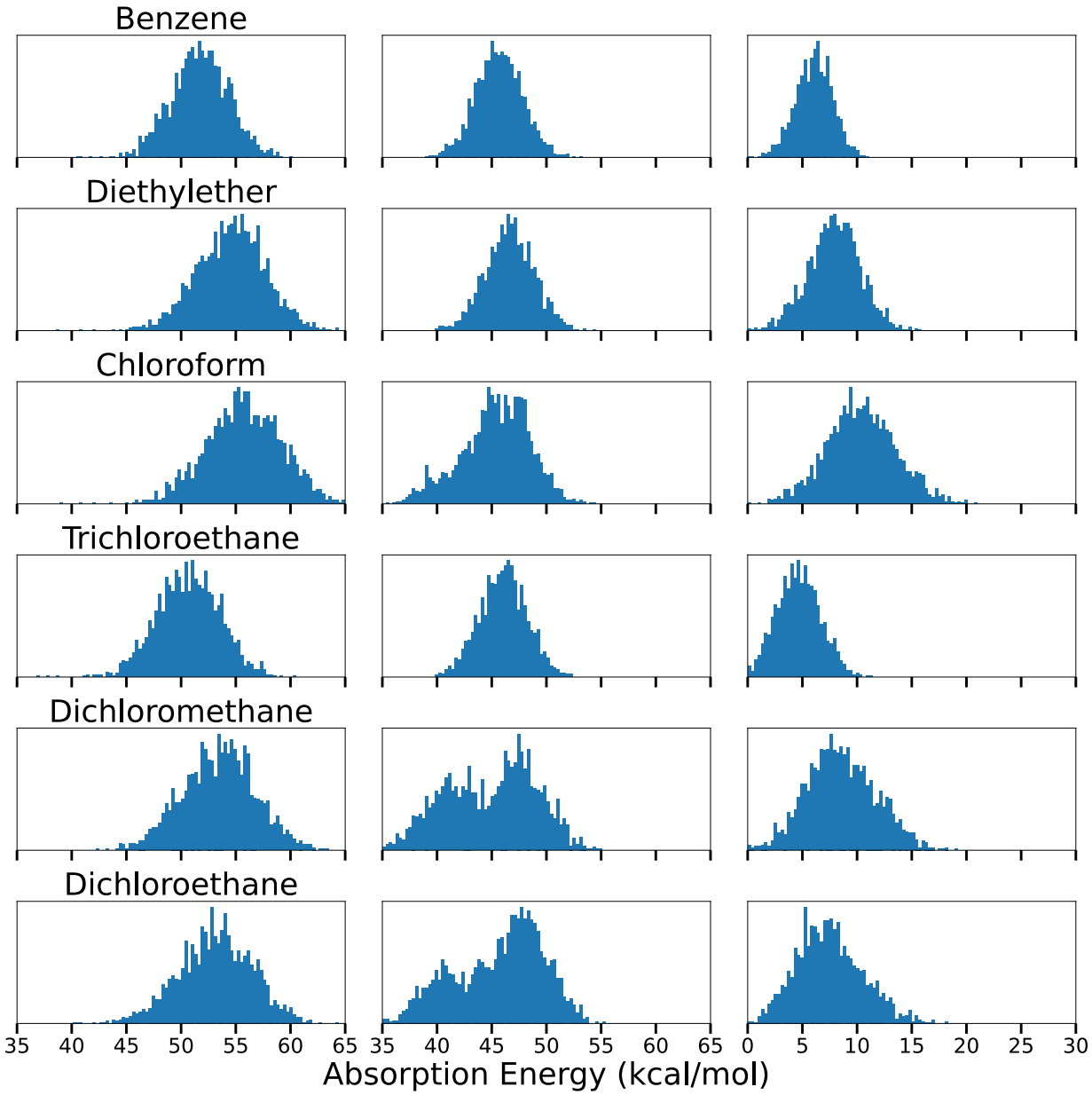

Figure 4.4: Histograms of the absorption energy of di-8-ANEPPS in solvent using nonpolarizable force fields Part 1 - left is the total absorption energy, middle is the absorption energy of just di-8-ANEPPS, and right is the absorption energy of the interaction between di-8-ANEPPS and the respective solvent

the energy difference of the isolated di-8-ANEPPS, which is computed by extracting the conformation of di-8-ANEPPS for each frame of the trajectory and calculating the energy of just that molecule with the ground and excited state parameters in vacuum. There are some shifts in the histogram of the isolated di-8-ANEPPS, which indicates that different geometries

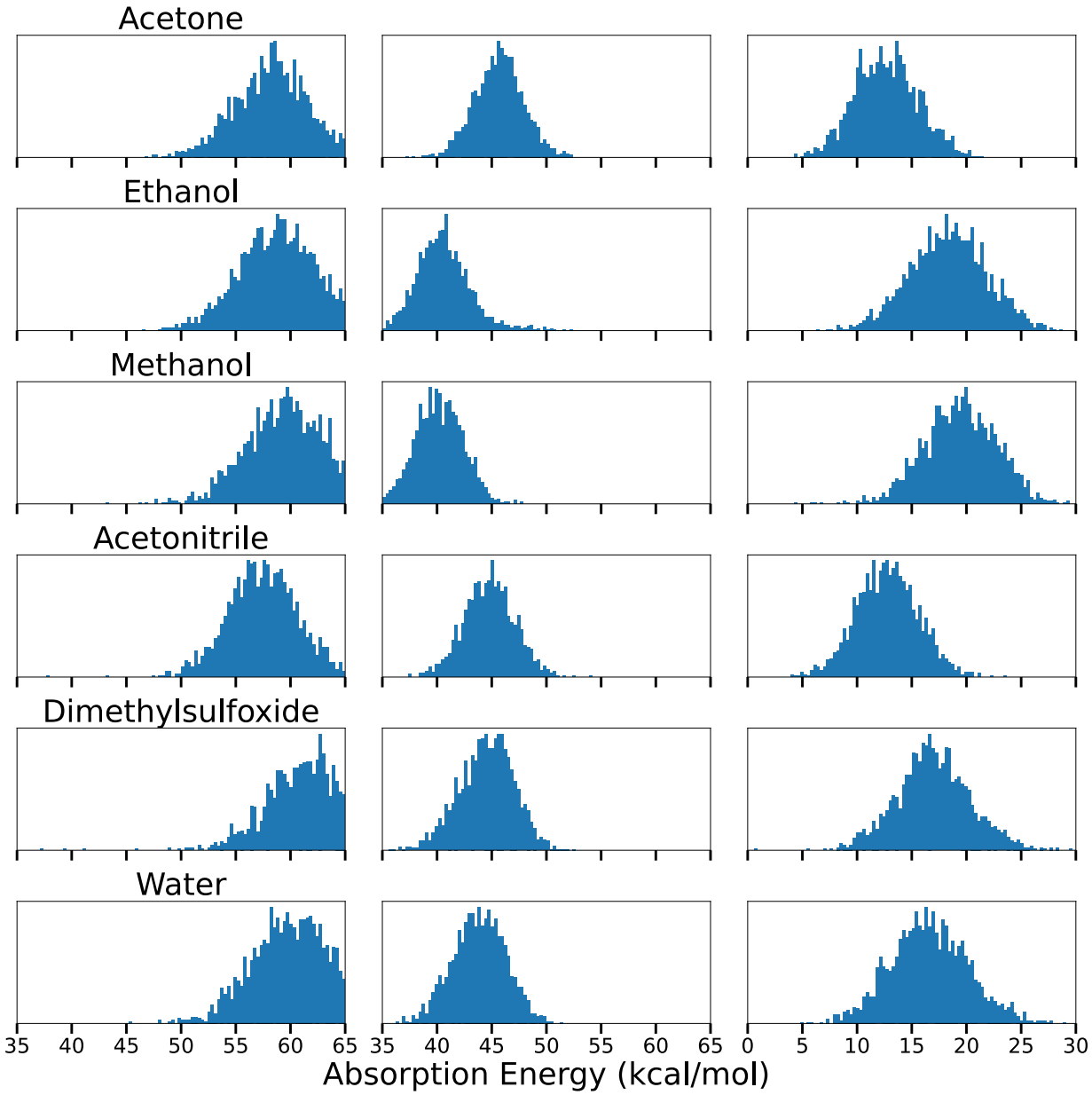

Figure 4.5: Histograms of the absorption energy of di-8-ANEPPS in solvent using nonpolarizable force fields Part 2 - left is the total absorption energy, middle is the absorption energy of just di-8-ANEPPS, and right is the absorption energy of the interaction between di-8-ANEPPS and the respective solvent

were more common in different solvent environments resulting in slightly different reported average energy absorption. The change in the peaks is only about 1 kcal/mol, but that definitely affects the shape of the data in the final column of histograms. The presence of two overlapping peaks in the histogram depicting the isolated di-8-ANEPPS energy absorption

is indicative of two common geometries sampled over the course of the simulation. The key feature differentiating them is whether the sulfonate head group is interacting more with the solvent or bent over towards the rest of the di-8-ANEPPS molecule. As an example, in the histogram of di-8-ANEPPS isolated from its simulation in 1,1-dichloroethane in the final row of Figure 4.4: the peak with higher energy corresponds to snapshots of the molecule where the sulfonate is bent towards the rest of the molecule and the peak with lower energy corresponds to when the sulfonate is not as bent. The third column of histograms shows the interaction energy between the di-8-ANEPPS and the solvent, which is calculated by subtracting the isolated di-8-ANEPPS energy difference from the total energy difference. Since the values of the isolated di-8-ANEPPS energy difference slightly decreases with increasing solvent polarity while the total energy is increasing, the resulting interaction energy difference shows a slightly greater range of energy differences with increasing solvent polarity than the total energy difference.

Solvent	All	stddev	error	Di8A	stddev	error	Interaction	stddev	error
Benzene	44.9	2.8	0.2	44.0	2.3	0.1	0.9	1.8	0.1
Diethylether	40.9	3.2	0.1	40.2	2.0	0.1	0.7	2.8	0.1
Chloroform	40.3	3.0	0.3	40.0	2.4	0.3	0.3	2.4	0.2
Trichloroethane	41.7	3.1	0.3	43.7	2.6	0.3	−2.0	2.2	0.1
Dichloromethane	40.6	3.1	0.1	39.6	2.1	0.1	1.0	2.6	0.1
Dichloroethane	40.5	3.0	0.1	39.5	2.1	0.1	1.1	2.4	0.2
Acetone	41.5	3.6	0.2	40.7	2.7	0.4	0.8	3.3	0.2
Ethanol	42.7	3.5	0.2	42.7	2.4	0.1	−0.0	3.0	0.2
Methanol	42.7	3.7	0.1	40.0	2.4	0.2	2.7	3.4	0.2
Acetonitrile	41.3	3.6	0.1	39.8	2.3	0.2	1.6	3.2	0.2
Dimethylsulfoxide	43.9	3.8	0.2	43.1	2.3	0.1	0.8	3.4	0.2
Water	43.0	3.7	0.1	40.9	2.6	0.4	2.2	3.5	0.3

Table 4.2: Emission energy of di-8-ANEPPS in solvent using nonpolarizable force fields - energies include added offset

In contrast, Table 4.2 shows that the emission wavelengths do not exhibit a consistent increase or decrease between solvents of increasing dielectric. This is true for both the results of this work as well as in experimental studies. In Le Goff et al.'s work the emission reported for the lowest dielectric solvent and the highest dielectric solvent considered differ by only by 7 nm, even though the range of this data is 57 nm with acetonitrile having the largest emission

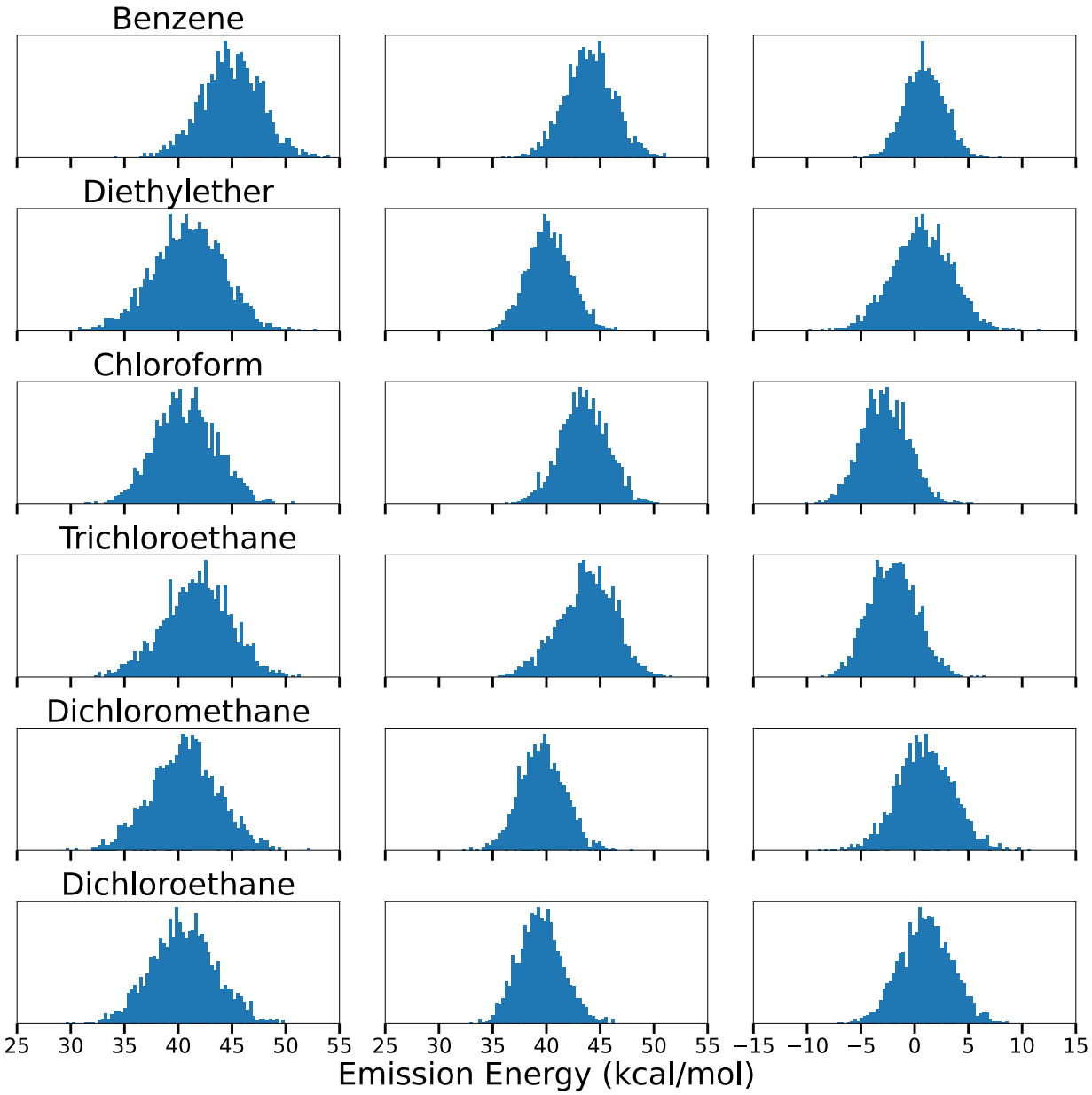

Figure 4.6: Histograms of the emission energy of di-8-ANEPPS in solvent using nonpolarizable force fields Part 1 - left is the total absorption energy, middle is the absorption energy of just di-8-ANEPPS, and right is the absorption energy of the interaction between di-8-ANEPPS and the respective solvent

wavelength and water having the lowest.[94] The work of Čmiel et al. (which is again for di-4-ANEPPS) shows an increase of 39 nm from chloroform to dimethylsulfoxide, but methanol is reported as having the highest emission wavelength.[29] And for Matson et al. the lowest and highest dielectric solvent differ by 12 nm, but the range is 61 nm with methanol having the

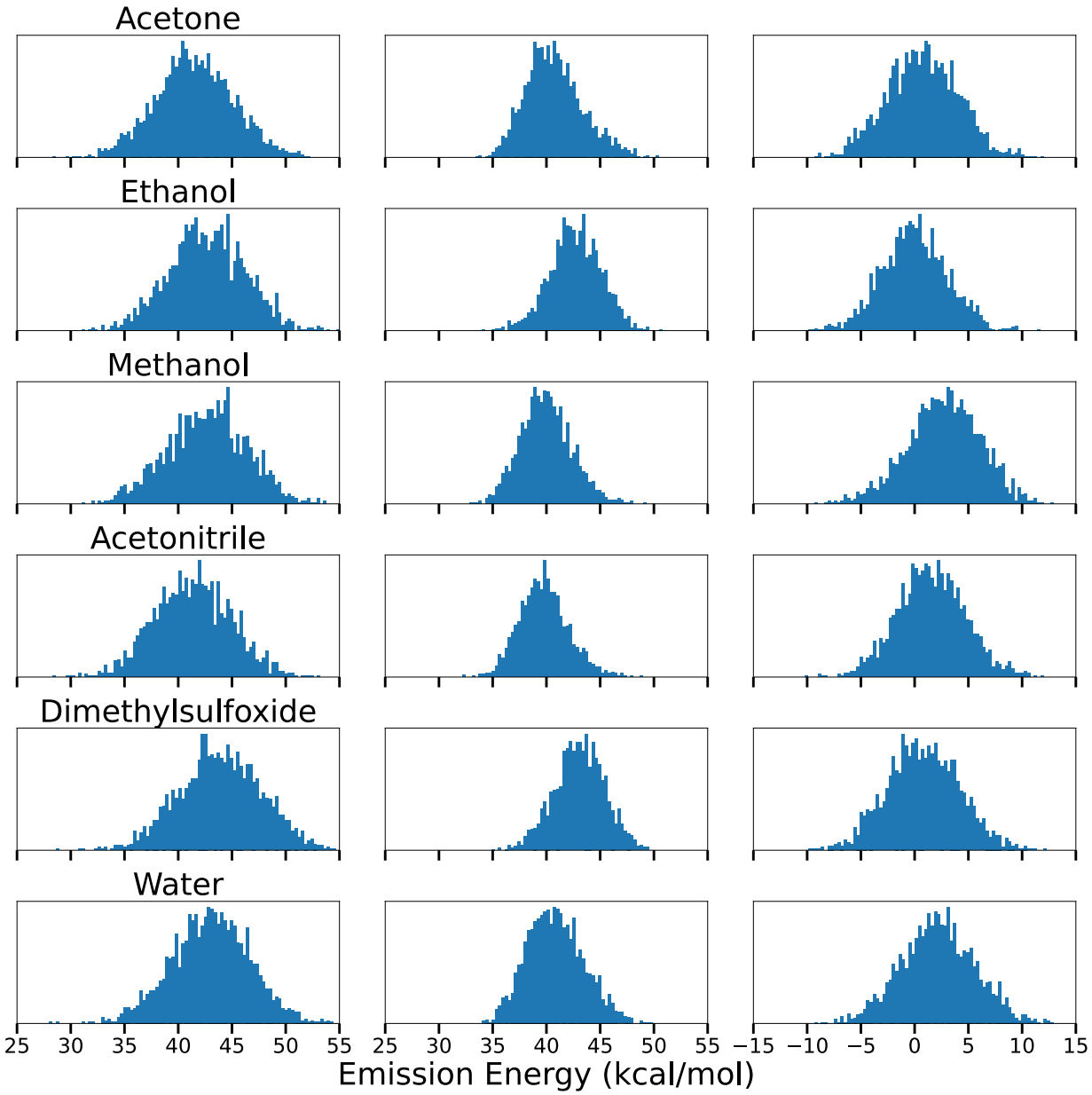

Figure 4.7: Histograms of the emission energy of di-8-ANEPPS in solvent using nonpolarizable force fields Part 2 - left is the total absorption energy, middle is the absorption energy of just di-8-ANEPPS, and right is the absorption energy of the interaction between di-8-ANEPPS and the respective solvent

largest emission wavelength and decanol being the lowest.[119] This seems to indicate that in general there is an overall increase in the emission wavelength with increased dielectric with some exceptions, especially with regards to water. The drop in the reported wavelength for water could be explained by the poor solubility of di-8-ANEPPS in water. Similar to the

experimental data, the emission wavelengths do not consistently increase with the increasing dielectric of the solvent. The range of this data is 68 nm, while the lowest and highest solvent dielectric produced di-8-ANEPPS emission wavelengths differing by only 27 nm.

The histograms produced based on the emission energies for nonpolarizable di-8-ANEPPS in Figures 4.6 and 4.7 do not show an obvious trend in the shift of the average energies, although the standard deviation does generally increases with increasing solvent polarity. There is some variation in the histogram of the energy difference for the extracted di-8-ANEPPS, but the separation into two peaks based on the proximity of the sulfonate head group with the rest of the molecule is not seen. This can be explained by the fact that these emission energies are based on simulations performed with the excited state parameters for di-8-ANEPPS, meaning that the localized positive charge that was on the pyridinium nitrogen during the ground state simulations is now spread out and further from the negatively charged sulfonate.

Solvent	Absorption	Emission	Stokes Shift
Benzene	552.9	636.5	83.6
Diethylether	524.5	698.9	174.4
Chloroform	549.6	709.6	160.0
Trichloroethane	564.7	685.5	120.8
Dichloromethane	535.1	704.7	169.6
Dichloroethane	538.2	705.9	167.7
Acetone	490.1	689.1	199.0
Ethanol	485.4	670.2	184.8
Methanol	479.6	670.2	190.6
Acetonitrile	497.1	691.8	194.7
Dimethylsulfoxide	465.2	651.3	186.1
Water	473.0	664.9	191.9

Table 4.3: Wavelengths of absorption, emission and Stokes shift of di-8-ANEPPS in solvent using nonpolarizable force fields

Looking at the comparison of absorption, emission and Stokes shift wavelengths in Table 4.3, the more polar solvents have a much greater Stokes shift than a solvent like benzene. Although most of these solvents report very similar wavelengths, there is still a clear trend. When graphing the Stokes shift (the difference between the absorption and emission wavelengths) the general positive trend in terms of increasing orientation polarizability is clearly

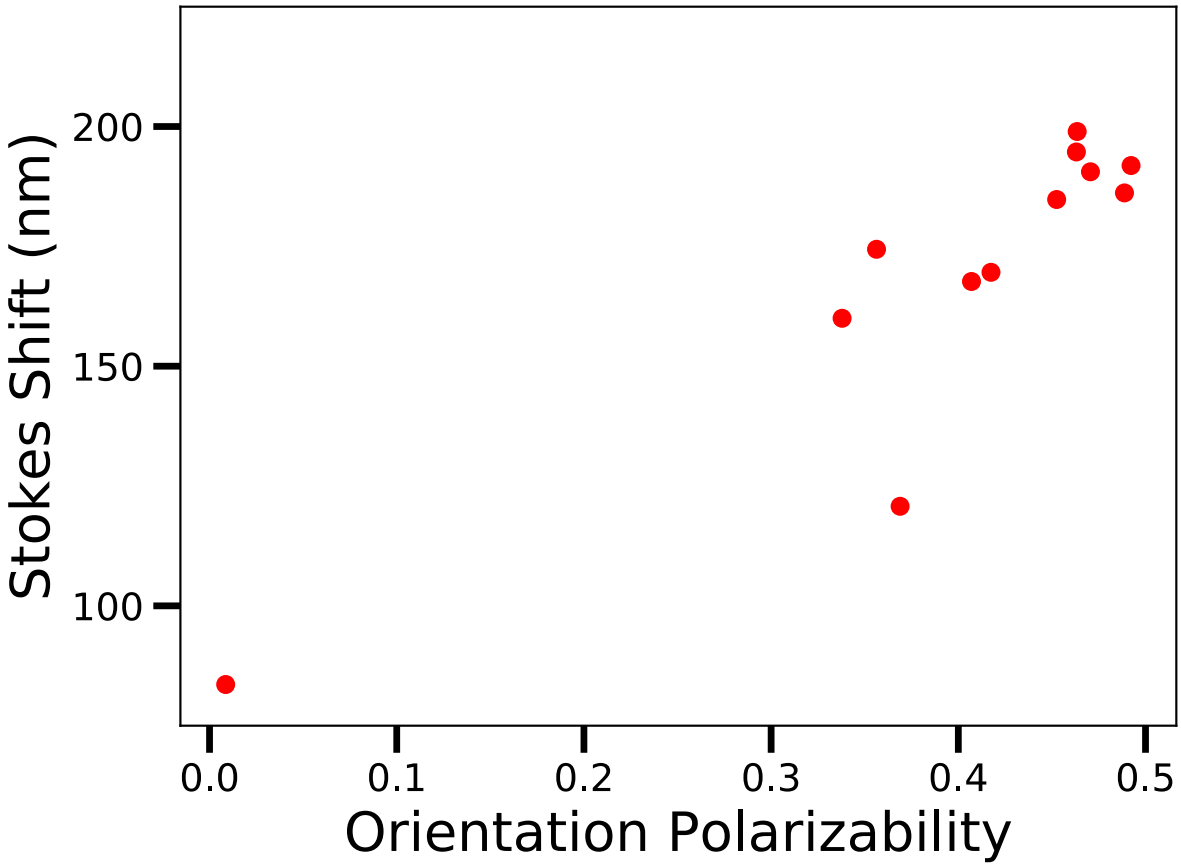

Figure 4.8: Lippert plot of Di-8-ANEPPS in twelve solvents using nonpolarizable force fields

overall linear as seen in Figure 4.8.

4.4.2 Polarizable Drude Solvent Models

A similarly small offset is expected to be appropriate for correcting the polarizable Drude data, considering the similarity between the two models. The molecular mechanics estimation of the the transition energy between the ground and excited parameters sets simulated in vacuum was found to be 35.013 kcal/mol. Subtracting this from the QM estimation from CASSCF from the truncated structure results in 28.376 kcal/mol and from di-4-ANEPPS structure results in 50.353 kcal/mol. As before, the exact values used as the absorption and emission offsets for this parameters set was determined by fitting this data to the data for

the seven solvents in common analyzed in Le Goff et al.'s work[94] which resulted in offsets of 5.303 kcal/mol for the absorption and 7.554 kcal/mol for the emission. These offsets are exceedingly close to what was calculated for the nonpolarizable version, which is to be expected considering how the polarizable Drude parameters set was designed to differ from the nonpolarizable parameters only by the addition of polarizabilities to the same set of partial charges.

Solvent	All	stddev	error	Di8A	stddev	error	Interaction	stddev	error
Benzene	56.3	3.6	0.3	51.6	4.7	0.4	4.7	2.1	0.2
Diethylether	54.9	2.7	0.1	50.2	2.3	0.1	4.8	1.9	0.1
Chloroform	52.5	2.4	0.1	50.1	2.3	0.1	2.4	1.3	0.0
Trichloroethane	55.0	3.2	0.2	51.8	3.6	0.2	3.2	1.7	0.1
Dichloromethane	56.2	3.2	0.1	51.7	3.5	0.2	4.5	2.0	0.1
Dichloroethane	55.9	3.0	0.1	51.2	3.1	0.2	4.7	1.9	0.1
Acetone	57.1	2.9	0.1	49.8	2.3	0.1	7.2	2.3	0.1
Ethanol	58.2	3.3	0.1	42.0	2.9	0.2	16.1	3.2	0.2
Methanol	58.5	3.5	0.2	43.2	4.2	0.4	15.3	3.9	0.3
Acetonitrile	57.8	3.8	0.2	45.1	5.3	0.5	12.7	3.7	0.3
Dimethylsulfoxide	59.7	3.8	0.2	44.1	5.2	0.5	15.6	4.1	0.3
Water	60.2	3.6	0.1	44.1	3.8	0.3	16.1	4.3	0.3

Table 4.4: Absorption energy of di-8-ANEPPS in solvent using polarizable Drude force fields - Drude particles are minimized and energy includes added offset

In Table 4.4 the absorption data for the polarizable Drude force fields was found to have a range of 7.7 kcal/mol (67 nm), which is actually narrower than was seen for the nonpolarizable parameter set despite the extreme similarity between the two models. Looking at just the seven solvents that Le Goff et al. has in common with this study (chloroform, dichloromethane, acetone, ethanol, methanol, acetonitrile, water),[94] the absorption wavelengths calculated with the polarizable Drude parameters differ from their experimental values for each solvent by about 3 to 23 nm. The smallest difference is for chloroform and the largest for dichloromethane. The range from chloroform to water is larger in Le Goff et al.'s experimental data than seen for the polarizable Drude set by about 20 nm, but if the range from chloroform to acetonitrile is considered instead the difference is only about 8.7 nm. The percent error between each solvent's absorption wavelengths averages to be about 2.36%. The largest difference is seen for the dichloromethane model at 4.28% and the lowest

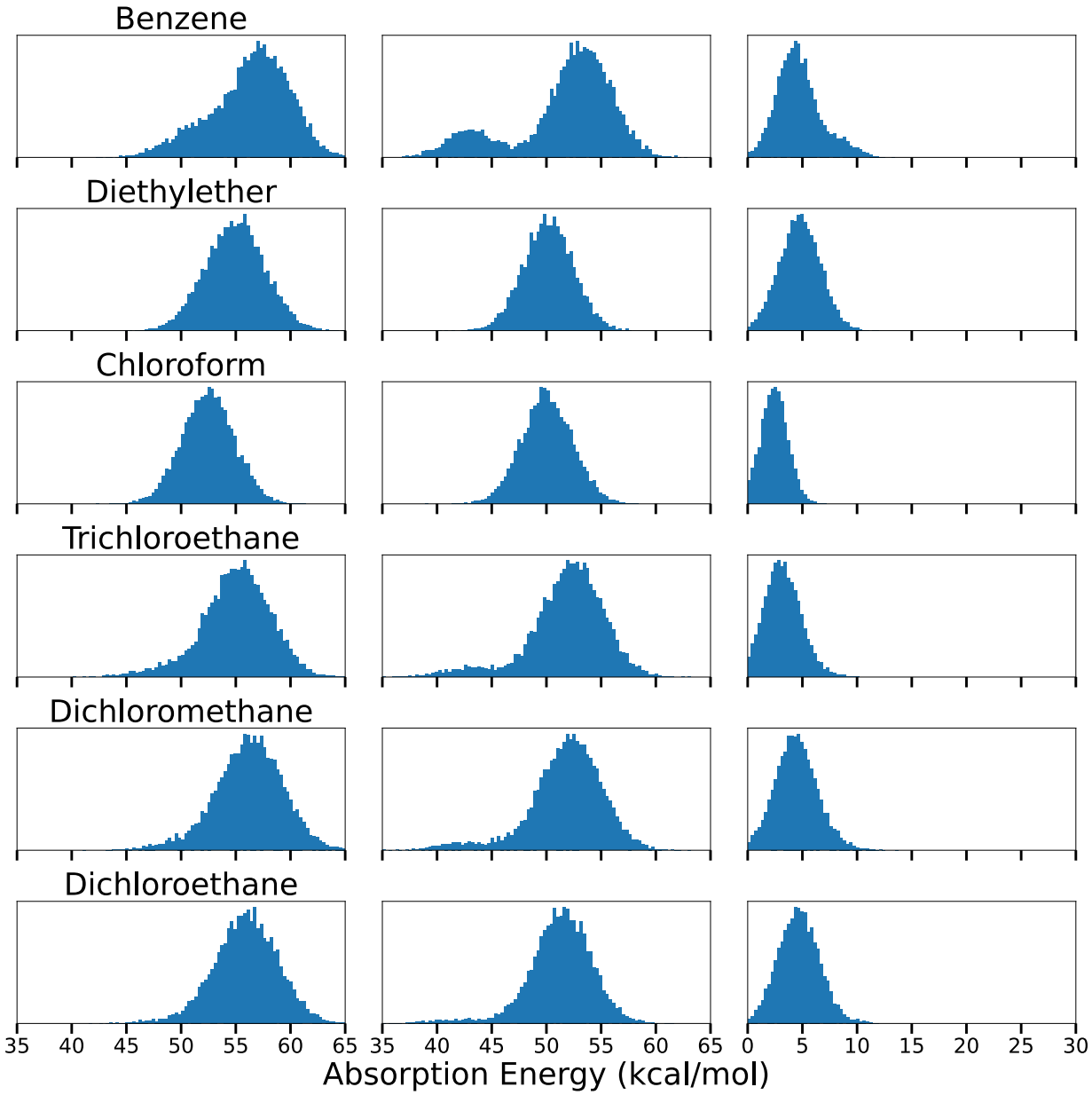

Figure 4.9: Histograms of the absorption energy of di-8-ANEPPS in solvent using polarizable Drude force fields Part 1 - left is the total absorption energy, middle is the absorption energy of just di-8-ANEPPS, and right is the absorption energy of the interaction between di-8-ANEPPS and the respective solvent

for acetonitrile at 0.54%. Performing the same comparison for the nonpolarizable parameter set revealed an average of 1.90%, meaning that even though the range for this model is a whole 10 nm smaller, the actual difference between each individual absorption wavelength and its corresponding experimental wavelength remains small. Of course, the experimental

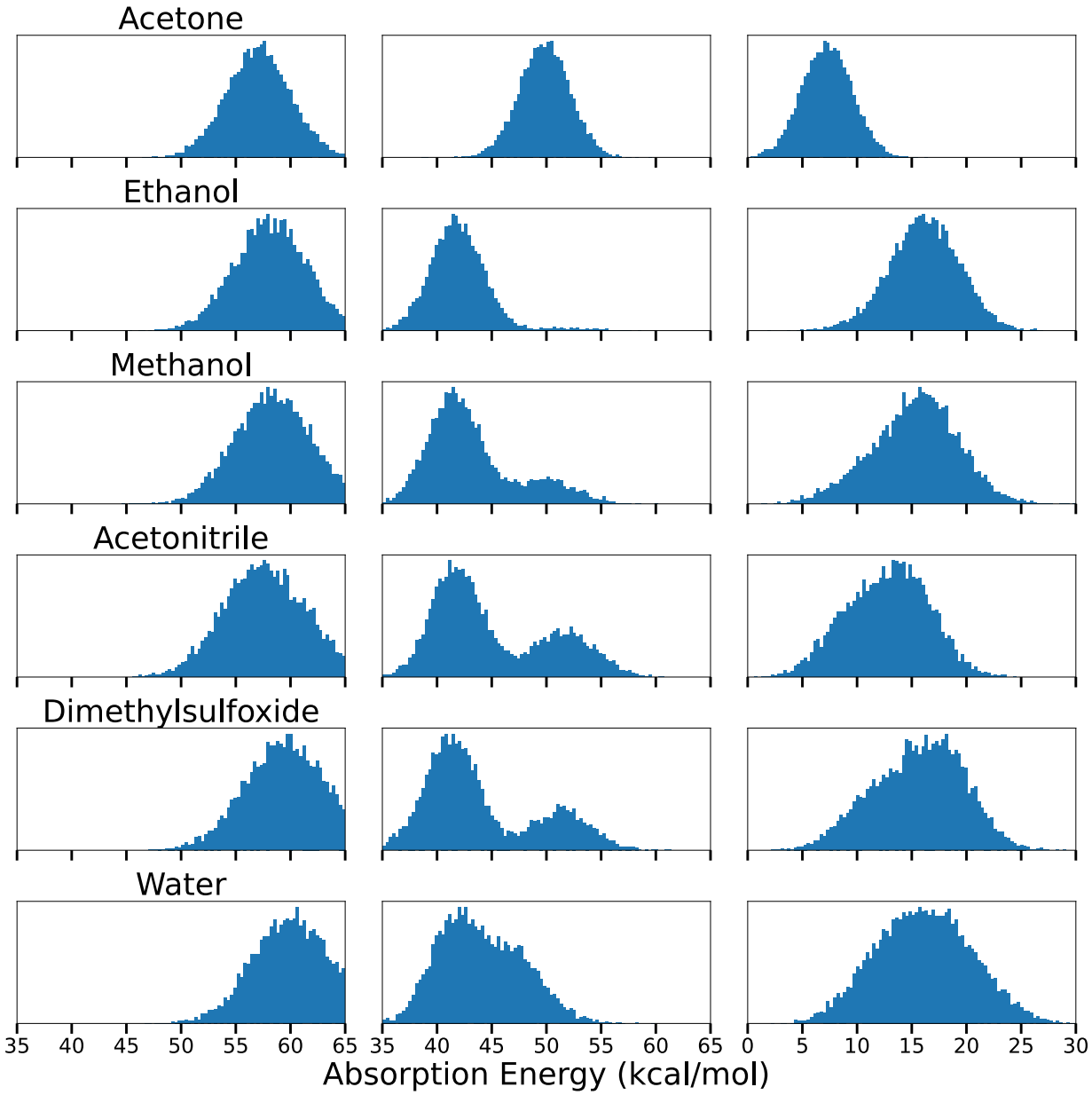

Figure 4.10: Histograms of the absorption energy of di-8-ANEPPS in solvent using polarizable Drude force fields Part 2 - left is the total absorption energy, middle is the absorption energy of just di-8-ANEPPS, and right is the absorption energy of the interaction between di-8-ANEPPS and the respective solvent

data reported by Le Goff et al. should not be considered the objectively correct values, as they are not perfectly agreed upon between different studies. Although the overall trends for a series of solvents are generally conserved within a given experimental study, different absorption and emission wavelengths have been reported for di-8-ANEPPS in the same

solvent.

The histograms of the absorption data produced by the polarizable Drude di-8-ANEPPS in solvent simulations are shown in Figures 4.9 and 4.10. The left column of histograms is the total energy difference of the whole system for each snapshot of the trajectory when calculated with parameters that differ only in whether they consider di-8-ANEPPS in its ground state or excited state. The greater the polarity of the solvent, the more the peak of this graph is shifted to higher energies. The middle column of histograms shows these same snapshots from simulation except it now only considers the di-8-ANEPPS molecule removed from the surrounding solvent (without updating its geometry from each snapshot of simulation in solvent).

Similar to the absorption histograms created for the nonpolarizable simulations of di-8-ANEPPS in solvent, the isolated di-8-ANEPPS absorption energy seems split somewhat into two peaks (as an example, the isolated di-8-ANEPPS absorption from its polarizable Drude simulation in acetonitrile in Figure 4.10). This is, as it was for the nonpolarizable absorption, due to two different geometry conformations of di-8-ANEPPS being common. The major differentiating characteristic is still the position of the sulfonate group: a higher energy difference is observed when the sulfonate bends over and is closer to the pyridinium nitrogen while the lower energy difference is seen when the sulfonate is farther away. The third column of histograms shows the interaction energy between the di-8-ANEPPS and the surrounding solvent by subtracting the energy contribution of the isolated di-8-ANEPPS. Despite the split in the peak in the isolated di-8-ANEPPS histograms, the interaction histograms are not split though there is an increased standard deviation of absorption energies with increasing solvent polarity.

In Table 4.5 the emission data range is about 2.0 kcal/mol (corresponding to a wavelength of about 32 nm), which is again lower than was seen for the nonpolarizable model. The emission wavelengths are all very close in magnitude to one another, making a consistent

Solvent	All	stddev	error	Di8A	stddev	error	Interaction	stddev	error
Benzene	42.1	2.5	0.1	38.4	2.1	0.0	3.7	1.8	0.1
Diethylether	40.3	2.7	0.1	38.3	2.3	0.1	2.0	2.1	0.1
Chloroform	42.3	3.0	0.2	40.4	3.4	0.3	1.9	1.6	0.1
Trichloroethane	41.3	2.9	0.2	39.0	3.0	0.2	2.3	1.9	0.1
Dichloromethane	41.4	2.6	0.1	38.4	2.3	0.1	3.0	2.1	0.1
Dichloroethane	41.1	2.6	0.1	38.1	2.2	0.1	3.0	2.0	0.1
Acetone	41.2	3.2	0.1	39.2	2.7	0.2	2.0	2.6	0.1
Ethanol	42.3	3.3	0.2	39.8	3.4	0.3	2.5	3.0	0.2
Methanol	41.6	3.3	0.1	37.9	2.2	0.1	3.7	2.9	0.1
Acetonitrile	42.3	3.4	0.1	39.3	3.3	0.3	3.0	3.1	0.1
Dimethylsulfoxide	42.0	3.4	0.1	38.4	2.4	0.2	3.6	3.1	0.1
Water	41.1	4.1	0.1	39.7	2.4	0.1	1.3	3.9	0.1

Table 4.5: Emission energy of di-8-ANEPPS in solvent using polarizable Drude force fields - Drude particles are minimized and energy includes added offset

trend unclear with increasing dielectric of the solvent. However, looking at the emission reported by Le Goff et al. the wavelengths for chloroform and water differ by only 7 nm (where water is actually reported to having a lower emission wavelength than chloroform). Ignoring water, the emission increases from 660 nm for chloroform to 710 nm for acetonitrile, a difference of 50 nm.[94] Unlike the nonpolarizable model which also showed the sudden drop for the emission for di-8-ANEPPS in water, the polarizable Drude model finds that water has the largest emission wavelength of this set of solvents, making the water solvent system have a percent error of 6.63% as compared to the emission data reported by Le Goff et al.. Yet despite this, the average error for the seven solvents in common between this study and Le Goff et al. is 3.01%. This difference is larger than was seen for the polarizable Drude absorption data (2.36%), but is actually smaller than the error percentage calculated for the nonpolarizable emission data: 3.64%.

Histograms of the emission energies from the polarizable Drude simulations are included as Figures 4.11 and 4.12. Similar to the emission histograms for the nonpolarizable simulations, these histograms based on the polarizable Drude simulations of the excited state of di-8-ANEPPS do not have the same separation of peaks in its isolated di-8-ANEPPS graphs that were present in the absorption histograms. Though the unsymmetrical shape of peaks like the isolated di-8-ANEPPS emission from the simulation in chloroform (the third row in

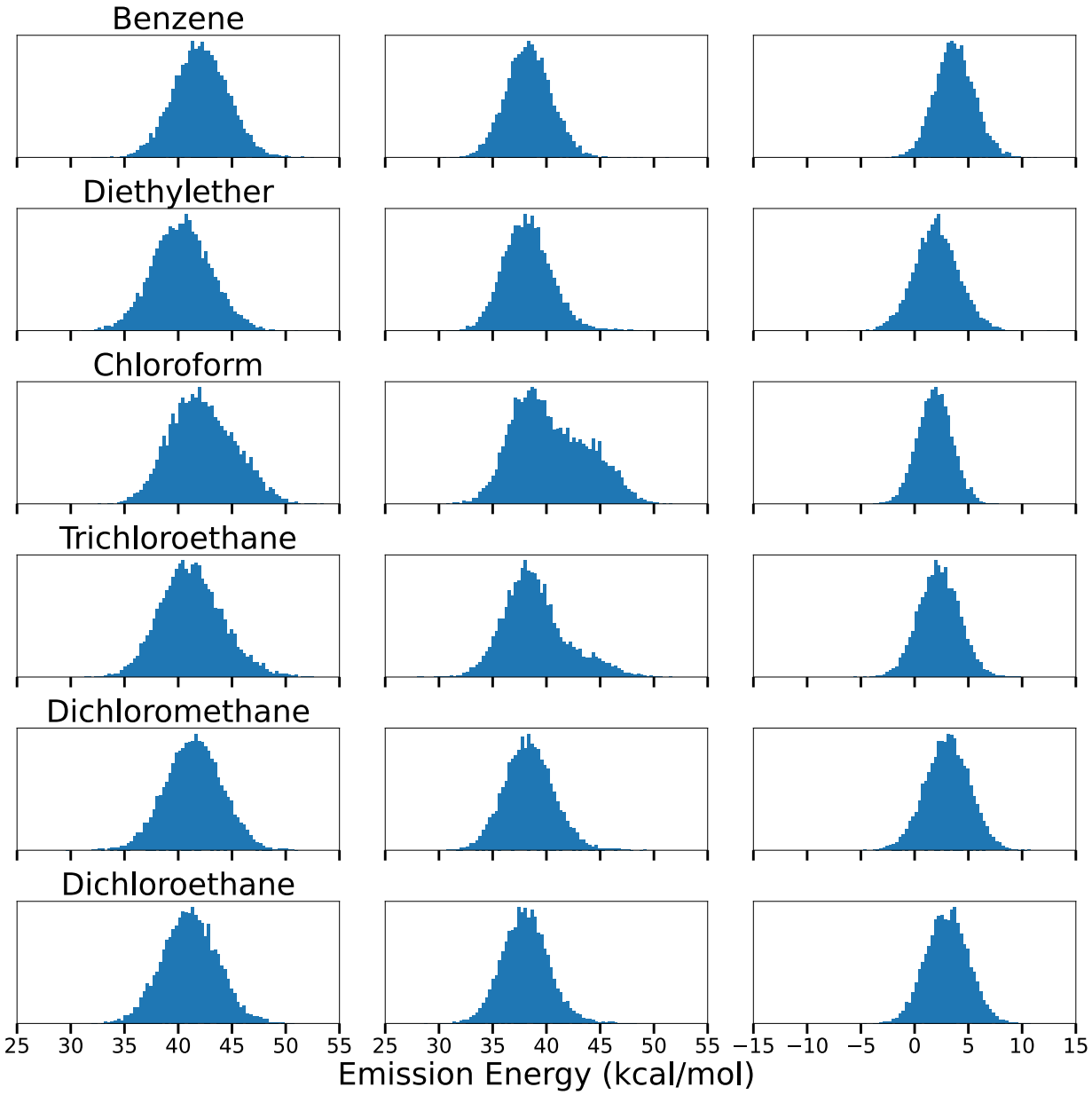

Figure 4.11: Histograms of the emission energy of di-8-ANEPPS in solvent using polarizable Drude force fields Part 1 - left is the total absorption energy, middle is the absorption energy of just di-8-ANEPPS, and right is the absorption energy of the interaction between di-8-ANEPPS and the respective solvent

Figure 4.11) and the isolated di-8-ANEPPS emission from its simulation in ethanol (the second row in Figure 4.12) is likely due to overlapping peaks from slightly different geometries. There is a definite increase in the width of the peak with increasing solvent polarity, which is seen in the total emission energies and interaction emission energies (the right and left

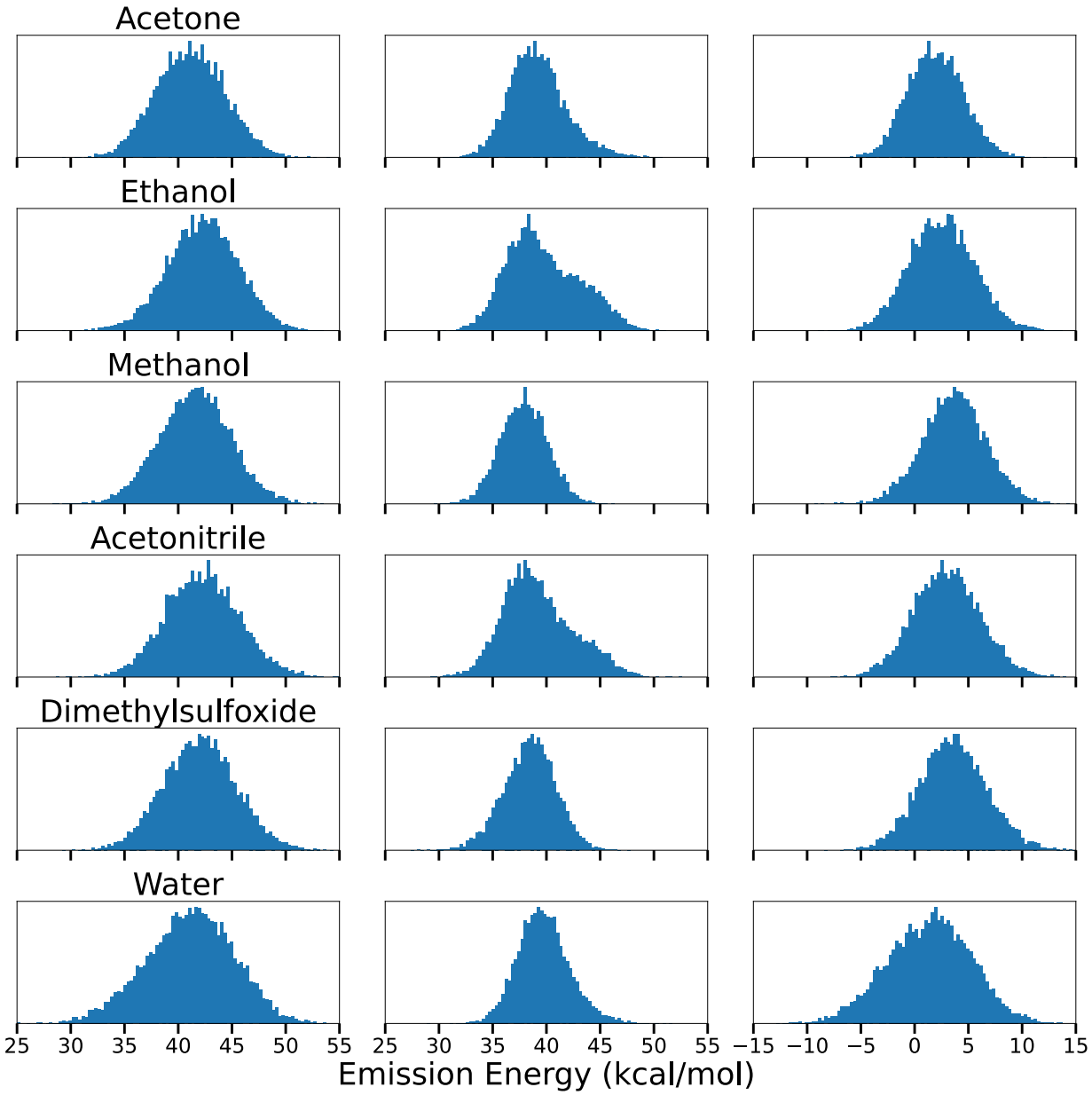

Figure 4.12: Histograms of the emission energy of di-8-ANEPPS in solvent using polarizable Drude force fields Part 2 - left is the total absorption energy, middle is the absorption energy of just di-8-ANEPPS, and right is the absorption energy of the interaction between di-8-ANEPPS and the respective solvent

columns of histograms respectively).

Contained in Table 4.6 is a summary of the total absorption and emission wavelengths calculated with the polarizable Drude model for the di-8-ANEPPS solvent systems along with the corresponding Stokes shifts. The Stokes shifts are then also graphed against the

Solvent	Absorption	Emission	Stokes Shift
Benzene	508.3	679.2	171.0
Diethylether	520.5	709.0	188.5
Chloroform	545.0	676.4	131.4
Trichloroethane	520.1	693.1	173.0
Dichloromethane	509.2	690.1	180.9
Dichloroethane	511.9	695.7	183.8
Acetone	501.1	694.7	193.6
Ethanol	491.5	676.2	184.7
Methanol	488.8	687.9	199.1
Acetonitrile	494.7	676.7	182.0
Dimethylsulfoxide	479.0	680.8	201.8
Water	475.4	696.3	220.9

Table 4.6: Wavelengths of absorption, emission and Stokes shift of di-8-ANEPPS in solvent using polarizable Drude force fields

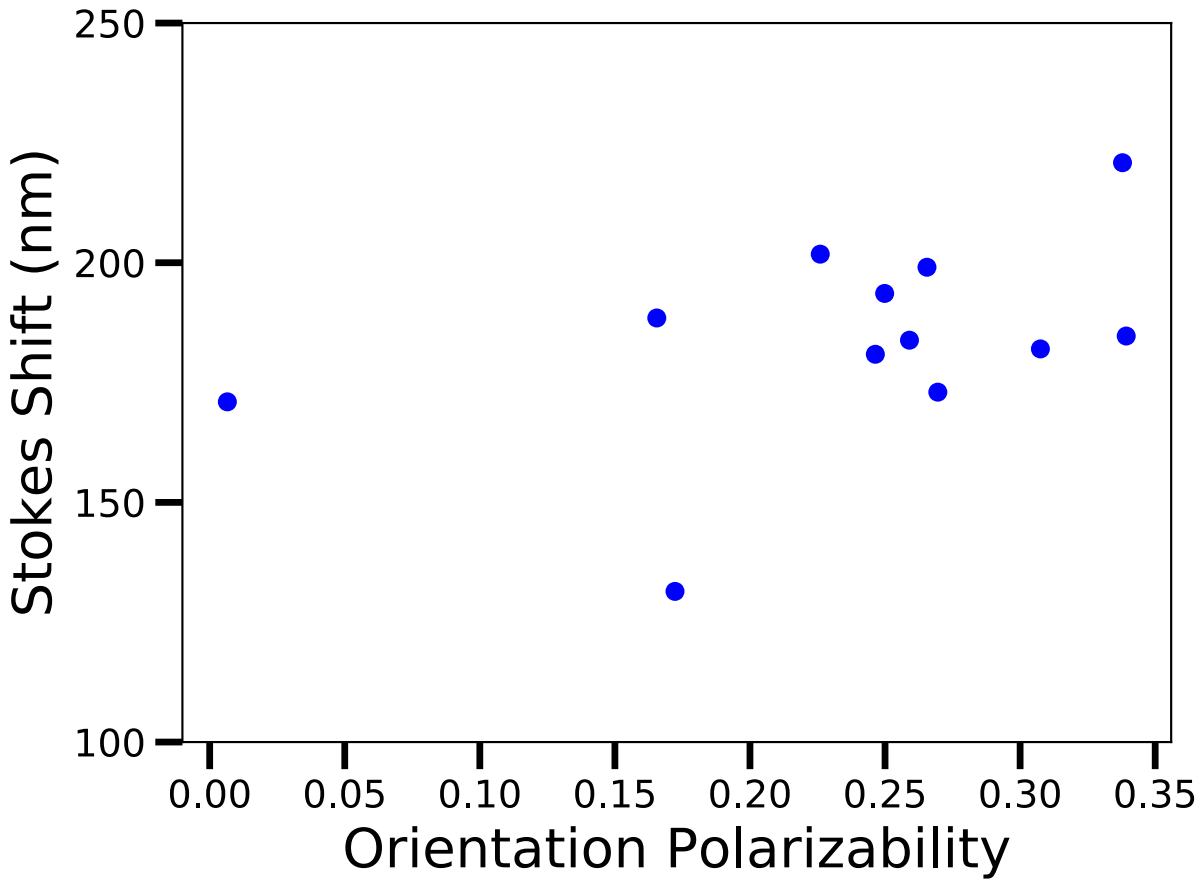

Figure 4.13: Lippert plot of di-8-ANEPPS in twelve solvents using polarizable Drude force fields

orientation polarizability of the corresponding solvent in Figure 4.13. Despite the lack of a clear trend with emission wavelengths, the Stokes shift shows an overall positive trend with increasing solvent polarity and solvent orientation polarizability.

4.5 Discussion

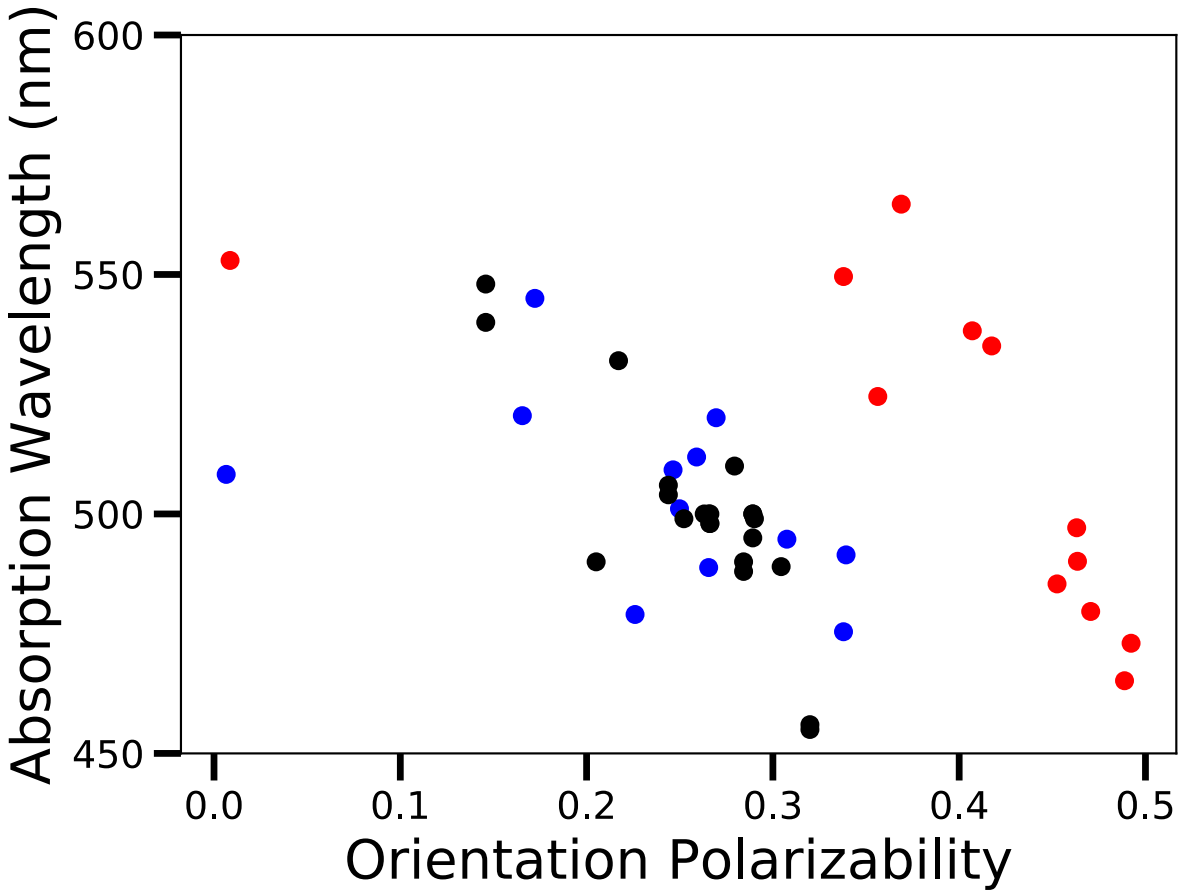

Figure 4.14: Absorption wavelengths of di-8-ANEPPS in solvent using nonpolarizable and polarizable Drude force fields, graphed with experimental data - nonpolarizable data is graphed in red, polarizable Drude data is graphed in blue and experimental data is graphed in black

Comparisons of the data are shown by graphing both the nonpolarizable and polarizable Drude data together against their respective solvent orientation polarizability calculated with each force field model, along with experimental data results. Figure 4.14 displays

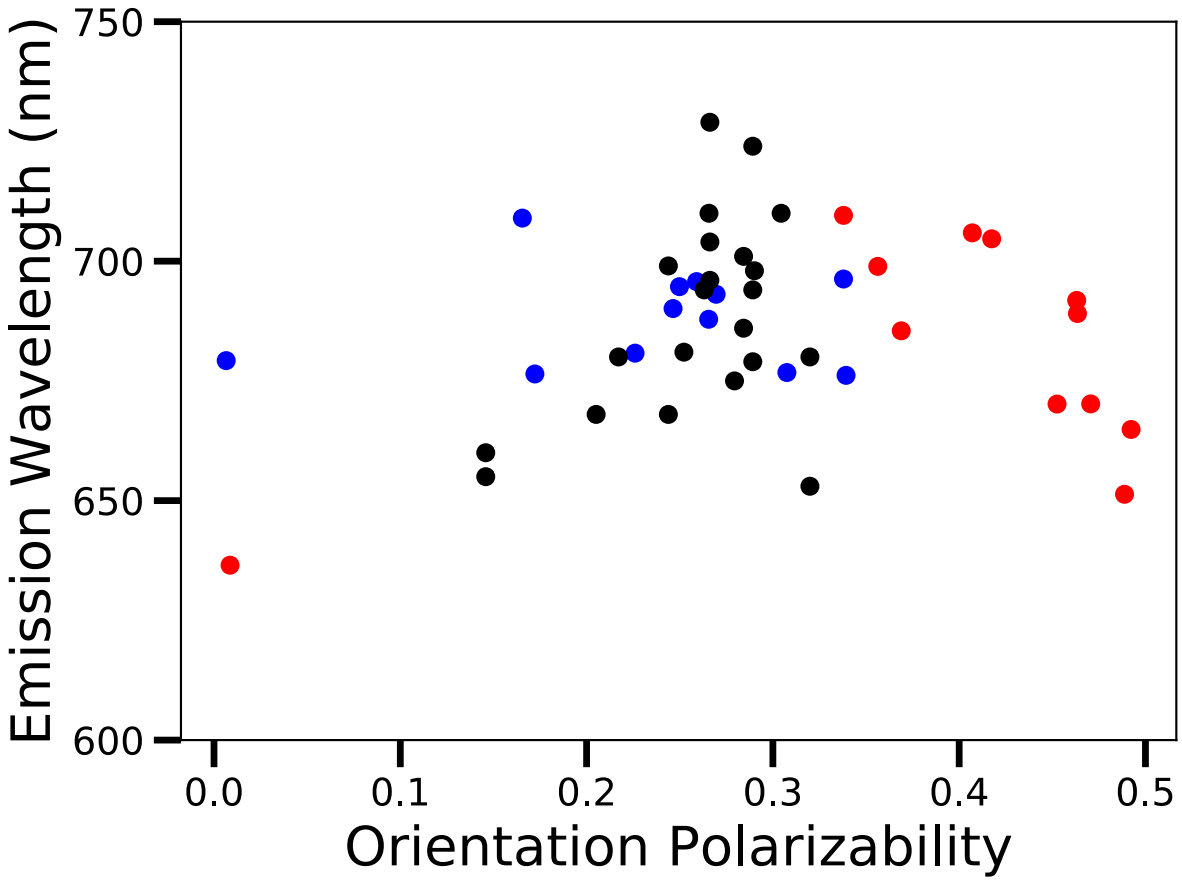

Figure 4.15: Emission wavelengths of di-8-ANEPPS in solvent using nonpolarizable and polarizable Drude force fields, graphed with experimental data - nonpolarizable data is graphed in red, polarizable Drude data is graphed in blue, and experimental data is graphed in black

the absorption wavelengths, Figure 4.15 displays the emission wavelengths and Figure 4.16 shows the Stokes shift (the difference between the absorption and emission wavelengths). The nonpolarizable data is graphed in red, the polarizable Drude data is graphed in blue and the experimental data points derived from several different papers are graphed in black. All solvents considered from the multiple experimental studies are included in the graphs even in cases where that particular solvent was not directly simulated in this work. Le Goff et al. reports the absorption and emission of di-8-ANEPPS in chloroform, dichloromethane, hexanol, methanol, ethanolamine, 2-propanol, acetone, ethanol, acetonitrile, and water.[94] Matson et al. considers both di-4-ANEPPS and di-8-ANEPPS in decanol, hexanol, methanol,

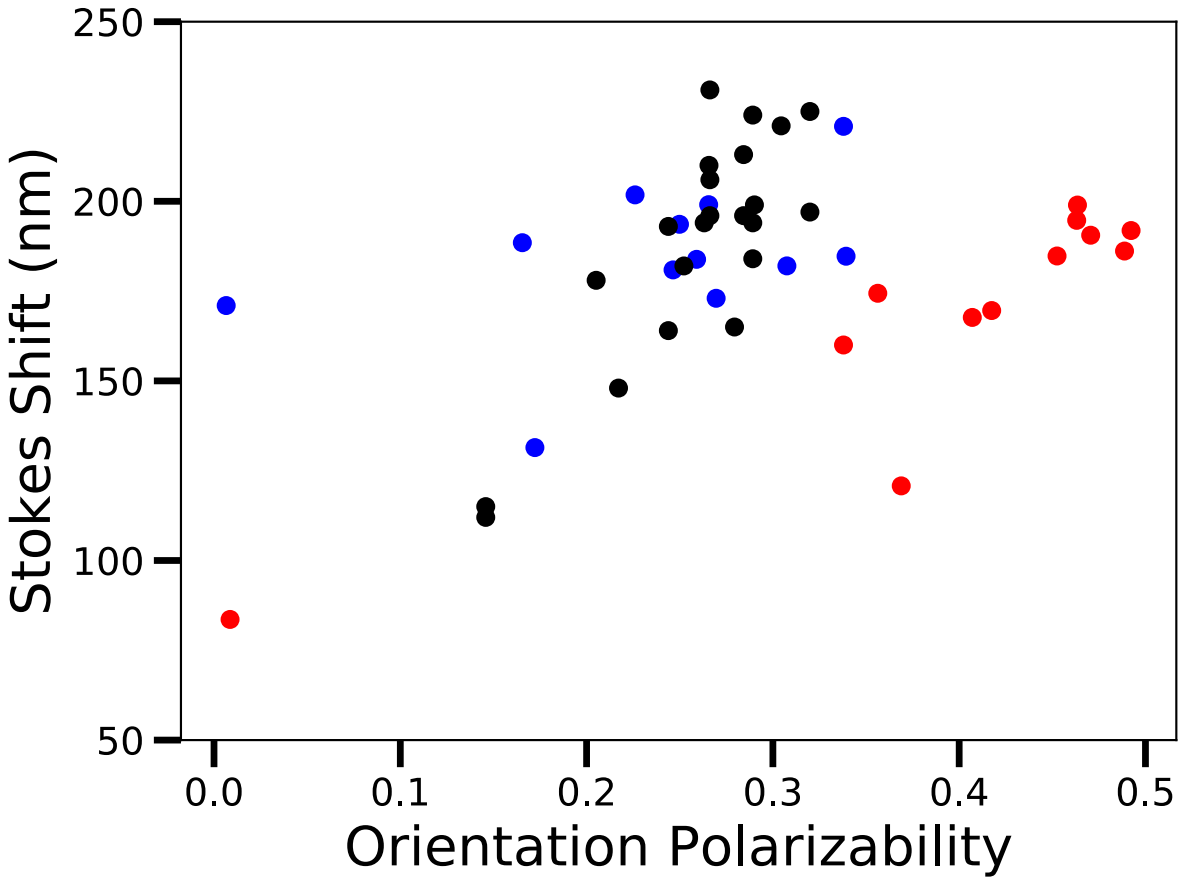

Figure 4.16: Stokes shift of di-8-ANEPPS in solvent using nonpolarizable and polarizable Drude force fields, graphed with experimental data - nonpolarizable data is graphed in red, polarizable Drude data is graphed in blue, and experimental data is graphed in black

iso-propanol, ethanol and water, and shows that apart from water these two molecules have practically identical wavelengths of absorption and emission (differing by 4 nm at most).[119] Čmiel et al.'s data of di-4-ANEPPS in chloroform, acetone, propanol, ethanol, methanol and dimethylsulfoxide from a third study are also included here for comparison.[29]

The difference in the values obtained for the solvent orientation polarizabilities results in the majority of the nonpolarizable data being further to the right along the $x - axis$ in the Lippert plot than the polarizable Drude data, making a direct comparison of the two models difficult. Plotting the Stokes shift calculated from both the nonpolarizable and polarizable Drude models versus the available experimental data results in Figure 4.17, the data used

Solvent	Nonpolarizable	Polarizable Drude	Experimental
Benzene	83.6	171.0	
Diethylether	174.4	188.5	
Chloroform	160.0	131.4	112[94] 115[119]
Trichloroethane	120.8	173.0	
Dichloromethane	169.6	180.9	148[94]
Dichloroethane	167.7	183.8	
Acetone	199.0	193.6	213[94] 196[119]
Ethanol	184.8	184.7	194[94] 184[119] 224[29]
Methanol	190.6	199.1	206[94] 196[119] 231[29]
Acetonitrile	194.7	182.0	221[94]
Dimethylsulfoxide	186.1	201.8	194[119]
Water	191.9	220.9	197[94] 225[29]

Table 4.7: Stokes shift of di-8-ANEPPS from nonpolarizable and polarizable Drude models compared to available experimental data

is included as Table 4.7. The solvents used in this graph are chloroform, dichloromethane, acetone, ethanol, methanol, acetonitrile, dimethylsulfoxide and water. Considering how the polarizable Drude force fields were constructed to be so similar to the nonpolarizable set, it is not surprising that the results are also very similar. After all the only difference in their construction is the inclusion of polarizability terms in the polarizable Drude parameters, which were applied to the same set of partial charges as is in the nonpolarizable parameters. Thus, the differences between them is a result entirely of the added Drude particles and the differences inherent between the Drude and nonpolarizable solvent parameters. The polarizable Drude model is generally slightly closer to the line for most solvents than the nonpolarizable parameters, and this is particularly true for benzene. The polarizable Drude parameters consistently estimate a greater difference between the emission and absorption wavelengths, which frequently is a value closer to the experimental value. It is important to note that the experimental data is from multiple sources with some overlapping solvents between them. This means that the there are some differences in the reported Stokes shift for the same solvent from different experiments: for example the experimental Stokes shift in methanol has been reported as 206 nm,[94] 196 nm,[119] and 231 nm.[29]. Using the nonpolarizable model the Stokes shift in methanol was found to be 190.6 nm while in the polarizable Drude model it is 199.1 nm.

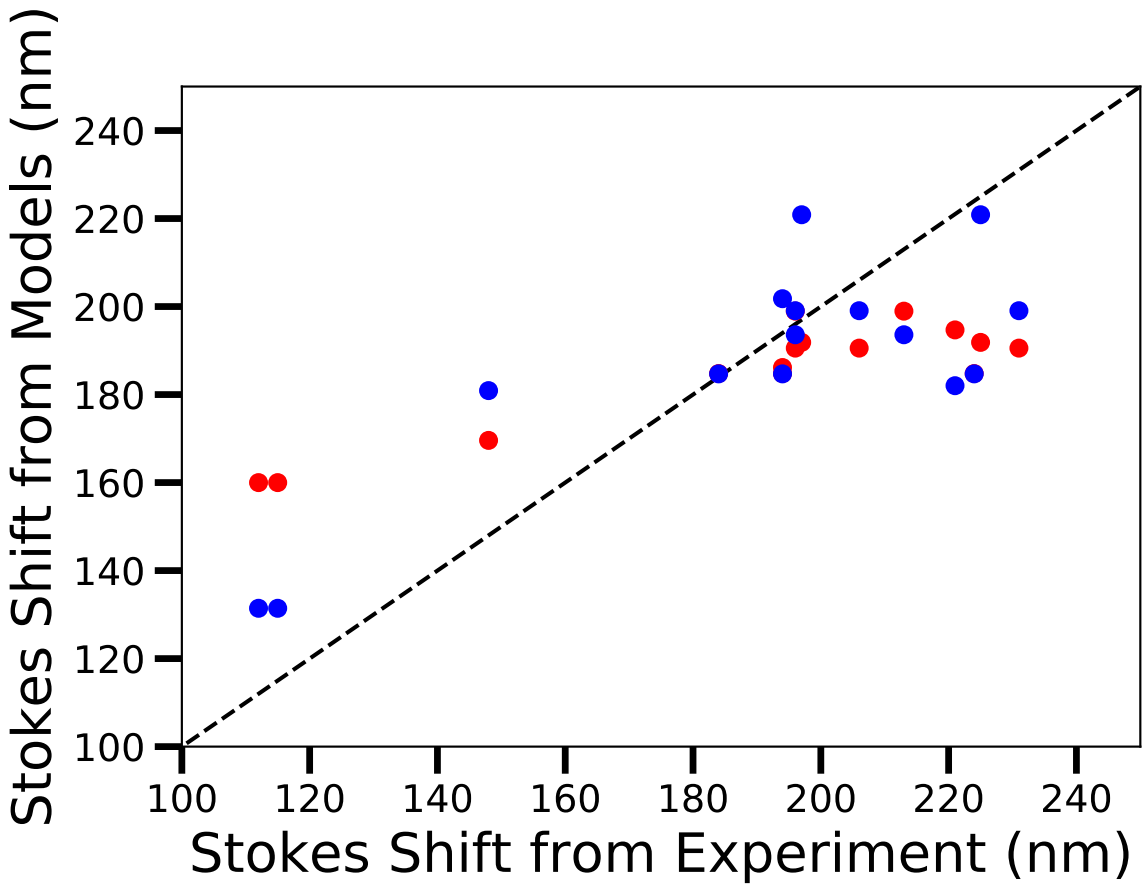

Figure 4.17: Stokes shift of di-8-ANEPPS in solvent using nonpolarizable (red) and polarizable Drude (blue) force fields plotted against the available experimental data

Breaking the Stokes shift down into absorption and emission wavelengths, Figure 4.18 shows the absorption wavelengths of the nonpolarizable and polarizable Drude di-8-ANEPPS graphed against the available experimental absorption wavelengths. The plotted absorption wavelengths are reported in Table 4.8. The more polar solvents typically have a smaller absorption wavelength and are thus found on the left side of the graph (the first two overlapping dots represent the comparisons to two experimental water absorption wavelengths: 456 nm[94]and 455 nm[29]). The greatest difference in absorption wavelength between the two models for the solvents considered is in dichloromethane, which according to experimental results has an absorption wavelength of 532 nm[94] (for nonpolarizable the absorption

Solvent	Nonpolarizable	Polarizable Drude	Experimental
Benzene	552.9	508.3	
Diethylether	524.5	520.5	
Chloroform	549.6	545.0	548[94] 540[119]
Trichloroethane	564.7	520.1	
Dichloromethane	535.1	509.2	532[94]
Dichloroethane	538.2	511.9	
Acetone	490.1	501.1	488[94] 490[119]
Ethanol	485.4	491.5	500[94] 495[119] 500[29]
Methanol	479.6	488.8	498[94] 500[119] 498[29]
Acetonitrile	497.1	494.7	489[94]
Dimethylsulfoxide	465.2	479.0	500[119]
Water	473.0	475.4	456[94] 455[29]

Table 4.8: Absorption wavelengths of di-8-ANEPPS from nonpolarizable and polarizable Drude models compared to available experimental data

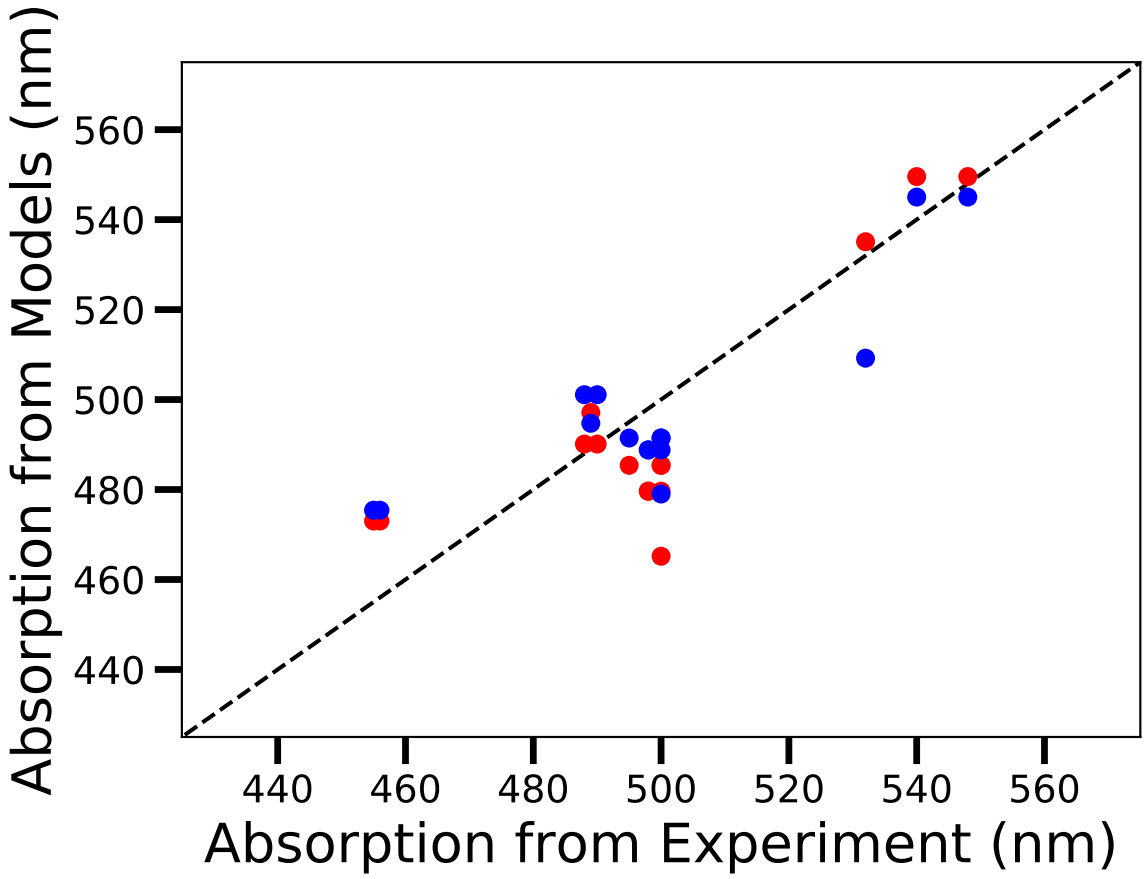

Figure 4.18: Absorption wavelengths of di-8-ANEPPS in solvent using nonpolarizable (red) and polarizable Drude (blue) force fields plotted against the available experimental data

of di-8-ANEPPS in dichloromethane was found to be 535.1 nm and while for polarizable Drude it was 509.2 nm). The final two sets of data points on the far right of the graph are both absorption wavelengths in chloroform, which has been reported to experimentally be 548 nm[94] and 540 nm[119] (as compared to the nonpolarizable and polarizable Drude model which calculated 549.6 nm and 545.0 nm respectively).

Solvent	Nonpolarizable	Polarizable Drude	Experimental
Benzene	636.5	679.2	
Diethylether	698.9	709.0	
Chloroform	709.6	676.4	660[94] 655[119]
Trichloroethane	685.5	693.1	
Dichloromethane	704.7	690.1	680[94]
Dichloroethane	705.9	695.7	
Acetone	689.1	694.7	701[94] 686[119]
Ethanol	670.2	676.2	694[94] 679[119] 724[29]
Methanol	670.2	687.9	704[94] 696[119] 729[29]
Acetonitrile	691.8	676.7	710[94]
Dimethylsulfoxide	651.3	680.8	694[119]
Water	664.9	696.3	653[94] 680[29]

Table 4.9: Emission wavelengths of di-8-ANEPPS from nonpolarizable and polarizable Drude models compared to available experimental data

In contrast when the two sets of emission wavelengths are graphed against the available experimental data, shown in Figure 4.19 and listed in Table 4.9, the data points between the nonpolarizable and polarizable Drude models are no longer as similar to each other. However, there are far more polarizable Drude data points that are closer to the experimental data than those produced by the nonpolarizable model. The nonpolarizable data shows an overall decrease in wavelength with increasing solvent polarity (which is most obvious when ignoring the benzene data point). The polarizable Drude data is less variable and shows a slight increase in emission wavelength with increasing solvent orientation polarizability. This is much more alike to the experimental data where most emission wavelengths increased with increasing solvent polarity. Looking at the two solvents that all three experimental sources include (ethanol and methanol) there is an increase in emission wavelength, however the magnitude of that increase is not consistent: 10 nm[94], 17 nm[119] and only 5 nm.[29] The nonpolarizable model doesn't report a difference between the emission wavelengths of

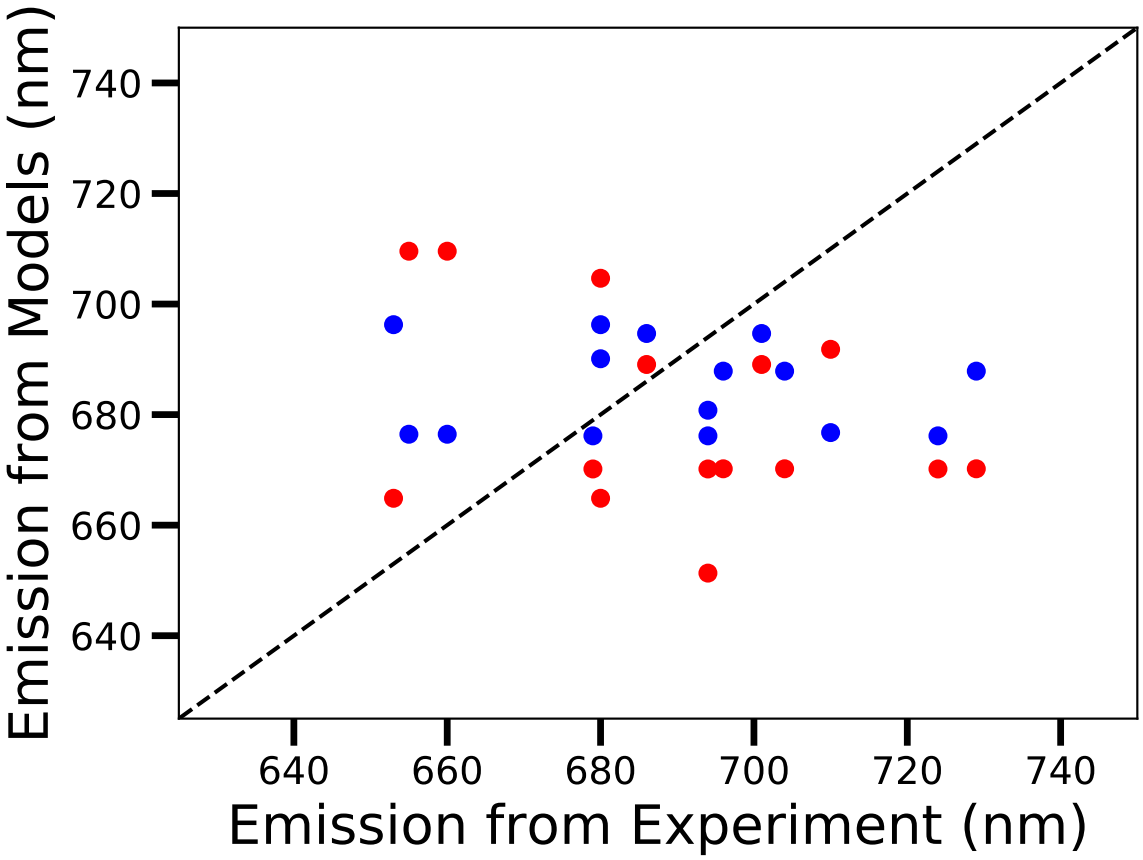

Figure 4.19: Emission wavelengths of di-8-ANEPPS in solvent using nonpolarizable (red) and polarizable Drude (blue) force fields plotted against the available experimental data

di-8-ANEPPS in these two solvents, while the polarizable Drude model has a much more reasonable increase of 11.7 nm. Despite the discrepancies in the emission wavelengths as compared to the available experimental data, the resulting Stokes shift does maintain the expected linear trend as was shown earlier in Figure 4.16. Even when the creation of the polarizable Drude parameters was heavily tied to the nonpolarizable system, to the extent that the literal partial charges of the atoms were not updated, it produces markedly improved results. Polarizable Drude parameters are indeed useful in replicating the experimental transitions in a theoretical format.

4.6 Conclusion

The results of this study can be summed up entirely by the two Lippert plots representing the data obtained from the simulations performed with the nonpolarizable (Figure 4.8) and polarizable Drude parameter sets (Figure 4.13). Especially when they are graphed together with available experimental data in Figure 4.16, which clearly shows the levels of success the theoretical models had in recreating the spectral shifts of di-8-ANEPPS in solvent. Direct comparisons of the Stokes shift of di-8-ANEPPS in the solvents in common between what was simulated and available experimental data, shown in Figure 4.17, also conveys the success of the nonpolarizable and polarizable Drude models. The general trend of the increasing Stokes shift of di-8-ANEPPS with the increasing orientation polarizability of the solvent is observed for both sets of force fields. The range of the data from the most nonpolar solvent (benzene) to the most polar solvent considered (water) is comparable to that seen in experimental studies. The differences between the construction of the two parameter sets is intentionally minor, as the polarizable Drude parameters were highly dependent on the nonpolarizable versions during their development. Yet despite their similarity, the polarizable Drude version shows a greater change in the Stokes shift over the course of considered solvents and better matches the available experimental data. The results of this work are evidence of the viability of representing each of the transitions in the fluorescence cycle of di-8-ANEPPS with molecular dynamics simulated using either the nonpolarizable or polarizable Drude force fields, though it has been shown that the polarizable Drude force fields are better equipped to handle the task.

CHAPTER 5

SIMULATING THE ABSORPTION AND FLUORESCENCE OF DI-8-ANEPPS EMBEDDED IN A LIPID MEMBRANE

5.1 Introduction

Changes to polarity or ion concentration can be reported by voltage-sensitive probes embedded in a membrane near a point of interest, such as a transporter protein. Small probes are particularly useful in this regard since their presence has little impact on the activity of the mechanism they are monitoring. It is ideal to have a dye whose fluorescence varies its wavelength rather than intensity in response to the property it is monitoring and has a fluorescence spectra range that is not overlapped by the spectra of any other molecule in the system. If only the fluorescence intensity changes, its signal can be affected by the quality of the emission detector, illumination intensity and dye concentration. Di-8-ANEPPS (di-8-amino-naphthyl-ethylene-pyridinium-propyl-sulfonate) is a small, fast-response probe molecule that is highly sensitive to its immediate surroundings and can be used to report changes in membrane potential through fluoresced photons at shifted wavelengths. It is a molecule that was specifically sought out for these characteristics.[110]

Dual-wavelength ratiometry is a procedure by which the fluorescence intensity is measured at two wavelengths and reported as the percent change of the ratio of those two values with respect to voltage. One major advantage of reporting results in this way is that this term is insensitive to the dye binding at different locations and insensitive to the specific concentration of the dye molecule in a given preparation.[30] These two wavelengths could either be excitation or emission wavelengths. In the case of excitation ratiometry, excitation is performed at two different wavelengths and the fluorescence intensity at a single wavelength is recorded for each. For emission ratiometry, a single excitation wavelength is used and measurements are made of the fluorescence intensity at two different emission wavelengths.[27,37]

The concept of performing dual wavelength ratiometric measurements was utilized with fluorescent cation detectors[57] and potentiometric indicators,[49] before being applied to a probe whose spectra shifts in response to membrane potential.[122] Emission ratiometry was shown to be a viable means of detecting transmembrane potential caused by externally applied electric field with di-8-ANEPPS,[18] but has been shown to be less effective when investigating intramembrane electric field strength due to membrane dipole potential and fluidity.[188] Overall di-8-ANEPPS has a very linear response to transmembrane potential in a physiological range of -280 to +140 mV, as was shown in a calibration of di-8-ANEPPS when simultaneously comparing the optical and electric measurements during voltage clamp. However, it was also found that this linearity was not maintained above or below that range.[20]

Di-8-ANEPPS has been shown to be a useful probe in monitoring more than just changes to membrane potential. For example, differences in membrane composition can be detected. A higher fluorescence ratio was reported for di-8-ANEPPS in the membranes of neurite (a projection from the cell body of a neuron) than soma (the cell body of a neuron), meaning that a more negative intramembrane electric field was detected in soma than in neurite.[13] Di-8-ANEPPS can even be used to detect shifts in the intramembrane dipole potential (caused by oriented dipoles at the membrane surface).[56] In a combination with the patch clamp technique (in which a high-resistance, electric seal is formed between a glass pipette and the cell membrane, allowing for accurate measurements of the transmembrane potential)[62,130] and measuring the ratio fluorescence of di-8-ANEPPS at two wavelengths calibrated against the voltage applied through the patch pipette, the voltage regulation of ion channels can be studied.[197] This last example highlights how it is only appropriate to use membrane-bound voltage sensitive dyes to report on relative (as opposed to absolute) changes to membrane potential due to how highly sensitive its fluorescence is to environmental factors. Extensive calibration with a given system is required to produce any meaningful results.

The work in this paper aims to determine the fluorescence shifts of di-8-ANEPPS in

a pure DPPC bilayer as a function of applied voltage across the membrane. Considering the probe in extremely simplistic environments is a necessary step to understanding how each factor can affect the spectra of di-8-ANEPPS, before including any additional complications. In Chapter 4 of this Thesis the solvent effects on the spectra of di-8-ANEPPS were investigated in a series of twelve solvents. The results of which showed that with increasing polarity of the solvent, more specifically increasing solvent orientation polarizability, the Stokes shift (the difference between the wavelengths of excitation and emission) is seen to increase. Next to investigate the property of the spectra of di-8-ANEPPS being sensitive to changing membrane potential, the same nonpolarizable models developed for the solvent study are used here, now inserted into membrane. The probe molecule was embedded in a simple, water-solvated DPPC membrane and was equilibrated with varying levels of an external electric field to demonstrate the change in absorption and emission as a function of voltage. The verification that this model responds to an applied electric field in the same manner as reported in experimental data, proves that the parameter set is a reasonable, theoretical representation of di-8-ANEPPS.

5.2 Theory

The parameterization of the di-8-ANEPPS model was performed prior for its simulation in solvents of various polarity and was discussed in Chapter 4 of this Thesis. The same set of nonpolarizable parameters are used here. Additionally, the same general procedure of switching parameter files to simulate the instantaneous electronic conversion of ground to excited state and equilibrating with the new parameter set to simulate the following relaxation used in Chapters 3 and 4 of this Thesis is also used here. The difference lies in the system surrounding the molecule of interest now being a DPPC membrane with a series of voltages applied across it instead of being a series of pure liquids of varying polarity. Di-8-ANEPPS has fewer atoms than a typical lipid molecule and is of a similar cylindrical

shape when anchored into a membrane, meaning that it is inserted parallel to the lipids. The hydrophobic octane tails interact directly with the lipid tails of a membrane bilayer while the more hydrophilic head group of the probe lines up with the corresponding polar lipid head groups. There exist many different approximations of the exact angle at which the molecule sits in a membrane, especially for the probe when it is in its excited state due to its greater charge separation as compared to its ground state. Since more of the molecule exhibits more polar character, the excited state is more likely to float up to interact more with the lipid head groups creating a more extreme angle with respect to the membrane normal. The angle with respect to the membrane normal for di-8-ANEPPS in membrane is typically reported to be very small, though there are experimental studies that find values as large as 37.8°.[91]

Membrane potential is the result of different concentrations of ions on either side of a membrane, enforced by facilitated transport and diffusion of those ions. This difference in electrical potential is used to evoke the activity of membrane-bound proteins and in transmitting signals in neurons and muscle tissue. The potential difference observed across a membrane is the result of charge separation at the membrane-solution interface, while the aqueous solution itself is on average electrically neutral. In order to model membrane potential in molecular dynamics, a uniform, external electric field acting on all charged particles is applied perpendicular to the plane of the membrane. Essentially this field is equivalent to the influence of two salt baths solutions each at different voltages by means of an electromotive force.[164] The total voltage of the system is the product of the electric field applied and the total length of the simulation box in the direction it is applied (this includes the membrane itself as well as the aqueous regions on either side of it).[58] This method of applying a constant electric field to simulate membrane potential has been demonstrated successfully in a variety of different systems including ascertaining the conductance of α-hemolysin,[1] voltage-regulated aquaporin water flux,[74] electroporation,[182] and conformational changes

in voltage-gated ion channel proteins.[133]

5.3 Methods

5.3.1 Parameterization of Di-8-ANEPPS

The generation of the nonpolarizable force fields for di-8-ANEPPS in its ground and first excited state was detailed in Chapter 4 of this Thesis. The same sets of parameters are used here. The parameters for the water and DPPC molecules were taken from Toppar files used in CHARMM-GUI.[81]

5.3.2 Simulation in Membrane

Initial simulations of a solvated DPPC membrane were performed. The system comprises 50 DPPC molecules in each leaflet and a total of 4143 water molecules. Five different versions of the system were simulated at a constant temperature of 323.15 K, under constant volume and where different constant electric fields were applied across the z-axis (which is aligned parallel with the membrane normal). One system served as a control while the other four had -500 mV, -100 mV, 100 mV and 500 mV applied across it. Each system was simulated for at least 250 ns under these constant conditions and respective electric fields. Using the PMEPot VMD plugin[1,75] to create a electrostatic potential grid for every frame output from simulation, the z-coordinate values were averaged to generate a smooth curve showing the effective voltage as a function of depth in the membrane. This can then be used as a baseline for what the di-8-ANEPPS would experience at a given location in the membrane. Additionally, these baselines can be subtracted out from the corresponding applied voltage system containing di-8-ANEPPS to show just the electrostatic potential contributed by the molecule. These membrane systems and versions where di-8-ANEPPS was inserted into one of the leaflets was built using CHARMM-GUI's membrane builder module.[80–82,95,96,192]

Additional systems were built for each selected applied voltage used for the pure DPPC membranes containing the same number of lipids and water molecules, but now also containing either the ground or excited state nonpolarizable version of di-8-ANEPPS. Each was run at a constant 323.15 K temperature, at constant volume and with the maintained external electric field when applicable for one microsecond. Similarly to the pure DPPC systems, each of these were analyzed with the PMEPot VMD plugin.[1,75] Rather than taking the average electrostatic potential along the z-coordinate (since these membrane systems are not homogeneous), the frames from simulation were shifted so that the di-8-ANEPPS head group is in a consistent coordinate position. Though the idealized conformation of the molecule is essentially cylindrical, with its carbon chains extended straight outward, over the course of simulation there is invariably some movement from the starting structure. In addition to the mingling of the carbon chains with the hydrophobic lipid tails, the angle of the molecule with respect to the membrane normal is also not constant. Thus, the averaged electrostatic potential data of that region can only give very general information about the given system.

Direct comparison of the simulated di-8-ANEPPS in membrane systems to experimental systems reported in other papers is accomplished in a similar way to the solvent system analysis. Energy differences between the ground and excited parameters sets for snapshots extracted from simulation performed with either the ground or excited di-8-ANEPPS were converted to the wavelengths of absorption and emission respectively. The dependence of the activity of di-8-ANEPPS on applied voltage is typically reported as a percent change in a ratio of the intensity between two wavelengths selected to be on either side of the intensity peak on the spectra. It is important to note that the most common procedure for this dual-wave ratiometric analysis of a molecule's sensitivity to voltage change often reports the two wavelengths used to excite the probe, a resulting peak emission wavelength and the graph of the fluorescence ratios.[56,113,122,148,173,194] In other words, excitation ratiometry is more prevalent than emission ratiometry (where results are reported as a function of the ratio

of two emission wavelengths). The data produced by the work presented here keeps the excitation and emission portions independent, meaning that there is no way to link a given excitation wavelength to the expected intensity of the corresponding fluorescence. However, it has been proven that the same analysis can be performed for a system where only a single wavelength was used for excitation and the ratio is instead between detected intensities at two emission wavelengths.[84] Taking the emission spectra graphed in that paper, the intensity peak was fit with a Lorentzian curve. A linear relationship between an applied voltage and the emission wavelength at the intensity peak is assumed, where the y-intercept is the wavelength at the intensity peak when no voltage is applied. The slope of this relationship was determined by recreating Kao et al.'s figure depicting the ratio of the two fluorescence peak intensities versus the voltage, based on the Lorentzian curve and only optimizing the slope term. This results in a linear relationship relaying the peak emission with respect to applied voltage that can be directly compared to the results produced in this work.

5.4 Results

5.4.1 Pure Membrane

Before inserting di-8-ANEPPS, a simple membrane system composed of 100 DPPC molecules (50 in each leaflet) and solvated with water molecules was considered. This is the same number of DPPC and water molecules used for the later simulations that contain the di-8-ANEPPS and is essentially the same size, since the di-8-ANEPPS is small enough not to disrupt the overall structure of the membrane. A full 250 ns of simulation was averaged to produce the electrostatic potential grid, although given the simplicity of pure solvent systems the general characteristics were already clear with less than 50 ns of simulation. 2D maps of the behavior in a sliced $y - z$ plane located at 0.0 in the x dimension were generated for the DPPC system where no voltage has been applied and for four systems where -500

mV, -100 mV, 100 mV and 500 mV external electric fields have been applied. Then for each (y, z) coordinate the 0V data was subtracted from the other four, effectively removing the self-potential of the molecules themselves and leaving only the overall transmembrane potential. Finally, the 2D maps that have subtracted out the 0V pure DPPC data have been converted into 1D along the z-axis by taking the average electrostatic potential with respect to the y-axis. The four normalized 1D maps are shown in Figure 5.1. This produces the expected smooth curves from 0 to the maximum transmembrane potential of each given system. These graphs allow for the visualization of what electric field is felt by the system, and more importantly di-8-ANEPPS itself, at given depths.

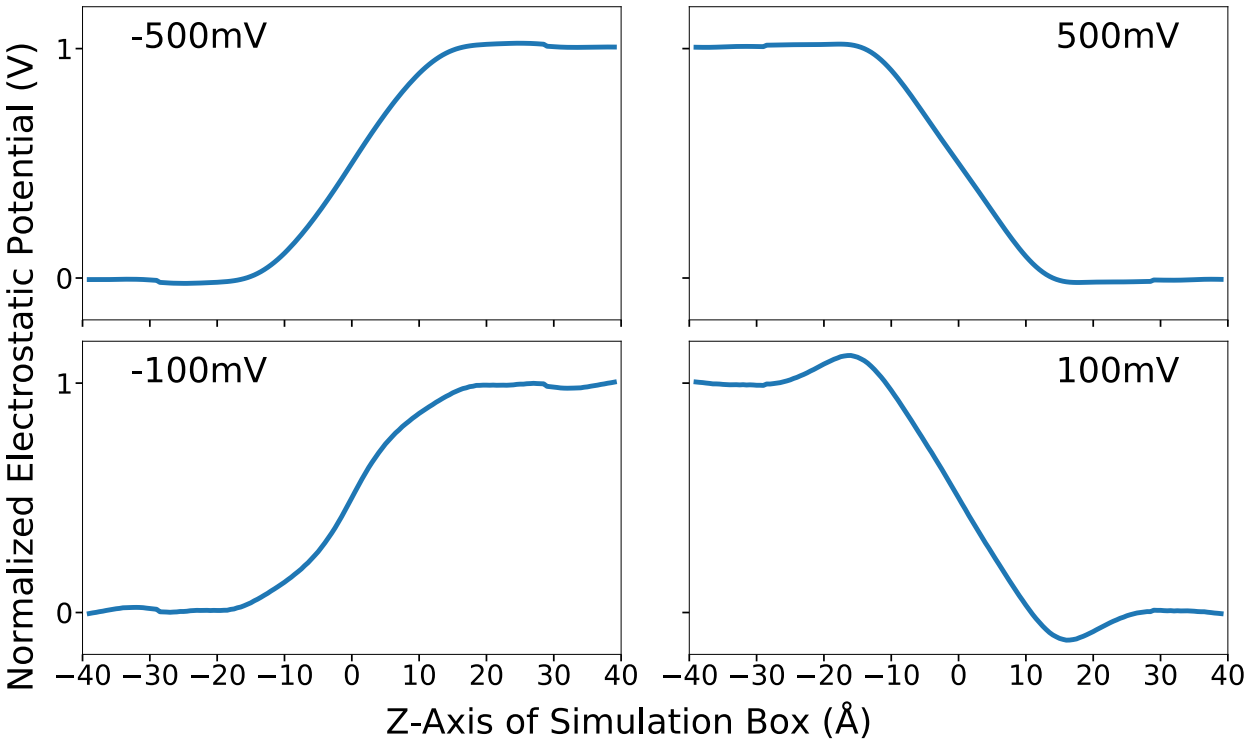

Figure 5.1: 1D normalized ($\phi(z)/V_{\text{mp}}$) PMEPot graphs along the z-axis of a pure DPPC membrane with applied voltages - after subtracting out the 0 mV PMEPot data

Di-8-ANEPPS was inserted into a DPPC membrane in an orientation parallel to the lipid chains. The molecule stretches from about the midpoint of the simulation box to about +20 Å along the z-axis. The propyl sulfonate of di-8-ANEPPS remains at the intersection

of the lipid head groups and the solvating water while the octane chains at the other end of the molecule entangle the lipid tails. The rigid, conjugated structure is composed of the pyridinium, ethylene and naphthyl ring. This middle portion of the molecule does somewhat interact with the lipid head groups especially if the di-8-ANEPPS is in an orientation not perfectly parallel with the membrane normal. Figure 5.2 shows a snapshot of di-8-ANEPPS in membrane with a normalized membrane potential overlaying it to display what parts of the molecule will be most influenced by the presence of an external electric field.

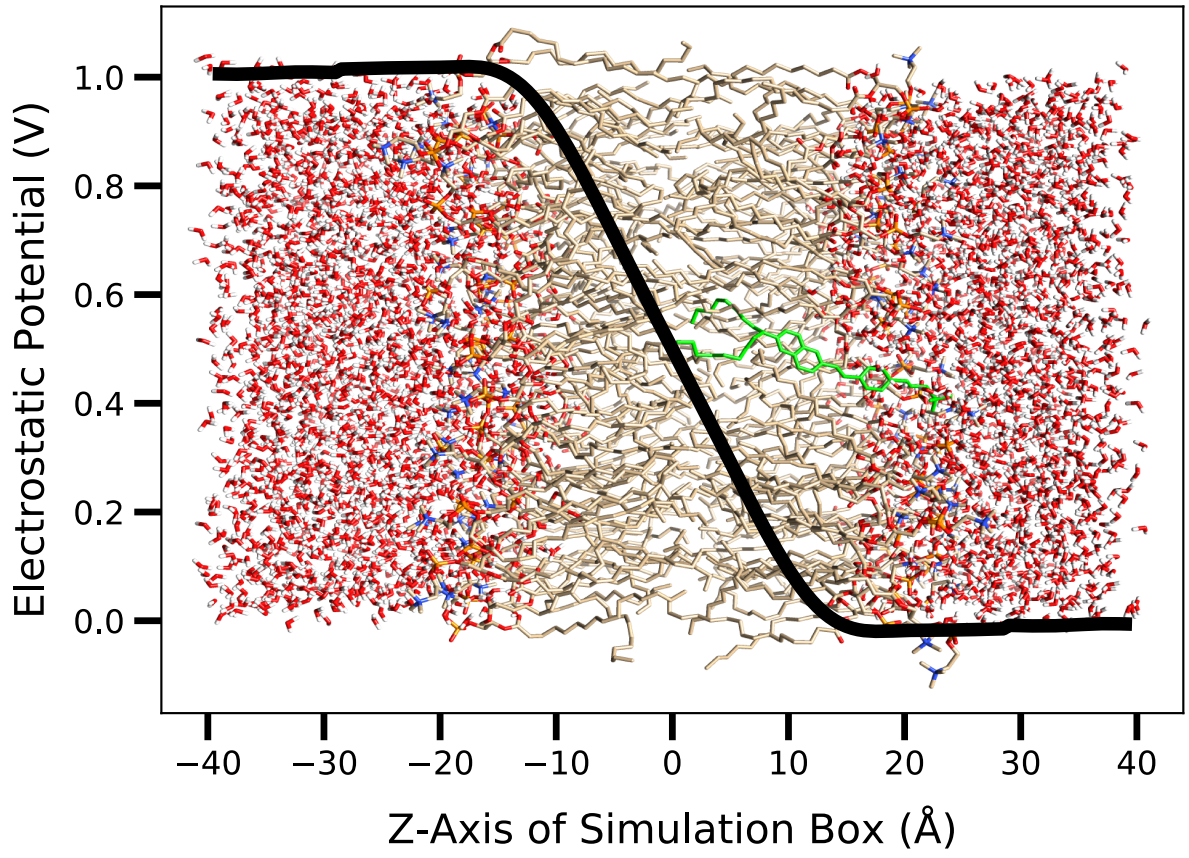

Figure 5.2: Image of di-8-ANEPPS (highlighted in green) in a DPPC membrane and water with 1D overlay of a normalized ($\phi(z)/V_{\mathrm{mp}}$) transmembrane potential

5.4.2 Di-8-ANEPPS in Membrane

Before considering the effect of applying external electric fields to these systems of di-8-ANEPPS in membrane, the orientation of the molecule in its ground and excited state without any additional factors is investigated. In order to follow the location of di-8-ANEPPS

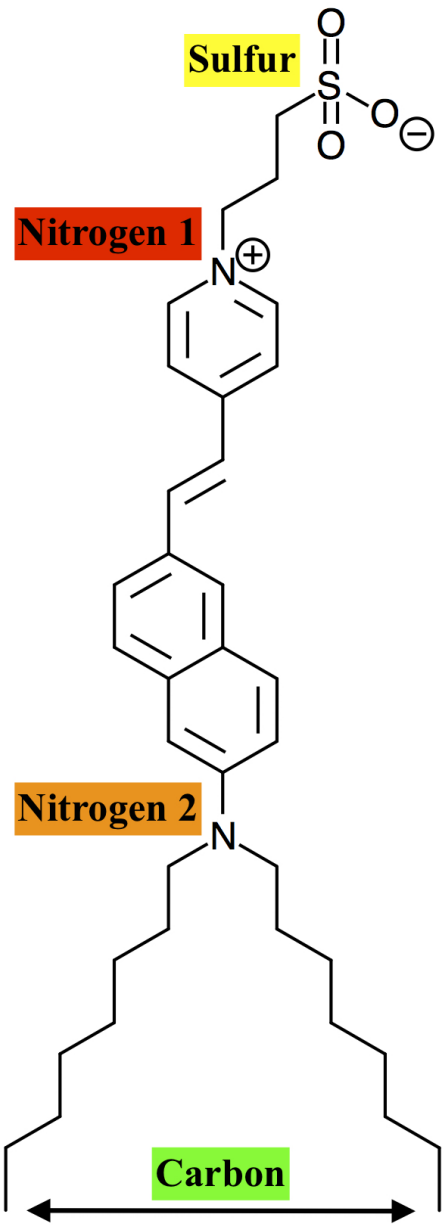

Figure 5.3: Labels of the selected atoms of di-8-ANEPPS that are tracked over the course of a simulation

during a simulation, the positions of several atoms were monitored and recorded for each snapshot of the trajectories. The first chosen atom is the sulfur in the head group, which of the chosen atoms should always have the most positive z-coordinate since it typically settles at the lipid head group-water intersection. The second atom chosen is the pyridinium nitrogen, which is at the top of the conjugated section of the molecule leading to the propyl sulfonate, and is a locally positively charged point when di-8-ANEPPS is in its ground state. The third atom chosen is the second nitrogen which is part of an amino group at the opposite end of the conjugated section of the molecule, and is a locally positively charged point when di-8-ANEPPS is in its excited state. Since the conjugated portion of the molecule is highly rigid, knowing the z-coordinates of these two nitrogen at either end indicates whether or not the molecule is angled with respect to the membrane normal. When the difference between these two z-coordinates shortens, it is a clear sign that the molecule is angled. Finally, the average of the final carbon in each of the two octane chains is also monitored, showing the total depth of the molecule in the membrane. These atoms are labelled and highlighted in Figure 5.3 with the colors that will be used in all future figures to indicate the z-coordinate data of that selection: yellow for sulfur, red for the pyridinium nitrogen, orange for the amino nitrogen and green for the final carbon of each octane.

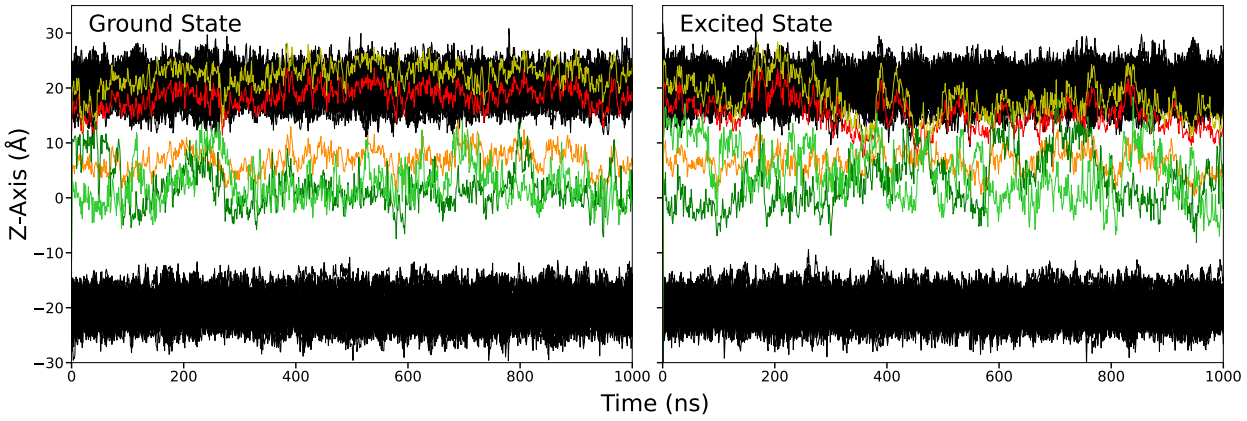

Figure 5.4: Tracking z-coordinates of the selected atoms in the ground and excited states of di-8-ANEPPS embedded in a DPPC membrane with no applied voltage - yellow is the sulfur, red is the pyridinium nitrogen, orange is the amino nitrogen, the two green shades are the final carbons in the octane chains, and black is the DPPC lipid head groups

Tracking the z-coordinates of several important atoms in the system containing the ground state di-8-ANEPPS over the course of a 1 microsecond simulation gives the left side of Figure 5.4. This is lined up with the same tracking for the system containing the excited di-8-ANEPPS, shown on the right side. The black lines track the head groups of the DPPC lipids to show the depth of di-8-ANEPPS and what part of the DPPC molecule each part of the di-8-ANEPPS is interacting directly with. It can be immediately apparent by comparing these two graphs that in general the excited state positions are much more volatile, and that the molecule in its excited state tends to be at a greater depth in the membrane. Overall the sulfur (yellow) still has the highest z-coordinate, and the distance between it and the pyridinium nitrogen (red) is approximately the same whether it is a ground state or excited state simulation. However, the position of the amino nitrogen (orange) with respect to the pyridinium nitrogen (red) is not at all consistent for the excited state, even though it is relatively uniform for the ground state. The orange line practically overlaps with the red line at a couple points over the course of the simulation, which when considering how rigid the structure is between those two atoms that are being tracked, shows that the excited state of di-8-ANEPPS can and does tilt. Effectively there are brief times during the excited state simulation where the conjugated ring structure is almost perpendicular to the membrane normal. The two terminal carbon of the octane chains (both green) are typically at a greater depth in the membrane than any other part of the molecule. Their positions are highly changeable resulting in one or the other sometimes existing at a similar depth to the amino nitrogen (orange), which exists at the end of the conjugated portion of the molecule. Of course, at the times when the molecule is more tilted, the positions of the final carbon are correspondingly pulled a bit higher in the membrane.

Mass density profiles of the ground and excited state of di-8-ANEPPS in DPPC are shown in Figure 5.5, which details the degree to which each component of di-8-ANEPPS is embedded in the membrane and is accessible to the water. The same set of atoms of di-8-

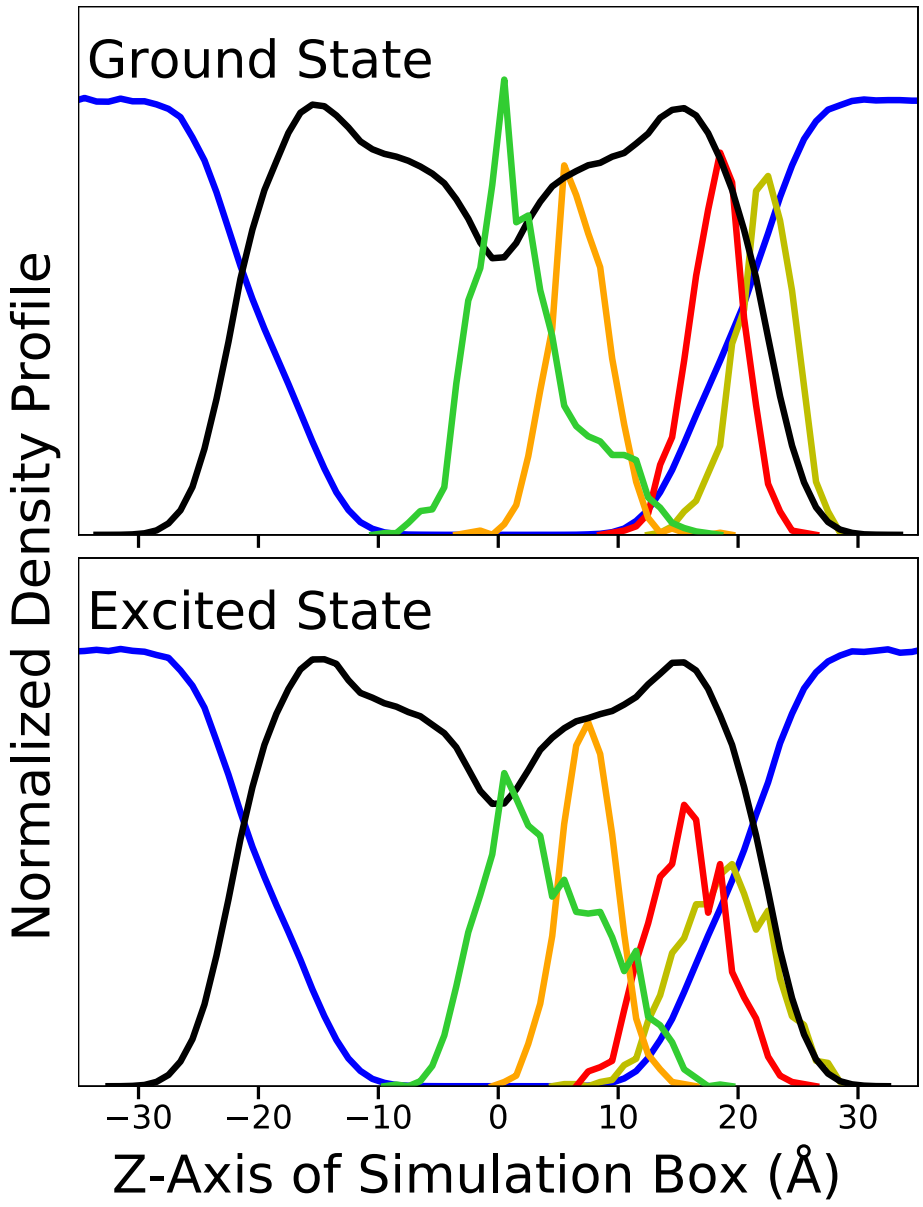

Figure 5.5: Density profiles of the selected atoms of the ground and excited states of di-8-ANEPPS in DPPC and water with no applied voltage, scaled relative to one another for clarity - yellow is the sulfur, red is the pyridinium nitrogen, orange is the amino nitrogen, green is the average of the final carbon in the octane chains, black is the DPPC lipids and blue is water

ANEPPS is chosen to track as described in Figure 5.3. Yellow is for the z-position of sulfur, red is for the pyridinium nitrogen, orange is for the amino nitrogen, green is the average z-position of the two final carbon in the octane chains, black is the DPPC and blue is water. As was seen when tracking the z-coordinate, both the ground and excited di-8-ANEPPS

embedded in membrane over the course of a simulation show that its head group remains at the intersection of water and DPPC, the middle portion of the molecule is somewhat deeper and the carbon chains exist entirely in the middle of the DPPC region (interacting exclusively with the hydrophobic tails of the lipids). The negatively charged sulfonate (tracked by its central sulfur atom, yellow) is always present at the interface between the water and DPPC, though its peak depth is slightly different between the ground and excited states. The excited state of di-8-ANEPPS shows the sulfur to be on average deeper in the membrane and with a greater range of positions therein. The two nitrogen that exist on either end of the fused pyridinium and naphthyl rings (red and orange respectively) have a smaller distance between their peaks for the excited state of di-8-ANEPPS than for the ground state, corresponding to situations where this part of the molecule's angle relative to the membrane normal changes. The fused rings peak position is deeper into the membrane than the sulfonate, though the overlap of the red and yellow lines shows that the propyl group connecting the sulfonate to the pyridinium is highly flexible and allows for the sulfur to easily visit the same depths as the pyridinium nitrogen. However, both the ground and excited state of di-8-ANEPPS show that typically the sulfur is at a shallower depth than the pyridinium nitrogen. The carbon tails are highly mobile and assumed a great number of conformations, resulting in the peak position of the averaged final two carbon from each octane chain (green) being over a large area. The peak position always remains deeper in the membrane anchoring the molecule, regardless of whether the di-8-ANEPPS is in its ground or excited state. There are a large number of configurations where the ends of the carbon tails reach depths closer to the other components of the molecule, as evidenced by the overlap of the green line with the other colors.

The same analyses were performed for the ground state of di-8-ANEPPS in DPPC while experiencing varying strengths of an electric field: -500 mV, -100 mV, 100 mV and 500 mV. Figure 5.6 shows the z-positions of the selected atoms tracked over the course of each simu-

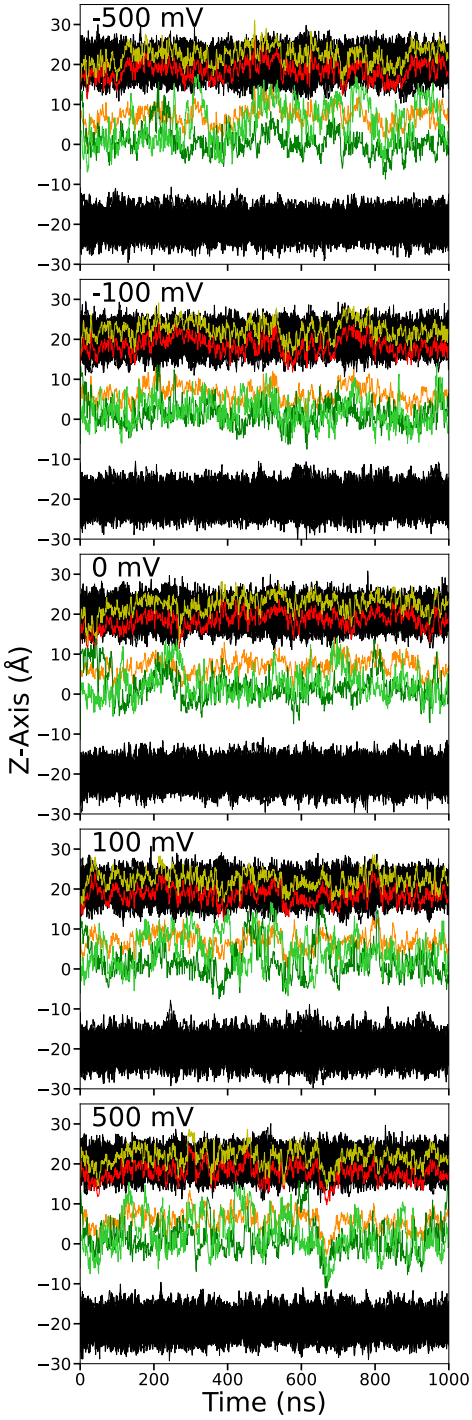

Figure 5.6: Tracking z-coordinates of the selected atoms in the ground state of di-8-ANEPPS embedded in a DPPC membrane with a range of applied voltages - yellow is the sulfur, red is the pyridinium nitrogen, orange is the amino nitrogen, the two green shades are the final carbons in the octane chains, and black is the DPPC lipid head groups

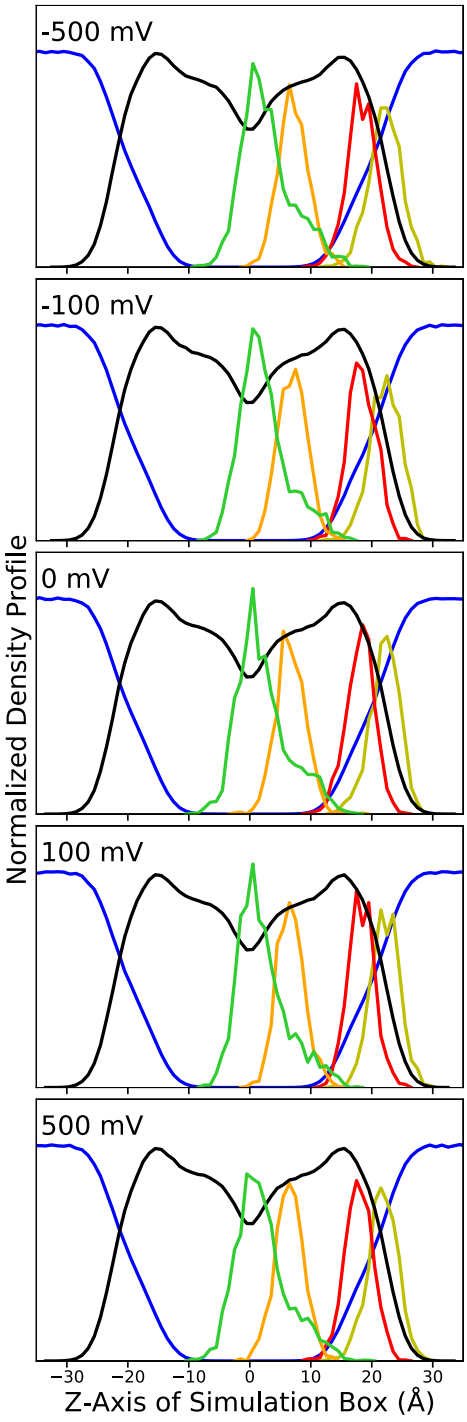

Figure 5.7: Density profiles of the selected atoms of the ground state of di-8-ANEPPS in DPPC and water with a range of applied voltages, scaled relative to one another for clarity - yellow is the sulfur, red is the pyridinium nitrogen, orange is the amino nitrogen, green is the average of the final carbon in the octane chains, black is the DPPC lipids and blue is water

lation, including the 0 mV system for comparison. And Figure 5.7 shows the corresponding density profiles of these chosen atoms for the same set of systems. Regardless of the strength of the electric field, very little change can be observed for the ground state: the positions of the tracked atoms hardly move and the width of these peaks are also relatively consistent. This can be explained by the fact that the greatest charge separation is between the locally negative sulfonate (tracked by the position of the central sulfur, yellow) and the locally positive pyridinium nitrogen (red) which occurs entirely at the interface between DPPC and water. This difference in charge is at a point where the electrostatic potential across the membrane is practically zero (which is its value for the water portion). In contrast the excited state of di-8-ANEPPS has a much greater spread of its charge, which penetrates much deeper into the membrane and makes it more sensitive than the ground state to the electrostatic potential across the membrane.

Comparing the ground and excited graphs before any external electric field is applied, the most obvious difference is the head group of the excited di-8-ANEPPS being positioned further into the membrane and that the fused ring portion is sometimes at an angle with respect to the membrane normal. These characteristics are the most important to keep in mind with tracking the same set of atoms in simulations when an external electric field is applied to see if the depths are affected. Figure 5.8 shows the z-positions of the selected atoms tracked over the course of each simulation of the excited state of di-8-ANEPPS in membrane where -500 mV, -100 mV, 100 mV and 500 mV are applied. Figure 5.9 shows the density profiles of these chosen atoms for the same set of systems containing the excited state of di-8-ANEPPS. For both the tracking and density profile graphs, the 0 mV system is included as well for comparison.

The excited state of di-8-ANEPPS can swing up so that everything apart from its octane tails are much closer to the head groups of the DPPC. The hydrophobic tails of di-8-ANEPPS are always mingling with the hydrophobic DPPC tails, regardless of which state

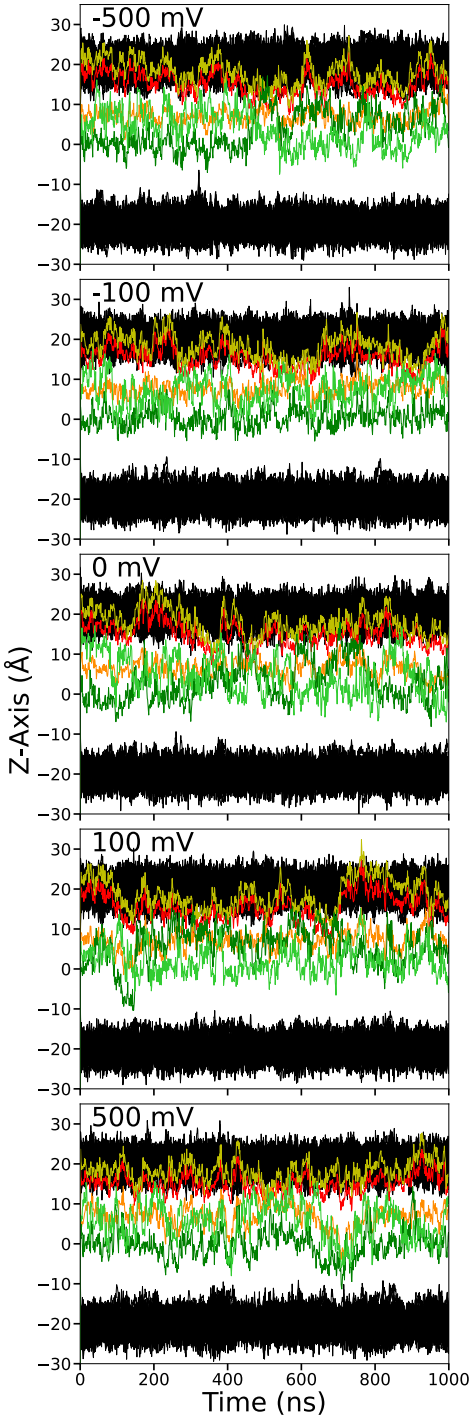

Figure 5.8: Tracking z-coordinates of the selected atoms in the excited state of di-8-ANEPPS embedded in a DPPC membrane with a range of applied Voltages - yellow is the sulfur, red is the pyridinium nitrogen, orange is the amino nitrogen, the two green shades are the final carbons in the octane chains, and black is the DPPC lipid head groups

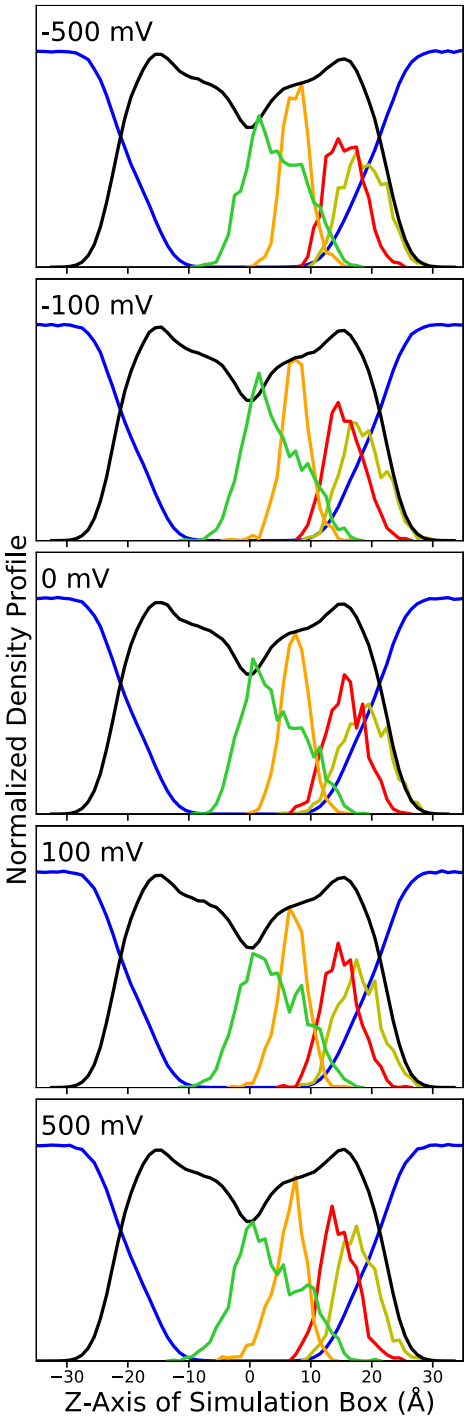

Figure 5.9: Density profiles of the selected atoms of the excited state of di-8-ANEPPS in DPPC and water with a range of applied voltages, scaled relative to one another for clarity - yellow is the sulfur, red is the pyridinium nitrogen, orange is the amino nitrogen, green is the average of the final carbon in the octane chains, black is the DPPC lipids and blue is water

di-8-ANEPPS is in. This prevents the rest of the molecule from moving further out of the depths of the membrane. However, it is still difficult to see any trends with these figures, it is more clear when tabulating the average z-position of each of the selected atoms over the course of each simulation. The results from each system simulated (containing either ground or excited di-8-ANEPPS with the range of applied voltages), are summarized in Table 5.1. Comparing the two extreme voltages applied, it can be immediately seen that each atom for both the ground and excited state ultimately settled at a greater depth into the membrane (closer to zero) when a more positive external electric field was applied. In the ground state the sulfur range is 0.4 Å, the pyridinium nitrogen range is about 0.5 Å, the amino nitrogen range is 0.7 Å and the final carbon range is also about 0.7 Å. The fact that the depths of the selected atoms do not change by the same amount is an indication of some angling of the molecule. At -500 mV the molecule is at a shallower depth, and its fused ring portion at a larger angle relative to the membrane normal, at +500 mV the molecules straightens out at a deeper position. Similarly, the excited state also has a slight difference in the change in depth for atoms at the top of the molecule versus atoms at its bottom. However, in systems containing the excited state each range of depths is greater: for sulfur it is about 0.9 Å, pyridinium nitrogen is also about 0.9 Å, the amino nitrogen range is 1.3 Å and the carbon range is about 1.1 Å. The larger depth changes show that indeed the excited state is more sensitive to the changing voltage potential across the membrane.

	Sulfur		Nitrogen 1		Nitrogen 2		Carbon	
	ground	excited	ground	excited	ground	excited	ground	excited
-500	22.2	18.7	18.4	15.7	7.2	7.6	2.8	4.3
-100	22.2	18.6	18.3	15.6	7.0	7.4	2.4	3.8
0	22.1	18.8	18.1	15.7	6.7	7.5	2.2	4.0
100	22.3	18.0	18.4	15.0	6.7	7.1	2.2	3.8
500	21.8	17.8	17.9	14.6	6.5	6.3	2.1	3.2

Table 5.1: Z-Coordinates of the selected atoms in the ground and excited state of di-8-ANEPPS in DPPC with a range of applied voltages

In Figure 5.10 the data from Table 5.1 is presented in two graphs, one for the ground

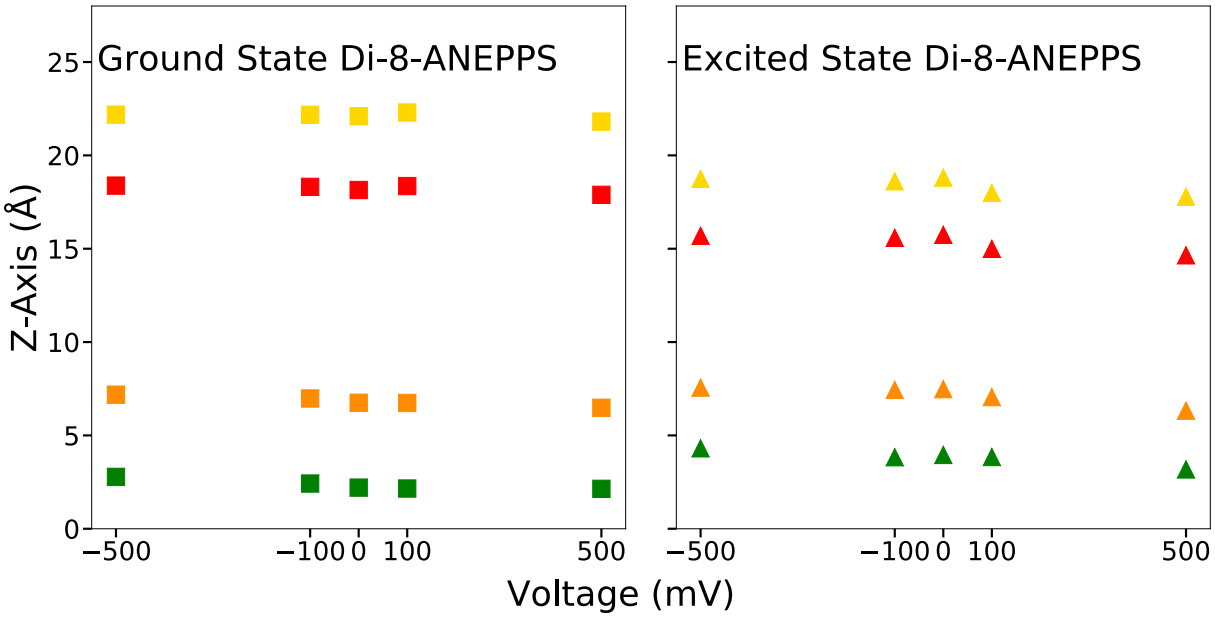

Figure 5.10: Z-coordinates of the selected atoms in the ground (squares) and excited (triangles) state di-8-ANEPPS in DPPC with a range of applied voltage - yellow is the sulfur, red is the pyridinium nitrogen, orange is the amino nitrogen, green is the average of the final carbon in the octane chains

state and one for the excited state of di-8-ANEPPS in DPPC with the range of applied voltage. Keeping consistent with the color scheme: each sulfur center of mass data point is in yellow, each pyridinium nitrogen center of mass is graphed in red, each amino nitrogen center of mass is graphed in orange and each of the average center of mass of the two final carbon in the octane chains is shown in green. Squares represent the ground state data and the triangles represent the excited state. Tracking these data points shows very clearly that the excited state tends to be deeper in the membrane than the ground state regardless of the magnitude of voltage applied across the membrane, that with increasing voltage overall it sinks a little deeper, and that the excited state tends to be angled in the membrane (resulting in a shorter distance between the two nitrogen - red and orange). Additionally Figure 5.11 separates this data by atom, allowing for a comparison of each between the ground and excited state with different voltage applied.

In a similar manner to how a linear relationship is expected between the Stokes shift and the orientation polarizability of the solvent containing the molecule of interest, a linear

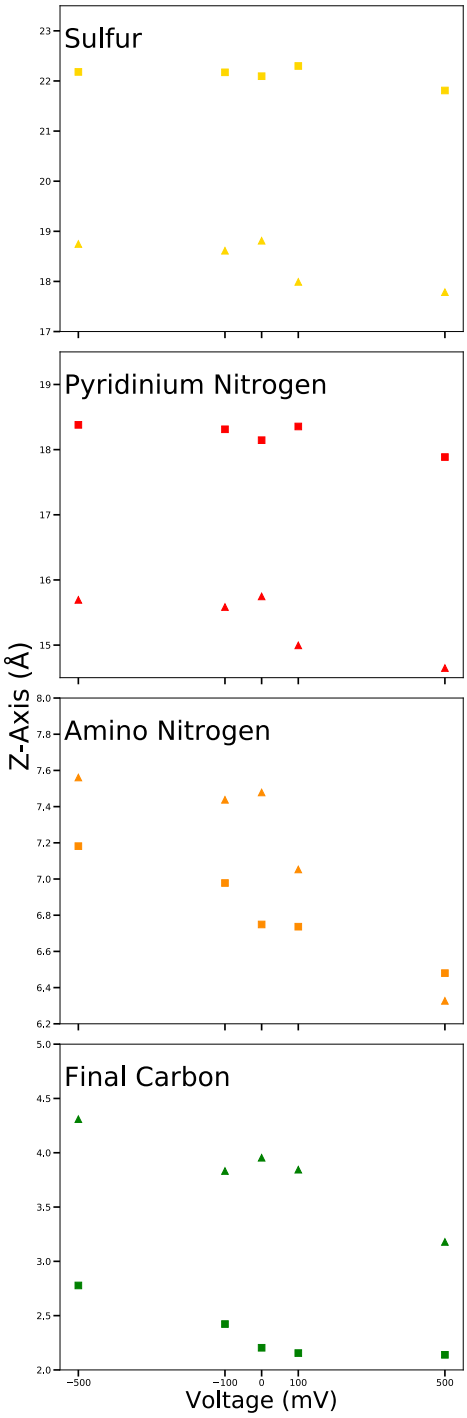

Figure 5.11: Z-coordinates of the selected atoms in the ground (squares) and excited (triangles) state di-8-ANEPPS in DPPC with a range of applied voltage

relationship can be drawn for the spectra as a function of the externally applied voltage. Since more differentiates the various solvents used than just each one's dielectric and index

of refraction, this trend is only generally followed. A more straight line of data could be extracted if the changes in polarizability are instead due to a change in concentration of that solvent in a mixture. In the membrane simulations performed in this study, the only changes between each iteration are the specific parameter set used to characterize di-8-ANEPPS (describing either its ground or excited state) and the voltage applied. Thus, unlike seeing just the broad trend being reproduced, it is expected that these results are much more linear. To keep the system more consistent and stable, it was performed under constant volume and constant temperature.

Voltage	Absorption (nm)	Emission (nm)	Stokes Shift (nm)
-500	466.4	608.6	142.1
-100	462.0	606.6	144.5
0	462.1	605.5	143.4
100	460.9	605.1	144.2
500	459.0	604.1	145.0

Table 5.2: Absorption and emission of nonpolarizable di-8-ANEPPS in DPPC membrane with a range of applied voltages

Studies that report changes in fluorescence of a probe molecule as a function of different voltages applied across its membrane do not report the changes in the peak of the absorption spectra. Often, they report two excitation wavelengths that are used to find a ratio of fluorescence intensity, but they do not report the absorption spectra directly. Meaning that the peak absorbance calculated for the -500 mV, -100 mV, 0 mV, 100 mV and 500 mV membrane systems cannot be directly compared to any available experimental data. Using the same offset calculated for the nonpolarizable absorption in solvents from Chapter 4 of this Thesis, 4.990 kcal/mol, the absorption wavelengths are reported in Table 5.2 and Figure 5.12. The total range of this data is 7.37 nm, meaning that it predicts a change of the peak intensity of the absorption spectra to be only 0.73 nm / 100 mV. Without any applied voltage, the absorbance wavelength is 460.6 nm which is quite close to the values reported for di-8-ANEPPS in various membrane systems. For example, in muscle fibers it was recorded to have an absorption peak at 470 nm.[38]

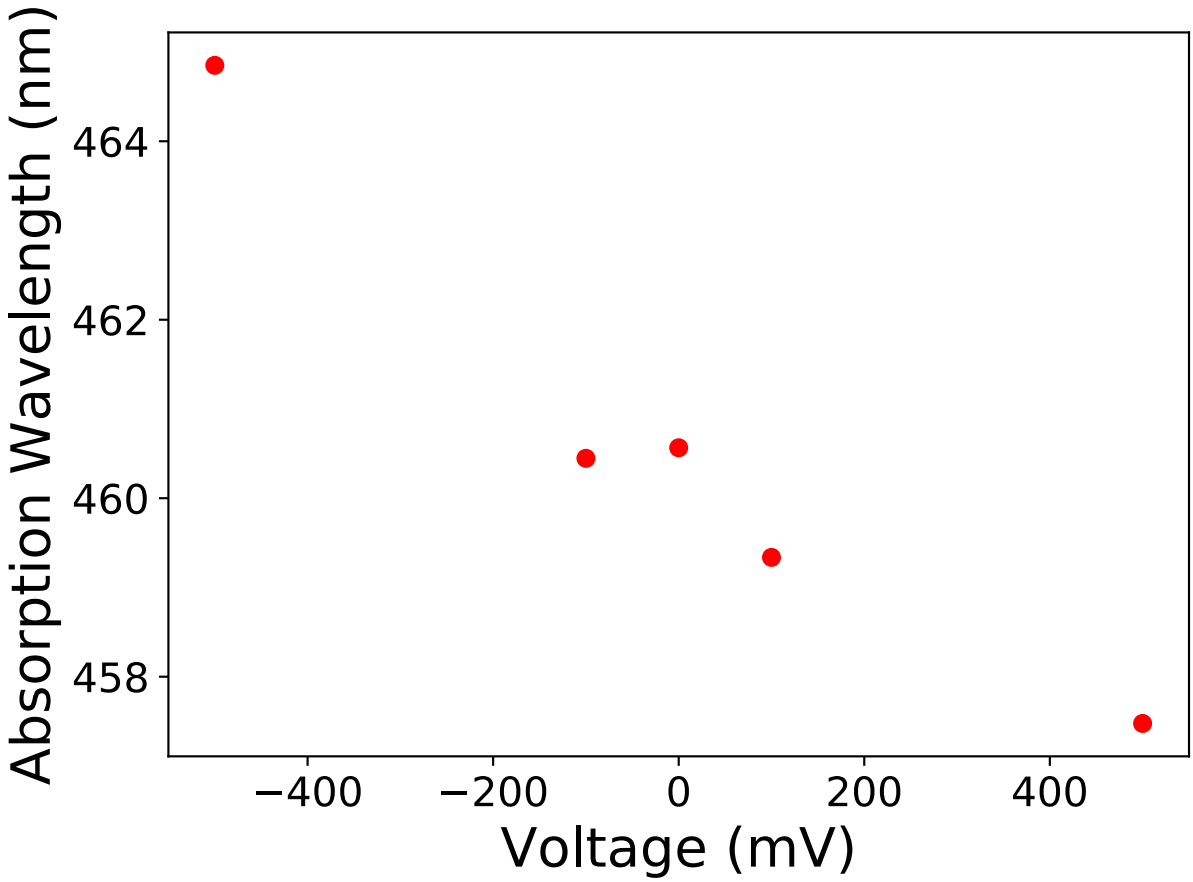

Figure 5.12: Absorption wavelengths for nonpolarizable di-8-ANEPPS in DPPC with a range of applied voltage

The membrane simulations performed in this study involved only DPPC and water for simplicity's sake, but there was not an experimental study performed looking at the effects of applied voltage field on di-8-ANEPPS in such a basic membrane. In the work of Kao et al., di-8-ANEPPS was inserted into Human Embryonic Kidney (HEK) cells and studied with voltages ranging from -80 to +60 mV applied across it.[84] Using their emission spectra reported in Figure 5 of their paper, a Lorentzian function was used to estimate the curve and reproduce the data in the bottom of Figure 3 in their paper. The Lorentzian curve fitting and the recreated graph of Kao et al's data showing the fluorescence ratio as a function of applied voltage is shown in Figure 5.13.

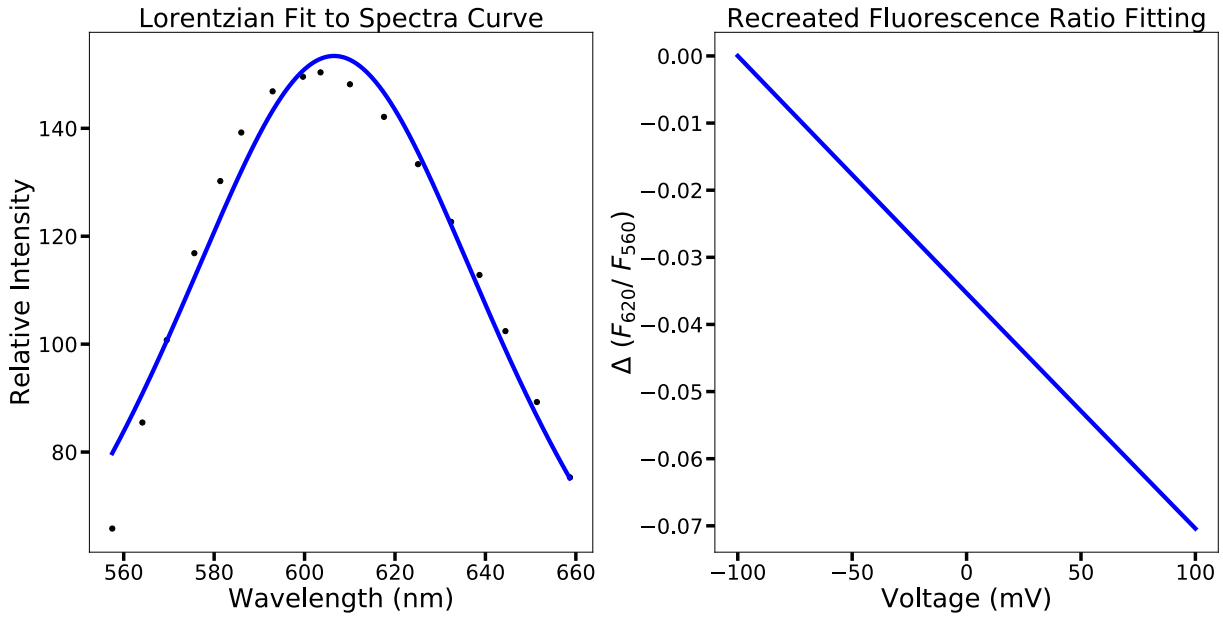

Figure 5.13: Recreation of Kao et al's data[84] to allow for direct comparison - on the left is the fitting of their emission peak with a Lorentzian function and on the right is graphing the change in the ratio of the fluorescence intensity at wavelengths of 620 nm and 560 nm using that Lorentzian function

Voltage (mV)	Emission (nm)	Experimental Emission (nm)[84]
-500	608.6	609.5
-100	606.6	606.7
0	605.5	606.0
100	605.1	605.3
500	604.1	602.4

Table 5.3: Emission wavelengths for nonpolarizable di-8-ANEPPS in DPPC with a range of applied voltages - compared to emission wavelengths deduced from fitting a Lorentzian to the data of Kao et al.[84]

Once the degree of shift of the spectra is known in terms of the membrane potential, it can be used to predict the maximum of the emission peak after it has been shifted. With these data points, the emission energies reported by this study's theoretical studies are directly compared and the added offset term is optimized in much the same way as it was for the di-8-ANEPPS in solvent systems (Chapter 4 of this Thesis). The offset was found to be 12.611 kcal/mol, which is a little over 2 kcal/mol larger than the emission offset found for the nonpolarizable model of di-8-ANEPPS in solvents (10.044 kcal/mol). The emission wavelengths reported in Table 5.2 use this new offset. And Table 5.3 directly compares these emission wavelengths to the extracted values of the emission wavelength at maximum

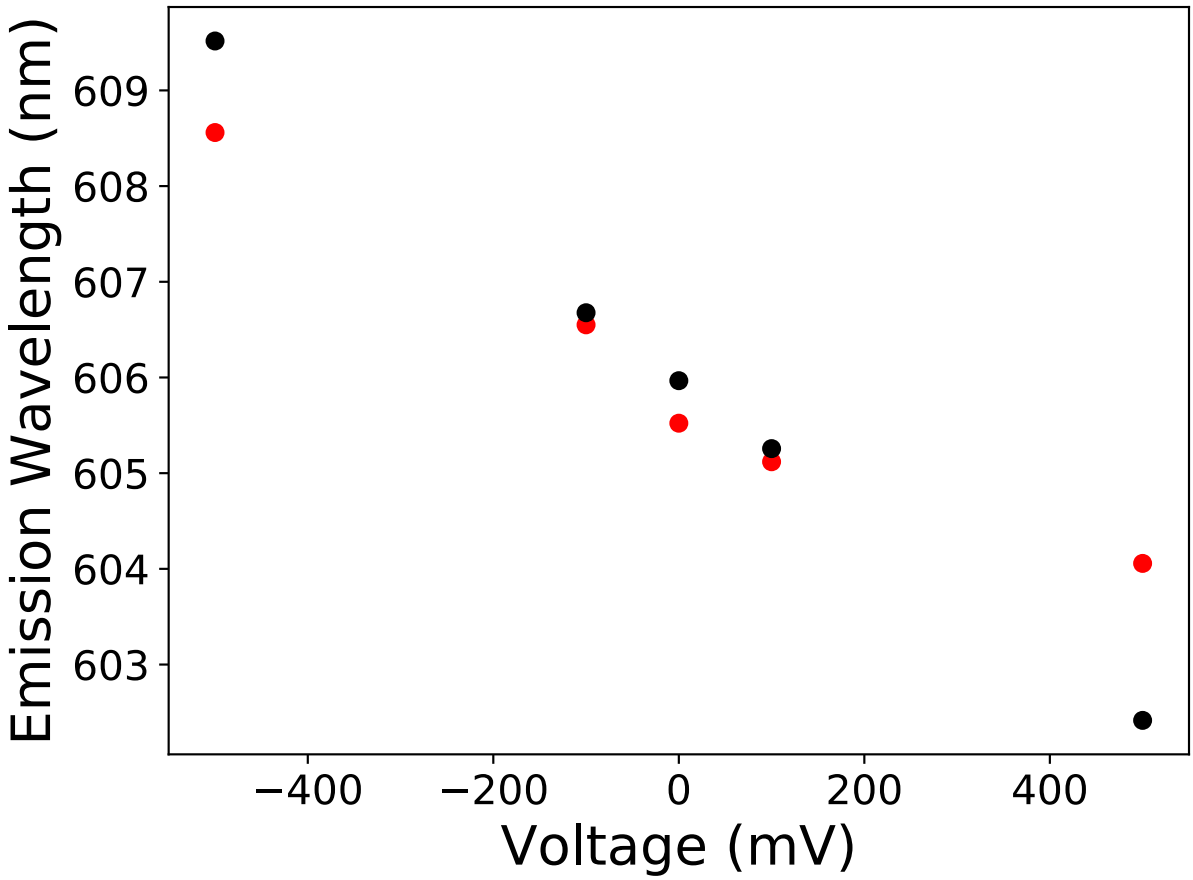

Figure 5.14: Emission wavelengths for nonpolarizable di-8-ANEPPS in DPPC with a range of applied voltages (red) - graphed with emission wavelengths deduced from fitting a Lorentzian to the data of Kao et al.[84] (black)

intensity from Kao et al.'s work. The precise values for the emission wavelengths were extracted from Kao et al.'s paper and those found in this study are also graphed together with the data from this study in Figure 5.14.

5.5 Discussion

The most important verification that this simulation of di-8-ANEPPS reflects reality is its calculated fluorescence, since that is what is directly measured in experiment. With increasing voltage potential across the membrane, there is a slight but noticeable decrease in the

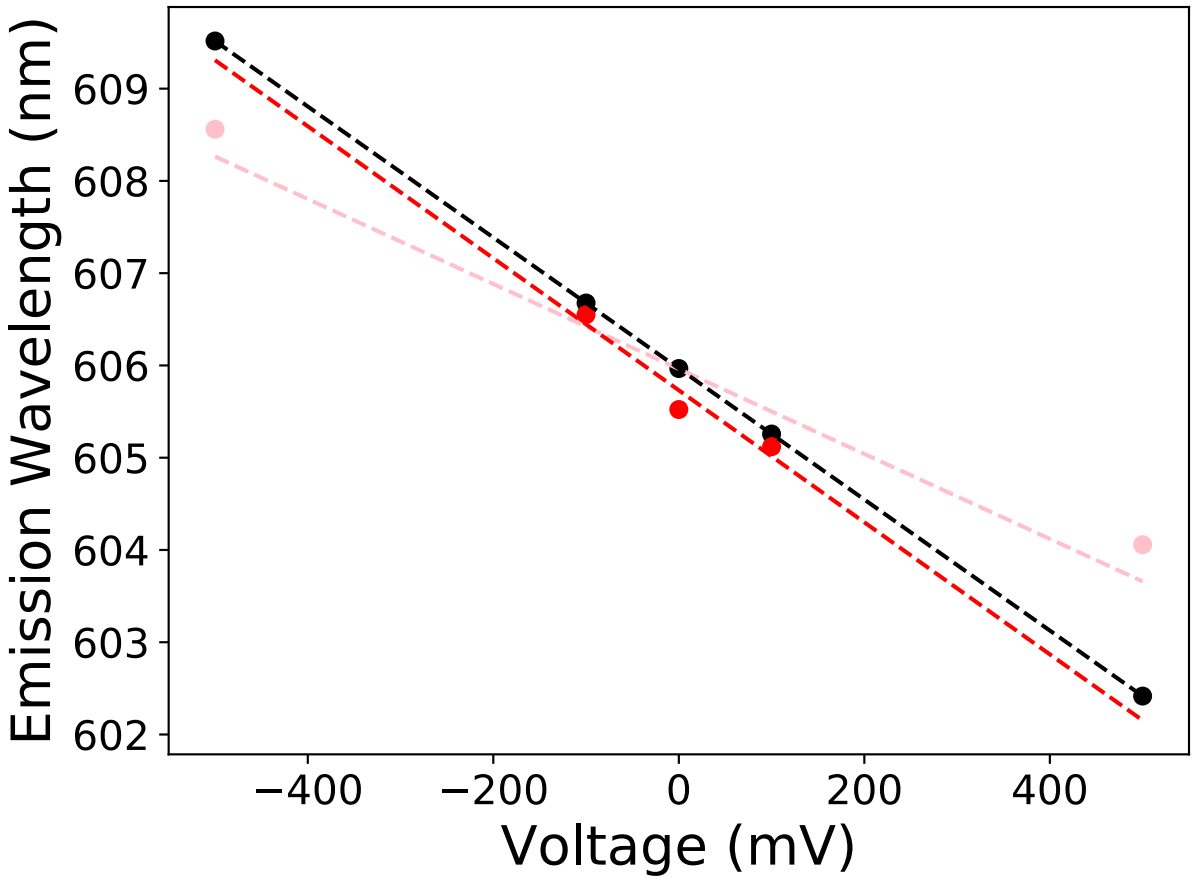

Figure 5.15: Emission wavelengths for nonpolarizable di-8-ANEPPS in DPPC with a range of applied voltages (red) - graphed with emission wavelengths deduced from fitting a Lorentzian to the data of Kao et al.[84] (black) - the pink trendline is of the nonpolarizable di-8-ANEPPS emissions based on the -500 to 500 mV range, the red trendline is of the nonpolarizable di-8-ANEPPS emissions based on the -100 to 100 mV range.

peak fluorescence predicted by this model. Considering the full range of data found from -500 to 500 mV: for every 100 mV, the wavelength of the fluorescence is shown to change by an average of 0.45 nm. This trendline is added to the emission wavelengths in Figure 5.15 in pink. However, if the range is shortened to just consider the simulations ranging from -100 to 100 mV: for every 100 mV, the wavelength of the fluorescence is shown to change by an average of 0.7155 nm, graphed as a red trendline in Figure 5.15. This discrepancy may be due to the larger effect of more extreme applied electric fields, resulting in the change no longer being linear at those values of applied voltages. This difference may seem minor, but

in comparison to the work of Kao et al. the linear relationship derived from the Lorentzian fit of their provided spectra predicted a change of 0.710 nm per 100 mV.[84] The work of Kao et al. tested a range of only -80 mV to 60 mV and others typically tested voltages of values at most ± 100 mV. It can be seen in this comparison that the fluorescence data produced by this study is highly in line with at least the experimental results of Kao et al. in the reduced range of voltages. Considering how the fluorescence data is dependent on both the ground and excited force fields (a trajectory of a simulation containing the excited state is analyzed to find the energy of each snapshot when considering both the ground and excited state parameters independently), a great deal of confidence can be placed in the viability of both parts of this theoretical model. Even though there is not a direct comparison that can be made for the absorption data in the same manner, its behavior is expected to be at least reasonable. Its trend is also highly linear, and when using the nonpolarizable absorption in solvent offset the predicted peak absorbance are all around 460 nm.

5.6 Conclusion

The success of the modeling of di-8-ANEPPS in membrane can be seen by the sensitivity of its fluorescence under varying applied electric fields. Largely this model is compared to the work of Kao et al. after converting the data they reported as a ratio of two emission intensities at wavelengths on either side of the peak to the peak intensity of emission itself. The extreme similarity displayed in Figure 5.15 shows the matching change in wavelength as a function of voltage in the range of -100 mV to 100 mV. The offset added to each energy difference was optimized slightly to line up the results of this study with that of Kao et al., but the difference between that offset and the one reached for simulating di-8-ANEPPS in solvents of varying polarity is only about 2 kcal/mol. And more importantly, the measure of success in this study is the slope of the relationship rather than the intercept matching experimental reports. Altering the offset value shifts all of the emissions the same amount and does not

affect the slope. This study demonstrates the feasibility of modeling the activities of a probe like di-8-ANEPPS in a membrane system and opens up the possibility of predicting the changes in its spectra in more complex environments simulated with molecular dynamics. Future work with this model will involve complicating the membrane system that the di-8-ANEPPS is inserted into. Considering how similar the results of di-8-ANEPPS in a simple DPPC-water theoretical system is to the cells investigated by Kao et al., which were Human Embryonic Kidney cells,[84] alterations to the membrane composition is likely to not cause drastic changes. However, it will be interesting to investigate what specific components could shift the fluorescence peaks significantly. The mobility of a probe in membrane has been tested in other studies by increasing the rigidity of the membrane with higher cholesterol content,[123] and varying osmotic pressures.[191]. In addition to investigating the effect of lipid composition and ion concentration, the contributions of each of these factors should also prove to be of interest.

CHAPTER 6

GENERAL CONCLUSION

The work accomplished in this study with the two molecules of interest (di-8-ANEPPS and DMABN) shows the viability of modeling fluorescent cycle transitions entirely by running molecular dynamic simulations. Quantum mechanical calculations were required during the process of parameterization, particularly in regards to generating the electrostatic potential data of the excited state used to create its partial charges. And an empirical constant was added to offset the transition energies to include the contributions from the vibrational changes within the fluorescing molecule. However, the literal simulations of the molecule of interest and its environment are entirely accomplished with molecular dynamics where the molecule is either treated as it is in its ground or excited state. Nonpolarizable and polarizable Drude force fields were generated for the molecules of interest, allowing for a comparison of these two models in handling the polar interactions of the immediate environment and of the molecule in its two states. The difference between these two models is particularly clear when looking at the calculation of the orientation polarizability of solvents in Chapter 2 of this Thesis. The nonpolarizable model treats the dynamic dielectric constant and thus the index of refraction as being equal to one, which drastically affects the resulting orientation polarizability estimation. In contrast the polarizable Drude model treats polarizability explicitly and consequentially can properly approximate the orientation polarizability term. An even more direct comparison of the two models was performed by parameterizing di-8-ANEPPS such that the polarizable Drude force fields were created with identical partial charges to the nonpolarizable force field; the only difference being the polarizability terms inherent in the polarizable Drude model. In Chapter 4 of this Thesis, di-8-ANEPPS simulated in a series of solvents showed clearly that the polarizable Drude model, although very similar, was a better recreation of experimental data than the nonpolarizable model.

The direct measurements of environmental effects on the absorption and emission of the

molecules of interest parameterized with the nonpolarizable and polarizable Drude force fields have largely been in rather simplistic systems: such as a pure solvent box. Chapters 3 and 4 of this Thesis explored the effects of changing the solvent surrounding DMABN and di-8-ANEPPS respectively. The accuracy of these models was determined by constructing Lippert plots where each data point represents the spectral shift of the molecule of interest in each solvent. By graphing the orientation polarizability of the specific solvent versus the Stokes shift of the molecule of interest (the difference between the emission and absorption wavelength), a perfectly linear result is expected in the case where there are no specific interactions between the molecules. Thus, a Lippert plot derived from experimental studies and the Lippert plot derived from simulations of the fluorescing molecule in explicit solvent is expected to generally follow a linear increase of the Stokes shift of the molecule with increasing solvent orientation polarizability, but there will be some variability. The fact that the energy differences extracted from those simulations result in linear Lippert plots consistent with those produced from experimental data is satisfactory. Some of the specific deviations of the Stokes shift of DMABN and di-8-ANEPPS reported for a given solvent system could easily be due to parameterization of the solvent itself. Specific molecular interactions between the solvent molecule and the solute can be assumed to be the cause of a departure from a perfect linear progression, and further improvement of these theoretical models could be made by investigating each solvent interaction more thoroughly. Yet despite these small improvements that might be made, the general trends are upheld and the range of data is consistent with reality.

Chapter 5 of this Thesis investigates di-8-ANEPPS in DPPC membrane simulated with varying applied external electric fields, which produced a gratifyingly linear result, especially in the -100 to 100 mV range. Both the absorption and emission showed a linear trend with respect to the membrane potential. Comparison was possible for the emission wavelengths calculated for di-8-ANEPPS with respect to applied electric field to those reported in experi-

mental systems, after converting the reported ratio of fluorescence to the fluorescence at peak intensity. Now that it has been shown that a simulated di-8-ANEPPS in membrane produces consistent results based on this comparison, additional factors that could cause a shift in fluorescence can now be investigated. Di-8-ANEPPS is known to be highly sensitive to the polarity, ion concentration, membrane composition and other local environmental factors. Now the model developed in this study can be used to explore to what degrees these factors contribute to the changes in the observed fluorescence, especially in regards to recreating a common experimental usage of the probe like its insertion into a neuronal membrane. The degree to which the excited state conformation deviates from that of the ground state under different environmental conditions would also be an interesting component to investigate. Additionally, the procedure outlined in this work can be followed with other probe molecules to answer such questions for other molecules of interest.

REFERENCES

[1] Aleksij Aksimentiev and Klaus Schulten. Imaging α-hemolysin with molecular dynamics: ionic conductance, osmotic permeability, and the electrostatic potential map. *Biophysical journal*, 88(6):3745–3761, 2005.

[2] KA Al-Hassan, MA Meetani, and ZFM Said. Fluorescence probes as molecular weight detectors of polymers. *Journal of fluorescence*, 8(1):93–100, 1998.

[3] Khader A Al-Hassan. The role of α-cyclodextrin cavity size on the fluorescence of 4-diethylaminobenzonitrile aqueous solution. *Chemical physics letters*, 227(4-5):527–532, 1994.

[4] A. P. Alivisatos, M. Chun, G. M. Church, R. J. Greenspan, M. L. Roukes, and R. Yuste. The brain activity map project and the challenge of functional connectomics. *Neuron*, 74(6):970–974, Jun 2012.

[5] S. Amoroso, V. V. Agon, T. Starke-Peterkovic, M. D. McLeod, H. J. Apell, P. Sebban, and R. J. Clarke. Photochemical behavior and Na+,K+-ATPase sensitivity of voltage-sensitive styrylpyridinium fluorescent membrane probes. *Photochem Photobiol*, 82(2): 495–502, 2006.

[6] Rômulo A Ando, Samantha E Brown-Xu, Lisa NQ Nguyen, and Terry L Gustafson. Probing the solvation structure and dynamics in ionic liquids by time-resolved infrared spectroscopy of 4-(dimethylamino) benzonitrile. *Physical Chemistry Chemical Physics*, 19(36):25151–25157, 2017.

[7] Peter W Atkins and Ronald S Friedman. *Molecular quantum mechanics*. Oxford university press, 2011.

[8] Tesfay Atsbeha, Ahmed M Mohammed, and Mesfin Redi-Abshiro. Excitation wavelength dependence of dual fluorescence of dmabn in polar solvents. *Journal of fluorescence*, 20(6):1241–1248, 2010.

[9] Alberto Baiardi, Julien Bloino, and Vincenzo Barone. General time dependent approach to vibronic spectroscopy including franck-condon, herzberg-teller, and duschinsky effects. *J. Chem. Theory Comput.*, 9(9):4097–4115, SEP 2013. ISSN 1549-9618. doi:10.1021/ct400450k.

[10] Dortmund Data Bank. Version 97. *DDBST Software and Separation Technology GmbH, Oldenburg, Germany*, 1997.

[11] Jay L Banks, George A Kaminski, Ruhong Zhou, Daniel T Mainz, BJ Berne, and Richard A Friesner. Parametrizing a polarizable force field from ab initio data. i. the fluctuating point charge model. *The Journal of chemical physics*, 110(2):741–754, 1999.

[12] SM Baylor and H Oetliker. Birefringence experiments on isolated skeletal muscle fibres suggest a possible signal from the sarcoplasmic reticulum. *Nature*, 253(5487):97–101, 1975.

[13] Richard S Bedlack Jr, Stephen H Fox, Eitan Gross, Leslie M Loew, et al. Distinct electric potentials in soma and neurite membranes. *Neuron*, 13(5):1187–1193, 1994.

[14] RS Bedlack Jr, LM Loew, et al. Localized membrane depolarizations and localized calcium influx during electric field-guided neurite growth. *Neuron*, 9(3):393–403, 1992.

[15] SM Blinder. Basic concepts of self-consistent-field theory. *American journal of physics*, 33(6):431–443, 1965.

[16] Bernard R Brooks, Charles L Brooks III, Alexander D Mackerell Jr, Lennart Nilsson, Robert J Petrella, Benoît Roux, Youngdo Won, Georgios Archontis, Christian Bartels, Stefan Boresch, et al. Charmm: the biomolecular simulation program. *Journal of computational chemistry*, 30(10):1545–1614, 2009.

[17] A. Bullen and P. Saggau. High-speed, random-access fluorescence microscopy: II. Fast quantitative measurements with voltage-sensitive dyes. *Biophys J*, 76(4):2272–2287, Apr 1999.

[18] A Bullen and P Saggau. High-speed, random-access fluorescence microscopy: Ii. fast quantitative measurements with voltage-sensitive dyes. *Biophysical journal*, 76(4): 2272–2287, 1999.

[19] R. Carr and M. Parrinello. Unified approach for molecular dynamics and density-functional theory. *Phys. Rev. Lett.*, 55:2471–2474, Nov 1985. doi:10.1103/PhysRevLett.55.2471. URL `https://link.aps.org/doi/10.1103/PhysRevLett.55.2471`.

[20] David Ker-Liang Cheng, Leslie Tung, and Eric A Sobie. Nonuniform responses of transmembrane potential during electric field stimulation of single cardiac cells. *American Journal of Physiology-Heart and Circulatory Physiology*, 277(1):H351–H362, 1999.

[21] Chi-Bin Chien and Jerome Pine. Voltage-sensitive dye recording of action potentials and synaptic potentials from sympathetic microcultures. *Biophysical journal*, 60(3): 697–711, 1991.

[22] C Chudoba, A Kummrow, J Dreyer, J Stenger, ETJ Nibbering, T Elsaesser, and KA Zachariasse. Excited state structure of 4-(dimethylamino) benzonitrile studied by femtosecond mid-infrared spectroscopy and ab initio calculations. *Chemical physics letters*, 309(5-6):357–363, 1999.

[23] R. J. Clarke. Effect of lipid structure on the dipole potential of phosphatidylcholine bilayers. *Biochim Biophys Acta*, 1327(2):269–278, Jul 1997.

[24] R. J. Clarke. The dipole potential of phospholipid membranes and methods for its detection. *Adv Colloid Interface Sci*, 89-90:263–281, Jan 2001.

[25] R. J. Clarke. Effect of Cholesterol on the Dipole Potential of Lipid Membranes. *Adv Exp Med Biol*, 1115:135–154, 2019.

[26] R. J. Clarke and C. Lopfert. Influence of anions and cations on the dipole potential of phosphatidylcholine vesicles: a basis for the Hofmeister effect. *Biophys J*, 76(5): 2614–2624, May 1999.

[27] Ronald J Clarke. Electric field sensitive dyes. *Advanced Fluorescence Reporters in Chemistry and Biology I*, pages 331–344, 2010.

[28] Ronald J Clarke and David J Kane. Optical detection of membrane dipole potential: avoidance of fluidity and dye-induced effects. *Biochimica et Biophysica Acta (BBA)-Biomembranes*, 1323(2):223–239, 1997.

[29] V Čmiel, F Mravec, T Halasová, J Sekora, and I Provazník. Emission properties of potential-responsive probe di-4-anepps. *Analysis of Biomedical Signals and Images*, 20:359–363, 2010.

[30] Lawrence B Cohen and Brian M Salzberg. Optical measurement of membrane potential. *Reviews of Physiology, Biochemistry and Pharmacology, Volume 83*, pages 35–88, 1978.

[31] LB Cohen, RD Keynes, and Bertil Hille. Light scattering and birefringence changes during nerve activity. *Nature*, 218(5140):438–441, 1968.

[32] LB Cohen, BM Salzberg, HV Davila, WN Ross, D Landowne, AS Waggoner, and CH Wang. Changes in axon fluorescence during activity: molecular probes of membrane potential. *The Journal of membrane biology*, 19(1):1–36, 1974.

[33] Edward Condon. A theory of intensity distribution in band systems. *Physical Review*, 28(6):1182, 1926.

[34] Edward U Condon. Nuclear motions associated with electron transitions in diatomic molecules. *Physical Review*, 32(6):858, 1928.

[35] EU Condon. The theory of complex spectra. *Physical Review*, 36(7):1121, 1930.

[36] Bernardo de Souza, Frank Neese, and Robert Izsak. On the theoretical prediction of fluorescence rates from first principles using the path integral approach. *J. Chem. Phys.*, 148(3), JAN 21 2018. ISSN 0021-9606. doi:10.1063/1.5010895.

[37] Alexander P Demchenko. The concept of λ-ratiometry in fluorescence sensing and imaging. *Journal of fluorescence*, 20(5):1099–1128, 2010.

[38] M DiFranco, J Capote, and JL Vergara. Optical imaging and functional characterization of the transverse tubular system of mammalian muscle fibers using the potentiometric indicator di-8-anepps. *The Journal of membrane biology*, 208(2):141–153, 2005.

[39] Marino DiFranco and Julio L Vergara. The na conductance in the sarcolemma and the transverse tubular system membranes of mammalian skeletal muscle fibers. *Journal of General Physiology*, 138(4):393–419, 2011.

[40] Marino DiFranco, Alvaro Herrera, and Julio L Vergara. Chloride currents from the transverse tubular system in adult mammalian skeletal muscle fibers. *Journal of General Physiology*, 137(1):21–41, 2011.

[41] P. A. M. Dirac. Quantum mechanics of many-electron systems . *Proc. R. Soc. Lond.* , A123: 714–733 , 1929.

[42] P Drude, RA Millikan, and RC Mann. The theory of optics longmans. *Green, and Co*, 1902.

[43] Benjamin Ehrenberg, Daniel L Farkas, Eric N Fluhler, Zenobia Lojewska, and Leslie M Loew. Membrane potential induced by external electric field pulses can be followed with a potentiometric dye. *Biophysical journal*, 51(5):833–837, 1987.

[44] Albert Einstein. Über einen die erzeugung und verwandlung des lichtes betreffenden heuristischen gesichtspunkt. 1905.

[45] Francisco Jose Avila Ferrer and Fabrizio Santoro. Comparison of vertical and adiabatic harmonic approaches for the calculation of the vibrational structure of electronic spectra. *Phys. Chem. Chem. Phys.*, 14(39):13549–13563, 2012. ISSN 1463-9076. doi:10.1039/c2cp41169e.

[46] Eric Fluhler, Valerie G Burnham, and Leslie M Loew. Spectra, membrane binding, and potentiometric responses of new charge shift probes. *Biochemistry*, 24(21):5749–5755, 1985.

[47] Vladimir Fock. Näherungsmethode zur lösung des quantenmechanischen mehrkörperproblems. *Zeitschrift für Physik*, 61(1):126–148, 1930.

[48] James Franck and EG Dymond. Elementary processes of photochemical reactions. *Transactions of the Faraday Society*, 21(February):536–542, 1926.

[49] JC Freedman and JF Hoffman. The relation between dicarbocyanine dye fluorescence and the membrane potential of human red blood cells set at varying donnan equilibria. *The Journal of general physiology*, 74(2):187–212, 1979.

[50] Peter Gedeck and Siegfried Schneider. Numerical self-consistent reaction field study of intramolecular charge transfer in p-(dimethylamino)-benzonitrile. *Journal of Photochemistry and Photobiology A: Chemistry*, 105(2-3):165–181, 1997.

[51] Zbigniew R Grabowski, Krystyna Rotkiewicz, and Wolfgang Rettig. Structural changes accompanying intramolecular electron transfer: focus on twisted intramolecular charge-transfer states and structures. *Chemical reviews*, 103(10):3899–4032, 2003.

[52] Jennifer N. Greeson and Robert M. Raphael. Application of fluorescence polarization microscopy to measure fluorophore orientation in the outer hair cell plasma membrane. *J. Biomed. Opt. S*, 12(2), MAR-APR 2007. ISSN 1083-3668. doi:10.1117/1.2717499.

[53] Amiram Grinvald, R Hildesheim, IC Farber, and L Anglister. Improved fluorescent probes for the measurement of rapid changes in membrane potential. *Biophysical Journal*, 39(3):301–308, 1982.

[54] Amiram Grinvald, A Fine, IC Farber, and R Hildesheim. Fluorescence monitoring of electrical responses from small neurons and their processes. *Biophysical journal*, 42(2): 195–198, 1983.

[55] David Gross, Leslie M Loew, and Watt W Webb. Optical imaging of cell membrane potential changes induced by applied electric fields. *Biophysical journal*, 50(2):339–348, 1986.

[56] Eitan Gross, Richard S Bedlack Jr, and Leslie M Loew. Dual-wavelength ratiometric fluorescence measurement of the membrane dipole potential. *Biophysical journal*, 67 (1):208–216, 1994.

[57] Grzegorz Grynkiewicz, Martin Poenie, and Roger Y Tsien. A new generation of ca2+ indicators with greatly improved fluorescence properties. *Journal of biological chemistry*, 260(6):3440–3450, 1985.

[58] James Gumbart, Fatemeh Khalili-Araghi, Marcos Sotomayor, and Benoît Roux. Constant electric field simulations of the membrane potential illustrated with simple systems. *Biochimica et Biophysica Acta (BBA)-Biomembranes*, 1818(2):294–302, 2012.

[59] S. Habib-E-Rasul Mullah, R. Komuro, P. Yan, S. Hayashi, M. Inaji, Y. Momose-Sato, L. M. Loew, and K. Sato. Evaluation of voltage-sensitive fluorescence dyes for monitoring neuronal activity in the embryonic central nervous system. *J Membr Biol*, 246(9):679–688, Sep 2013.

[60] MA Haidekker, TP Brady, D Lichlyter, and EA Theodorakis. Effects of solvent polarity and solvent viscosity on the fluorescent properties of molecular rotors and related probes. *Bioorganic chemistry*, 33(6):415–425, 2005.

[61] GG Hall. The molecular orbital theory of chemical valency viii. a method of calculating ionization potentials. *Proceedings of the Royal Society of London. Series A. Mathematical and Physical Sciences*, 205(1083):541–552, 1951.

[62] Owen P Hamill, A Marty, Erwin Neher, Bert Sakmann, and Frederick J Sigworth. Improved patch-clamp techniques for high-resolution current recording from cells and cell-free membrane patches. *Pflügers Archiv*, 391(2):85–100, 1981.

[63] Edward Harder, Victor M Anisimov, Igor V Vorobyov, Pedro EM Lopes, Sergei Y Noskov, Alexander D MacKerell, and Benoît Roux. Atomic level anisotropy in the electrostatic modeling of lone pairs for a polarizable force field based on the classical drude oscillator. *Journal of chemical theory and computation*, 2(6):1587–1597, 2006.

[64] Douglas R Hartree. The wave mechanics of an atom with a non-coulomb central field. part i. theory and methods. In *Mathematical Proceedings of the Cambridge Philosophical Society*, volume 24, pages 89–110. Cambridge university press, 1928.

[65] Douglas Rayne Hartree. The wave mechanics of an atom with a non-coulomb central field. part ii. some results and discussion. In *Mathematical Proceedings of the Cambridge Philosophical Society*, volume 24, pages 111–132. Cambridge University Press, 1928.

[66] Douglas Rayner Hartree and MM Black. A theoretical investigation of the oxygen atom in various states of ionisation. *Proceedings of the Royal Society of London. Series A, Containing Papers of a Mathematical and Physical Character*, 139(838):311–335, 1933.

[67] Douglas Rayner Hartree and William Hartree. Self-consistent field, with exchange, for beryllium. *Proceedings of the Royal Society of London. Series A-Mathematical and Physical Sciences*, 150(869):9–33, 1935.

[68] Douglas Rayner Hartree, W Hartree, and Bertha Swirles. Self-consistent field, including exchange and superposition of configurations, with some results for oxygen. *Philosophical Transactions of the Royal Society of London. Series A, Mathematical and Physical Sciences*, 238(790):229–247, 1939.

[69] DR Hartree. The wave mechanics of an atom with a non-coulomb central field. part iii. term values and intensities in series in optical spectra. In *Mathematical Proceedings of the Cambridge Philosophical Society*, volume 24, pages 426–437. Cambridge University Press, 1928.

[70] Judith A Heiny, Frances M Ashcroft, and Julio Vergara. T-system optical signals associated with inward rectification in skeletal muscle. *Nature*, 301(5896):164–166, 1983.

[71] Gerhard Herzberg. Zum aufbau der zweiatomigen moleküle. *Zeitschrift für Physik*, 57 (9):601–630, 1929.

[72] K. Hiyoshi, A. Shiraishi, N. Fukuda, and S. Tsuda. In vivo wide-field voltage imaging in zebrafish with voltage-sensitive dye and genetically encoded voltage indicator. *Dev Growth Differ*, 63(8):417–428, Oct 2021.

[73] Lei Huang and Benoît Roux. Automated force field parameterization for nonpolarizable and polarizable atomic models based on ab initio target data. *Journal of chemical theory and computation*, 9(8):3543–3556, 2013.

[74] Jochen S Hub, Camilo Aponte-Santamaría, Helmut Grubmüller, and Bert L de Groot. Voltage-regulated water flux through aquaporin channels in silico. *Biophysical journal*, 99(12):L97–L99, 2010.

[75] William Humphrey, Andrew Dalke, and Klaus Schulten. Vmd: visual molecular dynamics. *Journal of molecular graphics*, 14(1):33–38, 1996.

[76] Friedrich Hund. Zur deutung der molekelspektren. iv. *Zeitschrift für Physik*, 51(11): 759–795, 1928.

[77] A Jablonski. Efficiency of anti-stokes fluorescence in dyes. *Nature*, 131:839–840, JAN-JUN 1933. ISSN 0028-0836. doi:10.1038/131839b0.

[78] Christine Jamorski, James B Foresman, Carlo Thilgen, and Hans-Peter Lüthi. Assessment of time-dependent density-functional theory for the calculation of critical features in the absorption spectra of a series of aromatic donor–acceptor systems. *The Journal of chemical physics*, 116(20):8761–8771, 2002.

[79] H. C. Jankowiak, J. L. Stuber, and R. Berger. Vibronic transitions in large molecular systems: Rigorous prescreening conditions for franck-condon factors. *J. Chem. Phys.*, 127(23), DEC 21 2007. ISSN 0021-9606. doi:10.1063/1.2805398. 42nd Symposium on Theoretical Chemistry, Erkner, GERMANY, 2006.

[80] Sunhwan Jo, Taehoon Kim, and Wonpil Im. Automated builder and database of protein/membrane complexes for molecular dynamics simulations. *PloS one*, 2(9): e880, 2007.

[81] Sunhwan Jo, Taehoon Kim, Vidyashankara G Iyer, and Wonpil Im. Charmm-gui: a web-based graphical user interface for charmm. *Journal of computational chemistry*, 29(11):1859–1865, 2008.

[82] Sunhwan Jo, Joseph B Lim, Jeffery B Klauda, and Wonpil Im. Charmm-gui membrane builder for mixed bilayers and its application to yeast membranes. *Biophysical journal*, 97(1):50–58, 2009.

[83] George A Kaminski, Harry A Stern, Bruce J Berne, Richard A Friesner, Yixiang X Cao, Robert B Murphy, Ruhong Zhou, and Thomas A Halgren. Development of a polarizable force field for proteins via ab initio quantum chemistry: first generation model and gas phase tests. *Journal of computational chemistry*, 23(16):1515–1531, 2002.

[84] WY Kao, Cristina E Davis, YI Kim, and JM Beach. Fluorescence emission spectral shift measurements of membrane potential in single cells. *Biophysical journal*, 81(2): 1163–1170, 2001.

[85] M. Karplus. Development of multiscale models for complex chemical systems: from $H+H_2$ to biomolecules (Nobel Lecture). *Angew. Chem. Int. Ed. Engl.*, 53(38):9992–10005, Sep 2014.

[86] John G Kirkwood. The dielectric polarization of polar liquids. *The Journal of Chemical Physics*, 7(10):911–919, 1939.

[87] Gottfried Köhler, Peter Wolschann, and Krystyna Rotkiewicz. Solvent effects on intramolecular charge separation. In *Proceedings of the Indian Academy of Sciences-Chemical Sciences*, volume 104, pages 197–207. Springer, 1992.

[88] Maximilian Kohns. Molecular simulation study of dielectric constants of pure fluids and mixtures. *Fluid Phase Equilibria*, 506:112393, 2020.

[89] J. R. Lakowicz. *Principles of Fluorescence Spectroscopy, Second Edition.* Springer Science + Business Media, New York, 1999.

[90] A Lambacher and P Fromherz. Orientation of hemicyanine dye in lipid membrane measured by fluorescence interferometry on a silicon chip. *J. Phys. Chem. B*, 105(2): 343–346, JAN 18 2001. ISSN 1089-5647. doi:10.1021/jp002843i.

[91] Armin Lambacher and Peter Fromherz. Orientation of hemicyanine dye in lipid membrane measured by fluorescence interferometry on a silicon chip. *The Journal of Physical Chemistry B*, 105(2):343–346, 2001.

[92] Guillaume Lamoureux and Benoıt Roux. Modeling induced polarization with classical drude oscillators: Theory and molecular dynamics simulation algorithm. *The Journal of chemical physics*, 119(6):3025–3039, 2003.

[93] Guillaume Lamoureux, Alexander D MacKerell Jr, and Benoıt Roux. A simple polarizable model of water based on classical drude oscillators. *The Journal of chemical physics*, 119(10):5185–5197, 2003.

[94] Gaëlle Le Goff, Mark F Vitha, and Ronald J Clarke. Orientational polarisability of lipid membrane surfaces. *Biochimica et Biophysica Acta (BBA)-Biomembranes*, 1768 (3):562–570, 2007.

[95] Jumin Lee, Xi Cheng, Jason M Swails, Min Sun Yeom, Peter K Eastman, Justin A Lemkul, Shuai Wei, Joshua Buckner, Jong Cheol Jeong, Yifei Qi, et al. Charmm-gui input generator for namd, gromacs, amber, openmm, and charmm/openmm simulations using the charmm36 additive force field. *Journal of chemical theory and computation*, 12(1):405–413, 2016.

[96] Jumin Lee, Dhilon S Patel, Jonas Ståhle, Sang-Jun Park, Nathan R Kern, Seonghoon Kim, Joonseong Lee, Xi Cheng, Miguel A Valvano, Otto Holst, et al. Charmm-gui membrane builder for complex biological membrane simulations with glycolipids and lipoglycans. *Journal of chemical theory and computation*, 15(1):775–786, 2018.

[97] Mi Kyung Lee and David F Coker. Modeling electronic-nuclear interactions for excitation energy transfer processes in light-harvesting complexes. *The Journal of Physical Chemistry Letters*, 7(16):3171–3178, 2016.

[98] Mi Kyung Lee, Ksenia B Bravaya, and David F Coker. First-principles models for biological light-harvesting: Phycobiliprotein complexes from cryptophyte algae. *Journal of the American Chemical Society*, 139(23):7803–7814, 2017.

[99] Justin A Lemkul, Jing Huang, Benoît Roux, and Alexander D MacKerell Jr. An empirical polarizable force field based on the classical drude oscillator model: development history and recent applications. *Chemical reviews*, 116(9):4983–5013, 2016.

[100] John E Lennard-Jones. The electronic structure of some diatomic molecules. *Transactions of the Faraday Society*, 25:668–686, 1929.

[101] Frank Leresche, Urs Von Gunten, and Silvio Canonica. Probing the photosensitizing and inhibitory effects of dissolved organic matter by using n, n-dimethyl-4-cyanoaniline (dmabn). *Environmental Science & Technology*, 50(20):10997–11007, 2016.

[102] Gilbert N Lewis. The conservation of photons. *Nature*, 118(2981):874–875, 1926.

[103] Xinbi Li, Sergei Y Ponomarev, Daniel L Sigalovsky, John P Cvitkovic, and George A Kaminski. Possim: parameterizing complete second-order polarizable force field for proteins. *Journal of chemical theory and computation*, 10(11):4896–4910, 2014.

[104] Lun-De Liao, Vassiliy Tsytsarev, Ignacio Delgado-Martínez, Meng-Lin Li, Reha Erzurumlu, Ashwati Vipin, Josue Orellana, Yan-Ren Lin, Hsin-Yi Lai, You-Yin Chen, et al. Neurovascular coupling: in vivo optical techniques for functional brain imaging. *Biomedical engineering online*, 12(1):1–20, 2013.

[105] Cui-Ying LIN, Jian-Xi ZHAO, and Li SONG. Determination of the critical micelle concentration of surfactant in aqueous nabr or n-butanol solution by dmabn. *Acta Physico-Chimica Sinica*, 24(4):709–714, 2008.

[106] E Lippert and A Teil. 10 (1955) 541; 2. *Elektrochem*, 61:962, 1957.

[107] E Lippert, W LiJder, E Moll, W Ntigele, H Boos, and H Prigge. 1. seibold-blankenstein. *Angew. Chem*, 73:695, 1961.

[108] E Lippert, W Lüder, and H Boos. Fluoreszenzspektrum und franck-condon-prinzip in lösungen aromatischer verbindungen. In *Advances in molecular spectroscopy*, pages 443–457. Elsevier, 1962.

[109] Yi-Ping Liu, Kyungsun Kim, BJ Berne, Richard A Friesner, and Steven W Rick. Constructing ab initio force fields for molecular dynamics simulations. *The Journal of chemical physics*, 108(12):4739–4755, 1998.

[110] Leslie M Loew. Potentiometric dyes: imaging electrical activity of cell membranes. *Pure and applied chemistry*, 68(7):1405–1409, 1996.

[111] Leslie M Loew and LL Simpson. Charge-shift probes of membrane potential: a probable electrochromic mechanism for p-aminostyrylpyridinium probes on a hemispherical lipid bilayer. *Biophysical journal*, 34(3):353–365, 1981.

[112] Leslie M Loew, George W Bonneville, and Jason Surow. Charge shift optical probes of membrane potential. theory. *Biochemistry*, 17(19):4065–4071, 1978.

[113] Leslie M Loew, Lawrence B Cohen, James Dix, Eric N Fluhler, Valerie Montana, Guy Salama, and Wu Jian-young. A naphthyl analog of the aminostyryl pyridinium class of potentiometric membrane dyes shows consistent sensitivity in a variety of tissue, cell, and model membrane preparations. *The Journal of membrane biology*, 130(1):1–10, 1992.

[114] LM Loew, LB Cohen, BM Salzberg, AL Obaid, and F Bezanilla. Charge-shift probes of membrane potential. characterization of aminostyrylpyridinium dyes on the squid giant axon. *Biophysical journal*, 47(1):71–77, 1985.

[115] Zenobia Lojewska, DL Farkas, B Ehrenberg, and LM Loew. Analysis of the effect of medium and membrane conductance on the amplitude and kinetics of membrane potentials induced by externally applied electric fields. *Biophysical journal*, 56(1): 121–128, 1989.

[116] Uwe Lommatzsch and Bernhard Brutschy. Ab initio calculations and supersonic jet studies on the geometry of 4-dimethylaminobenzonitrile (dmabn) and related compounds in the ground and excited state. *Chemical physics*, 234(1-3):35–57, 1998.

[117] Leandro Martínez, Ricardo Andrade, Ernesto G Birgin, and José Mario Martínez. Packmol: A package for building initial configurations for molecular dynamics simulations. *Journal of computational chemistry*, 30(13):2157–2164, 2009.

[118] Noboru Mataga, Yozo Kaifu, and Masao Koizumi. Solvent effects upon fluorescence spectra and the dipolemoments of excited molecules. *Bulletin of the Chemical Society of Japan*, 29(4):465–470, 1956.

[119] Maria Matson, Nils Carlsson, Tamas Beke-Somfai, and Bengt Nordén. Spectral properties and orientation of voltage-sensitive dyes in lipid membranes. *Langmuir*, 28(29): 10808–10817, 2012.

[120] E. Merzbacher. *Quantum Mechanics, 3rd Ed.* John Wiley & Sons, Inc., New York, New York, 1998.

[121] Chr Møller and Milton S Plesset. Note on an approximation treatment for many-electron systems. *Physical review*, 46(7):618, 1934.

[122] Valerie Montana, Daniel L Farkas, and Leslie M Loew. Dual-wavelength ratiometric fluorescence measurements of membrane potential. *Biochemistry*, 28(11):4536–4539, 1989.

[123] Soumi Mukherjee, H Raghuraman, and Amitabha Chattopadhyay. Membrane localization and dynamics of nile red: effect of cholesterol. *Biochimica et Biophysica Acta (BBA)-Biomembranes*, 1768(1):59–66, 2007.

[124] W Müller, H Windisch, and HA Tritthart. Fast optical monitoring of microscopic excitation patterns in cardiac muscle. *Biophysical journal*, 56(3):623–629, 1989.

[125] Robert S Mulliken. Bonding power of electrons and theory of valence. *Chemical Reviews*, 9(3):347–388, 1931.

[126] Robert S Mulliken. The interpretation of band spectra part iii. electron quantum numbers and states of molecules and their atoms. *Reviews of modern physics*, 4(1):1, 1932.

[127] Robert S Mulliken. Electronic structures of polyatomic molecules and valence. ii. general considerations. *Physical Review*, 41(1):49, 1932.

[128] Frank Neese. The orca program system. *Wiley Interdisciplinary Reviews: Computational Molecular Science*, 2(1):73–78, 2012.

[129] Frank Neese. Software update: the orca program system, version 4.0. *Wiley Interdisciplinary Reviews-Computational Molecular Science*, 8(1):73–78, 2017.

[130] Erwin Neher and Bert Sakmann. Single-channel currents recorded from membrane of denervated frog muscle fibres. *Nature*, 260(5554):799–802, 1976.

[131] Antje Neubauer, Sukumaran Murali, and Wolfgang Rettig. Charge transfer control by substituents: Donor pyrroles and fluoro-anilines. *International Journal of Photoenergy*, 7(3):121–124, 2005.

[132] Martin Neumann. Dipole moment fluctuation formulas in computer simulations of polar systems. *Molecular Physics*, 50(4):841–858, 1983.

[133] Manami Nishizawa and Kazuhisa Nishizawa. Molecular dynamics simulation of kv channel voltage sensor helix in a lipid membrane with applied electric field. *Biophysical journal*, 95(4):1729–1744, 2008.

[134] Yingli Niu, Qian Peng, Chunmei Deng, Xing Gao, and Zhigang Shuai. Theory of excited state decays and optical spectra: Application to polyatomic molecules. *J. Phys. Chem. A*, 114(30):7817–7831, AUG 5 2010. ISSN 1089-5639. doi:10.1021/jp101568f.

[135] K. Okumura, H. Kakinuma, R. Amo, H. Okamoto, K. Yamasu, and S. Tsuda. Optical measurement of neuronal activity in the developing cerebellum of zebrafish using voltage-sensitive dye imaging. *Neuroreport*, 29(16):1349–1354, 11 2018.

[136] Alexander A Oliferenko, Sergei A Pisarev, Vladimir A Palyulin, and Nikolai S Zefirov. Atomic charges via electronegativity equalization: generalizations and perspectives. *Advances in Quantum Chemistry*, 51:139–156, 2006.

[137] Myeongkee Park, Chul Hoon Kim, and Taiha Joo. Multifaceted ultrafast intramolecular charge transfer dynamics of 4-(dimethylamino) benzonitrile (dmabn). *The Journal of Physical Chemistry A*, 117(2):370–377, 2013.

[138] Sandeep Patel and Charles L Brooks III. Charmm fluctuating charge force field for proteins: I parameterization and application to bulk organic liquid simulations. *Journal of computational chemistry*, 25(1):1–16, 2004.

[139] Sandeep Patel, Alexander D Mackerell Jr, and Charles L Brooks III. Charmm fluctuating charge force field for proteins: Ii protein/solvent properties from molecular dynamics simulations using a nonadditive electrostatic model. *Journal of computational chemistry*, 25(12):1504–1514, 2004.

[140] Wolfgang Pauli. Über den zusammenhang des abschlusses der elektronengruppen im atom mit der komplexstruktur der spektren. *Einführung und Originaltexte*, page 229, 1925.

[141] Linus Pauling. The application of the quantum mechanics to the structure of the hydrogen molecule and hydrogen molecule-ion and to related problems. *Chemical Reviews*, 5(2):173–213, 1928.

[142] F Pérez Salgado, Jurek Herbich, AGM Kunst, and RPH Rettschnick. Structure and picosecond excited-states dynamics in isolated, supercooled 4-(n, n-dimethylamino) benzonitrile. *The Journal of Physical Chemistry A*, 103(17):3184–3192, 1999.

[143] Taras Petrenko and Frank Neese. Analysis and prediction of absorption band shapes, fluorescence band shapes, resonance raman intensities, and excitation profiles using the time-dependent theory of electronic spectroscopy. *J. Chem. Phys.*, 127(16), OCT 28 2007. ISSN 0021-9606. doi:10.1063/1.2770706.

[144] James C Phillips, David J Hardy, Julio DC Maia, John E Stone, João V Ribeiro, Rafael C Bernardi, Ronak Buch, Giacomo Fiorin, Jérôme Hénin, Wei Jiang, et al. Scalable molecular dynamics on cpu and gpu architectures with namd. *The Journal of chemical physics*, 153(4):044130, 2020.

[145] Max Planck. Uber das gesetz der energieverteilung im normalspektrum. *Annalen Der Physik*, 4, 1901.

[146] Jay W Ponder, Chuanjie Wu, Pengyu Ren, Vijay S Pande, John D Chodera, Michael J Schnieders, Imran Haque, David L Mobley, Daniel S Lambrecht, Robert A DiStasio Jr, et al. Current status of the amoeba polarizable force field. *The journal of physical chemistry B*, 114(8):2549–2564, 2010.

[147] S. Preuss and W. Stein. Comparison of two voltage-sensitive dyes and their suitability for long-term imaging of neuronal activity. *PLoS One*, 8(10):e75678, 2013.

[148] Gorazd Pucihar, Tadej Kotnik, B Valič, and D Miklavčič. Numerical determination of transmembrane voltage induced on irregularly shaped cells. *Annals of biomedical engineering*, 34(4):642–652, 2006.

[149] Gorazd Pucihar, Tadej Kotnik, and Damijan Miklavčič. Measuring the induced membrane voltage with di-8-anepps. *JoVE (Journal of Visualized Experiments)*, (33):e1659, 2009.

[150] Dmitrij Rappoport and Filipp Furche. Photoinduced intramolecular charge transfer in 4-(dimethyl) aminobenzonitrile- a theoretical perspective. *Journal of the American Chemical Society*, 126(4):1277–1284, 2004.

[151] Wolfgang Rettig. Charge separation in excited states of decoupled systems—tict compounds and implications regarding the development of new laser dyes and the primary process of vision and photosynthesis. *Angewandte Chemie International Edition in English*, 25(11):971–988, 1986.

[152] Wolfgang Rettig, Barbara Bliss, and Klaus Dirnberger. Pseudo-jahn–teller and tict-models: a photophysical comparison of meta-and para-dmabn derivatives. *Chemical physics letters*, 305(1-2):8–14, 1999.

[153] Justin M Rhinehart, Randy D Mehlenbacher, and David McCamant. Probing the charge transfer reaction coordinate of 4-(dimethylamino) benzonitrile with femtosecond stimulated raman spectroscopy. *The Journal of Physical Chemistry B*, 114(45):14646–14656, 2010.

[154] Justin M Rhinehart, J Reddy Challa, and David W McCamant. Multimode charge-transfer dynamics of 4-(dimethylamino) benzonitrile probed with ultraviolet femtosecond stimulated raman spectroscopy. *The Journal of Physical Chemistry B*, 116(35): 10522–10534, 2012.

[155] Steven W Rick and BJ Berne. Dynamical fluctuating charge force fields: the aqueous solvation of amides. *Journal of the American Chemical Society*, 118(3):672–679, 1996.

[156] Steven W Rick, Steven J Stuart, and Bruce J Berne. Dynamical fluctuating charge force fields: Application to liquid water. *The Journal of chemical physics*, 101(7): 6141–6156, 1994.

[157] RS Ries, H Choi, R Blunck, F Bezanilla, and JR Heath. Black lipid membranes: visualizing the structure, dynamics, and substrate dependence of membranes. *J. Phys. Chem. B*, 108(41):16040–16049, OCT 14 2004. ISSN 1520-6106. doi:10.1021/jp048098h.

[158] David Robinson, Nicholas A Besley, Paul O'Shea, and Jonathan D Hirst. Di-8-anepps emission spectra in phospholipid/cholesterol membranes: a theoretical study. *The Journal of Physical Chemistry B*, 115(14):4160–4167, 2011.

[159] Björn O Roos. The complete active space self-consistent field method and its applications in electronic structure calculations. *Advances in chemical physics*, 69:399–445, 1987.

[160] Clemens Carel Johannes Roothaan. New developments in molecular orbital theory. *Reviews of modern physics*, 23(2):69, 1951.

[161] WN Ross, BM Salzberg, LB Cohen, A Grinvald, HV Davila, AS Waggoner, and Ch H Wang. Changes in absorption, fluorescence, dichroism, and birefringence in stained giant axons: optical measurement of membrane potential. *The Journal of membrane biology*, 33(1):141–183, 1977.

[162] K Rotkiewicz, KH Grellmann, and ZR Grabowski. Reinterpretation of the anomalous fluorescense of pn, n-dimethylamino-benzonitrile. *Chemical Physics Letters*, 19(3): 315–318, 1973.

[163] B. Roux. *Computational Modeling and Simulations of Biomolecular Systems*. World Scientific Pupblishing, Singapore, 2021.

[164] Benoît Roux. The membrane potential and its representation by a constant electric field in computer simulations. *Biophysical journal*, 95(9):4205–4216, 2008.

[165] C. Rupakheti, G. Lamoureux, A. D. MacKerell, and B. Roux. Statistical mechanics of polarizable force fields based on classical Drude oscillators with dynamical propagation by the dual-thermostat extended Lagrangian. *J Chem Phys*, 153(11):114108, Sep 2020.

[166] C. R. Rupakheti, A. D. MacKerell, and B. Roux. Global Optimization of the Lennard-Jones Parameters for the Drude Polarizable Force Field. *J Chem Theory Comput*, 17 (11):7085–7095, Nov 2021.

[167] Chetan Rupakheti, Guillaume Lamoureux, Alexander D MacKerell Jr, and Benoît Roux. Statistical mechanics of polarizable force fields based on classical drude oscillators with dynamical propagation by the dual-thermostat extended lagrangian. *The Journal of Chemical Physics*, 153(11):114108, 2020.

[168] Catalin F Rusu, Harald Lanig, Olaf G Othersen, Carola Kryschi, and Timothy Clark. Monitoring biological membrane-potential changes: a ci qm/mm study. *The Journal of Physical Chemistry B*, 112(8):2445–2455, 2008.

[169] Erwin Schrödinger. An undulatory theory of the mechanics of atoms and molecules. *Physical review*, 28(6):1049, 1926.

[170] Wouter Schuddeboom, Stephan A Jonker, John M Warman, Uwe Leinhos, Wolfgang Kuehnle, and Klaas A Zachariasse. Excited-state dipole moments of dual fluorescent 4-(dialkylamino) benzonitriles: influence of alkyl chain length and effective solvent polarity. *The Journal of Physical Chemistry*, 96(26):10809–10819, 1992.

[171] Luis Serrano-Andres, Manuela Merchan, Bjoern O Roos, and Roland Lindh. Theoretical study of the internal charge transfer in aminobenzonitriles. *Journal of the American Chemical Society*, 117(11):3189–3204, 1995.

[172] Yue Shi, Zhen Xia, Jiajing Zhang, Robert Best, Chuanjie Wu, Jay W Ponder, and Pengyu Ren. Polarizable atomic multipole-based amoeba force field for proteins. *Journal of chemical theory and computation*, 9(9):4046–4063, 2013.

[173] Vasyl V Shynkar, Andrey S Klymchenko, Guy Duportail, Alexander P Demchenko, and Yves Mély. Two-color fluorescent probes for imaging the dipole potential of cell plasma membranes. *Biochimica et Biophysica Acta (BBA)-Biomembranes*, 1712(2): 128–136, 2005.

[174] John C Slater. The theory of complex spectra. *Physical Review*, 34(10):1293, 1929.

[175] John C Slater. Note on hartree's method. *Physical Review*, 35(2):210, 1930.

[176] John C Slater. Molecular energy levels and valence bonds. *Physical Review*, 38(6): 1109, 1931.

[177] T. Starke-Peterkovic and R. J. Clarke. Effect of headgroup on the dipole potential of phospholipid vesicles. *Eur Biophys J*, 39(1):103–110, Dec 2009.

[178] T. Starke-Peterkovic, N. Turner, M. F. Vitha, M. P. Waller, D. E. Hibbs, and R. J. Clarke. Cholesterol effect on the dipole potential of lipid membranes. *Biophys J*, 90 (11):4060–4070, Jun 2006.

[179] Harry A Stern, George A Kaminski, Jay L Banks, Ruhong Zhou, BJ Berne, and Richard A Friesner. Fluctuating charge, polarizable dipole, and combined models: parameterization from ab initio quantum chemistry. *The Journal of Physical Chemistry B*, 103(22):4730–4737, 1999.

[180] George Gabriel Stokes. Xxx. on the change of refrangibility of light. *Philosophical transactions of the Royal Society of London*, (142):463–562, 1852.

[181] SJ Strickler and RA Berg. Relationship between absorption intensity and fluorescence lifetime of molecules. *J. Chem. Phys.*, 37(4):814–&, 1962. ISSN 0021-9606. doi:10.1063/1.1733166.

[182] Mounir Tarek. Membrane electroporation: a molecular dynamics simulation. *Biophysical journal*, 88(6):4045–4053, 2005.

[183] I Tasaki, A Watanabe, R Sandlin, and L Carnay. Changes in fluorescence, turbidity, and birefringence associated with nerve excitation. *Proceedings of the National Academy of Sciences*, 61(3):883–888, 1968.

[184] Amanda D. Torres, Carlos E. de Moura, V, Ricardo R. Oliveira, and Alexandre B. Rocha. Comparison among several vibronic coupling methods. *J. Mol. Mod.*, 28(9), SEP 2022. ISSN 1610-2940. doi:10.1007/s00894-022-05230-8.

[185] Nicholas J Turro. *Modern molecular photochemistry*. University science books, 1991.

[186] Kenno Vanommeslaeghe, Elizabeth Hatcher, Chayan Acharya, Sibsankar Kundu, Shijun Zhong, Jihyun Shim, Eva Darian, Olgun Guvench, P Lopes, Igor Vorobyov, et al. Charmm general force field: A force field for drug-like molecules compatible with the charmm all-atom additive biological force fields. *Journal of computational chemistry*, 31(4):671–690, 2010.

[187] M. F. Vitha and R. J. Clarke. Comparison of excitation and emission ratiometric fluorescence methods for quantifying the membrane dipole potential. *Biochim Biophys Acta*, 1768(1):107–114, Jan 2007.

[188] Mark F Vitha and Ronald J Clarke. Comparison of excitation and emission ratiometric fluorescence methods for quantifying the membrane dipole potential. *Biochimica et Biophysica Acta (BBA)-Biomembranes*, 1768(1):107–114, 2007.

[189] Igor V Vorobyov, Victor M Anisimov, and Alexander D MacKerell. Polarizable empirical force field for alkanes based on the classical drude oscillator model. *The Journal of Physical Chemistry B*, 109(40):18988–18999, 2005.

[190] Junmei Wang, Romain M Wolf, James W Caldwell, Peter A Kollman, and David A Case. Development and testing of a general amber force field. *Journal of computational chemistry*, 25(9):1157–1174, 2004.

[191] Dora Toledo Warshaviak, Michael J Muellner, and Mirianas Chachisvilis. Effect of membrane tension on the electric field and dipole potential of lipid bilayer membrane. *Biochimica et Biophysica Acta (BBA)-Biomembranes*, 1808(10):2608–2617, 2011.

[192] Emilia L Wu, Xi Cheng, Sunhwan Jo, Huan Rui, Kevin C Song, Eder M Dávila-Contreras, Yifei Qi, Jumin Lee, Viviana Monje-Galvan, Richard M Venable, et al. Charmm-gui membrane builder toward realistic biological membrane simulations, 2014.

[193] C. Xu and L. M. Loew. The effect of asymmetric surface potentials on the intramembrane electric field measured with voltage-sensitive dyes. *Biophys J*, 84(4):2768–2780, Apr 2003.

[194] Chang Xu and Leslie M Loew. The effect of asymmetric surface potentials on the intramembrane electric field measured with voltage-sensitive dyes. *Biophysical journal*, 84(4):2768–2780, 2003.

[195] Xuefei Xu, Zexing Cao, and Qianer Zhang. Theoretical study of photoinduced singlet and triplet excited states of 4-dimethylaminobenzonitrile and its derivatives. *The Journal of chemical physics*, 122(19):194305, 2005.

[196] Klaas A Zachariasse. Comment on "pseudo-jahn–teller and tict-models: a photophysical comparison of meta-and para-dmabn derivatives"[chem. phys. lett. 305 (1999) 8]: The pict model for dual fluorescence of aminobenzonitriles. *Chemical Physics Letters*, 320(1-2):8–13, 2000.

[197] Jing Zhang, Robert M Davidson, Leslie M Loew, et al. Membrane electric properties by combined patch clamp and fluorescence ratio imaging in single neurons. *Biophysical Journal*, 74(1):48–53, 1998.

[198] Tim J Zuehlsdorff and Christine M Isborn. Combining the ensemble and franck-condon approaches for calculating spectral shapes of molecules in solution. *The Journal of Chemical Physics*, 148(2):024110, 2018.

[199] Tim J. Zuehlsdorff, Sapana V. Shedge, Shao-Yu Lu, Hanbo Hong, Vincent P. Aguirre, Liang Shi, and Christine M. Isborn. Vibronic and environmental effects in simulations of optical spectroscopy. In MA Johnson and TJ Martinez, editors, *Ann. Rev. Phys. Chem., Vol 72*, volume 72 of *Annual Review of Physical Chemistry*, pages 165–188. 2021. ISBN 978-0-8243-1072-1. doi:10.1146/annurev-physchem-090419-051350.

[200] Tim J Zuehlsdorff, Sapana V Shedge, Shao-Yu Lu, Hanbo Hong, Vincent P Aguirre, Liang Shi, and Christine M Isborn. Vibronic and environmental effects in simulations of optical spectroscopy. *Annual Review of Physical Chemistry*, 72(1), 2021.